

# The theory and phenomenology of perturbative QCD based jet quenching

A. Majumder

Department of Physics, The Ohio-State University, Columbus, OH 43210, USA

M. Van Leeuwen,

Department of Physics, Utrecht University, Utrecht, The Netherlands.

February 24, 2019

## Abstract

The study of the structure of strongly interacting dense matter via hard jets is reviewed. High momentum partons produced in hard collisions produce a shower of gluons prior to undergoing the non-perturbative process of hadronization. In the presence of a dense medium this shower is modified due to scattering of the various partons off the constituents in the medium. The modified pattern of the final detected hadrons is then a probe of the structure of the medium as perceived by the jet. Starting from the factorization paradigm developed for the case of particle collisions, we review the basic underlying theory of medium induced gluon radiation based on perturbative Quantum Chromo Dynamics (pQCD) and current experimental results from Deep Inelastic Scattering on large nuclei and high energy heavy-ion collisions, emphasizing how these results constrain our understanding of energy loss. This review contains introductions to the theory of radiative energy loss, elastic energy loss, and the corresponding experimental observables and issues. We close with a discussion of important calculations and measurements that need to be carried out to complete the description of jet modification at high energies at future high energy colliders.

## Contents

<b>1</b>	<b>Introduction</b>	<b>3</b>
1.1	Background . . . . .	4
1.2	pQCD and factorization . . . . .	5
1.3	Hard jets in Semi-inclusive DIS on a nucleus and heavy-ion collisions . . . . .	7
1.4	Medium transport properties: what can be learnt from jets . . . . .	10
1.5	Other approaches and medium response observables . . . . .	12
<b>2</b>	<b>Scattering induced single gluon radiation.</b>	<b>14</b>
2.1	DIS on a proton and vacuum radiation . . . . .	14
2.2	Multiple scattering induced single gluon radiation . . . . .	18
2.2.1	Multiple scattering without gluon radiation . . . . .	18
2.2.2	Multiple scattering of quark and radiated gluon . . . . .	22
2.2.3	Length dependence of energy loss and extensions to heavy-ion reactions . . . . .	26
2.3	Other approaches and pictures of the medium . . . . .	27
2.3.1	AMY approach: Hard Thermal Loop field theory . . . . .	27

2.3.2	GLV approach: Opacity expansion . . . . .	28
2.3.3	ASW approach: Multiple-soft gluon exchange . . . . .	29
2.4	Parametrizing the effect of the medium: $\hat{q}$ , $dN/dy$ , $T$ and $\alpha_s$ . . . . .	30
<b>3</b>	<b>Incorporating Multiple radiations</b>	<b>33</b>
3.1	Higher twist: In medium DGLAP . . . . .	33
3.2	ASW and GLV: Poisson convolution . . . . .	34
3.3	AMY: rate equations. . . . .	35
3.4	Comparison of the different energy loss formalisms . . . . .	36
<b>4</b>	<b>Heavy flavors and elastic energy loss</b>	<b>39</b>
4.1	Dead cone effect in radiative energy loss . . . . .	39
4.2	Longitudinal drag and diffusion: other transport coefficients . . . . .	40
<b>5</b>	<b>Parton energy loss in collisions: modeling of the medium</b>	<b>44</b>
5.1	Nuclear overlap geometry . . . . .	44
5.2	Modeling the produced matter: hydrodynamic evolution . . . . .	45
5.3	Energy loss in a non-uniform medium . . . . .	46
5.4	Calculating observables . . . . .	47
<b>6</b>	<b>Comparison to experiment</b>	<b>48</b>
6.1	Choosing observables . . . . .	48
6.2	Perturbative QCD in p+p collisions . . . . .	48
6.3	Cold nuclear matter effects . . . . .	50
6.3.1	Energy loss in cold nuclear matter . . . . .	50
6.3.2	Experimental study of initial state: d+Au . . . . .	51
6.4	Heavy ion collisions at RHIC . . . . .	52
6.4.1	Verifying initial production rates: Photon production . . . . .	52
6.4.2	Light hadron suppression . . . . .	53
6.4.3	Di-hadron correlations and $I_{AA}$ . . . . .	55
6.4.4	Model comparisons of $R_{AA}$ and $I_{AA}$ . . . . .	58
6.4.5	Path length dependence of energy loss . . . . .	58
6.4.6	Colour factor dependence: quark versus gluon energy loss . . . . .	60
6.4.7	Heavy quark energy loss . . . . .	61
6.4.8	$\gamma$ -hadron and jet based measurements at RHIC . . . . .	63
6.5	Outlook: how to reduce uncertainties . . . . .	65
<b>7</b>	<b>Outlook: parton energy loss at LHC</b>	<b>68</b>
7.1	Experimental capabilities at the LHC . . . . .	68
7.2	Theoretical issues: From analytical approaches to Monte-Carlo . . . . .	68
<b>8</b>	<b>Conclusion</b>	<b>70</b>

# 1 Introduction

During the past nine years, high energy heavy-ion collisions have been studied at the the Relativistic Heavy-Ion Collider (RHIC) at Brookhaven National Laboratory (BNL). The three most striking findings in heavy-ion collisions at RHIC are the observation of a large azimuthal asymmetry in soft ( $p_T < 2$  GeV) hadron production, denoted as elliptic flow; the observation of a large suppression of hadron yields at high transverse momentum ( $p_T > 6$ ) GeV and the finding that the yields and the elliptic flow at intermediate  $p_T$  follow a scaling behaviour that separates baryons and mesons by a factor of 3/2. Each of these observations indicates that hot and dense strongly interacting matter is formed in collisions at RHIC, possibly a deconfined Quark-Gluon Plasma. Soon, the LHC will start colliding nuclei at much larger energies, which will provide critical tests of the current understanding of hot and dense QCD matter at RHIC.

In this review, we will concentrate solely on the suppression of high- $p_T$  hadron production and specifically its theoretical description within a perturbative QCD (pQCD) based formalism. In the collision of two heavy-ions at very high energies, most of the hard valence partons go through the collision un-deflected. The prevalent interaction is that between the softer “sea” partons. It is these soft interactions which lead to the formation of the hot and dense matter. Here “soft” means involving momentum scales of the order of  $\Lambda_{QCD}$ . Occasionally the hard partons undergo hard scattering (at scales much larger than  $\Lambda_{QCD}$ ) leading to the formation of two back-to-back hard partons with a large  $p_T$ . High- $p_T$  hadrons originate in the fragmentation of such high  $p_T$  partons after their escape from the medium. The hard partons lose energy through interactions with the hot and dense medium. High  $p_T$  signatures are of special interest, because they are expected to be described by perturbative QCD due to the hard scale of the jets. At the LHC, it will be possible to reach  $p_T \sim 100 - 200$  GeV, i.e. a factor of 10 increase in the hard scale of the jets compared to RHIC. Jet physics based on perturbative QCD is therefore expected to play a central role in the study of hot QCD matter at the LHC.

While the development of the theoretical framework to describe parton energy loss was started a little less than 20 years ago [1], the basic observation that high- $p_T$  hadrons are suppressed was only made with the first RHIC data [2, 3]. Since then there has been significant progress in our understanding of parton energy loss. On the experimental side, the variety of measurements has greatly increased, now extending to a variety of di-hadron and heavy flavour measurements. The precision and momentum reach of these measurements is also much more extended compared to the first results from RHIC. Phenomenological calculations have become much more detailed, incorporating a variety of initial state effects such as shadowing, Cronin broadening [4] and more realistic models of the collision geometry based on hydrodynamical calculations constrained to describe the soft hadron spectrum. There are now four different theoretical schemes for energy loss calculations, which incorporate different physical assumptions regarding the scales involved and the microscopic structure of the medium. These approaches can be compared and contrasted to provide insight into the essential aspects of the dynamics of energy loss in heavy ion collisions.

In this review, we aim to provide a survey of the current state of the theoretical understanding of parton energy loss and the experimental tests of this understanding. Our objective is not to provide an exhaustive compilation of all experimental results and theoretical calculations that have been performed, but rather to provide an overview of the current understanding and methods which can serve as a ‘reading guide’ for the extensive literature on the subject. The theoretical part of the review introduces the pQCD based formalism of jet quenching as an extension of the standard factorized approach to hard processes in vacuum and then discusses the similarities and differences between the four different theoretical approaches to parton energy loss in some detail. In the experimental part of the review the emphasis is on a subset of observables which are, or can be, rigorously calculated within pQCD and focus on what has been learnt from these. This field is under active development, both theoretically and experimentally. On the theory side, the topic of most current interest is the development of Monte

Carlo routines to address some of the shortcomings of the analytical approaches and to compute more exclusive jet based observables. On the experimental side, measurements have been extended to include photon-jet events and multi-hadron observables, including first attempts to reconstruct jets in heavy ion collisions at RHIC. In conclusion, we will discuss these developments and how they are expected to address some of the main open question about parton energy loss.

In the remainder of this chapter we provide a very brief introduction of how the factorized formalism arises in pQCD. In Chapter 2, we re-derive the multiple scattering induced single gluon emission cross section within this language. This is most straightforwardly achieved in a particular variant of what has come to be denoted as the higher twist approach. After this we relate our results to the derivations in other schemes. In Chapter 3, we describe the inclusion of multiple emissions. This is as yet a theoretically unsettled regime and we review the three different means by which multiple emissions have been included. This is followed by a direct comparison of the various formalisms, where the medium modified fragmentation function is calculated in an identical medium. In Chapter 4 we extend our formalism to include heavy flavor modification along with elastic loss and diffusion. In Chapter 5 we describe the phenomenological setup used to compute jet modification in a static large nucleus and in a dynamically evolving quark gluon plasma. In Chapter 6, we compare the results of recent calculations in the literature on single hadron, dihadron, photon triggered and heavy flavor observables to measurements in Deep-Inelastic Scattering (DIS) from HERA and those in high-energy nuclear collisions from RHIC. In Chapter 7, we provide an outlook to the LHC and forthcoming theory calculations.

## 1.1 Background

Quantum chromodynamics (QCD) is now the accepted theory of strong interactions. In spite of the large diversity of hadronic states observed in nature, the Lagrangian of QCD is rather simple, involving only two types of fundamental fields: quarks and gluons, interacting via an  $SU(N_c = 3)$  gauge theory [5]

$$\mathcal{L}_{QCD}(x) = -\frac{1}{4}F_{\mu\nu}^a(x)F^{a\mu\nu}(x) + \sum_{q=1}^{n_f} \bar{\psi}_i^q(x) \left[ i\gamma^\mu \mathfrak{D}_{\mu,i,j} + m_q \right] \psi_j^q(x), \quad (1)$$

where  $i, j$  run from 1 to  $N_c$  representing the colors of the fundamental quarks of flavor  $q$  and  $a$  runs from 1 to  $N_c^2 - 1$  representing the colors of the adjoint gluon gauge field. For the purposes of this review  $n_f$  will mostly be limited to 3, for the light quarks  $u, d$ , and  $s$ , which will be treated as massless. The heavy flavors charm and bottom will be discussed separately and will have non-zero mass terms. The top quark will not be included in this review (thus  $n_f \leq 5$ ). The covariant derivative and the adjoint field strength have the usual definitions,

$$\mathfrak{D}_{\mu,i,j}^\mu = \delta_{i,j} \partial^\mu - ig t_{i,j}^a A^{a\mu} \quad \text{and} \quad F_{\mu\nu}^a = \partial_\mu A_\nu^a - \partial_\nu A_\mu^a + gf^{abc} A_\mu^b A_\nu^c. \quad (2)$$

In the equation above,  $A_\mu^a$  is the gluon four-vector potential with adjoint color  $a$ ,  $t_{i,j}^a$  are the Gell-Mann matrices,  $f^{abc}$  is the completely antisymmetric tensor and  $g = \sqrt{4\pi\alpha_s}$  is the strong interaction coupling constant. In this review, we will often refer to the fine structure constant  $\alpha_s$  also as the ‘‘coupling’’. Which is meant, will be denoted using the appropriate symbol.

Like all renormalizable quantum field theories, the coupling depends on the renormalization scale  $\mu$ , usually chosen as the relevant hard scale in the problem  $Q^2$  to minimize the effect of higher order contributions. Unlike the case of QED or weak interactions, QCD is asymptotically free, which implies that the coupling becomes weaker as the scale is raised [6, 7]. Solving the (one loop) renormalization group equation, and comparing with experimental data to obtain the initial condition, one obtains,

$$\alpha_s(Q^2) = \frac{4\pi}{\left(\frac{11N_c}{3} - \frac{2n_f}{3}\right) \log\left(\frac{Q^2}{\Lambda_{QCD}^2}\right)}. \quad (3)$$

The above equation implies that at scales far above  $\Lambda_{QCD} \sim 200\text{MeV}$ , QCD should be weakly coupled and a perturbative expansion in terms of  $\alpha_s$  should become feasible. The applicability of this statement, of course, depends on the process in question. In the case of the total cross section in  $e^+e^-$  annihilation, single hadron inclusive  $e^+e^-$  annihilation, the total cross section in Deep Inelastic Scattering (DIS), single hadron inclusive DIS and the Drell-Yan effect, pQCD begins to become applicable beyond a  $Q^2 \gtrsim 2 \text{ GeV}^2$  [8, 9, 10]. The quantity  $Q^2$  here refers to the relevant invariant mass that sets the hard scale in the problem. In all the three cases mentioned, this is the invariant mass squared of the intermediate photon. In the case of hadron-hadron scattering, one requires a specific hard momentum transfer process, such as the production of a high transverse momentum (high  $p_T$ ) particle. The hard interaction in this case is mediated by the strong force (meaning the higher order corrections are of a different type) and such processes seem to need a minimum  $p_T \gtrsim 2 \text{ GeV}$  ( $Q^2 \gtrsim 4 \text{ GeV}^2$ ) for pQCD to be applicable [11].

With the diminishing of momentum transfers, the strong coupling fine structure constant  $\alpha_s(Q^2)$  continues to grow and confines all particles which carry color charge within composite color singlet hadrons. While one may still construct an effective Lagrangian using the underlying symmetries of QCD and carry out a perturbative analysis, such theories will not constitute any part of this review. All interactions with a momentum scale below a  $Q^2 \sim 2 \text{ GeV}^2$  will be considered as non-perturbative and will usually be contained in a non-perturbative distribution such as a fragmentation function, a parton distribution function or an in-medium transport coefficient. The separation of the non-perturbative part from the hard perturbative part of the calculation will be discussed in the next subsection.

## 1.2 pQCD and factorization

The ability to apply pQCD to describe a particular process should not be confused with the application of perturbative expansions in other gauge theories such as QED, the electro-weak theory or even in low energy effective theories of QCD such as chiral perturbation theory. In those theories, the incoming and outgoing asymptotic states in a scattering event carry the quantum numbers of the fields in the respective Lagrangian densities. While the QCD Lagrangian is cast in terms of quarks and gluons and by pQCD we do mean a diagrammatic expansion involving those fields, asymptotic states in strong interactions, due to confinement, are never quarks or gluons but composite hadrons. The ability to apply pQCD thus means simply the ability to isolate a section of the interaction which can be systematically described using a perturbative expansion in  $\alpha_s$  involving quarks and gluons, from the remaining part of the process which is non-perturbative.

In all the reactions mentioned above where pQCD is applicable, there exist sub-processes over a range of energy scales up to the hard scale  $Q^2$ . Most of these cannot be described using pQCD and need to be separated from those sub-processes which involve hard scales. The technical machinery which demonstrates this separation order-by-order in the coupling constant is called “factorization” [12, 13, 14]. The result of factorization is usually stated as a theorem with corrections power suppressed at very large  $Q^2$ . We illustrate an example of this theorem for the case of a high energy  $p$ - $p$  collision leading to the formation of a high  $p_T$  hadron. Assume the collision is in the center of mass frame with each proton carrying a momentum  $P(-P)$ . The physical picture of this process is one where a hard parton in one of the incoming nucleons, carrying a light-cone momentum fraction  $x_a$  ( $p_a = x_a P^+$ ) scatters off a hard parton in the other nucleon with light-cone momentum fraction  $x_b$  ( $p_b = -x_b P^-$ ) and produces two back-to-back partonic jets. Light-cone momenta are defined as  $P^+ = (P^0 + P^3)/\sqrt{2}$  and  $P^- = (P^0 - P^3)/\sqrt{2}$ . The hadronization products of one of these jets ( $c$ ) will yield the high  $p_T$  hadron  $h$  carrying a momentum fraction  $z$  of the original jet’s momentum. The factorization theorem for the differential cross section (in  $p_T$  and rapidity  $y$ ) states that the process can be expressed as [13, 15],

$$\frac{d^2\sigma^h}{dyd^2p_T} = \int dx_a dx_b G_a(x_a, \mu_f) G_b(x_b, \mu_f) \frac{d\sigma_{ab \rightarrow cX}(\mu_R, \mu_f, \mu'_f, x_a P, x_b P, p_T/z)}{d\hat{t}} \frac{D_c^h(z, \mu'_f)}{\pi z} + \mathcal{O}\left(\frac{\Lambda^2}{Q^2}\right), \quad (4)$$

where  $G_a(x_a)[G_b(x_b)]$  is the parton distribution function (PDF) to find a hard parton with a momentum fraction  $x_a$  ( $x_b$ ) in the incoming proton,  $d\sigma/d\hat{t}$  is the hard partonic cross section (with a partonic Mandelstam variable  $\hat{t}$ ) and  $D^h(z)$  is the fragmentation function (FF), the distribution of hadrons with a momentum fraction  $z$  produced in the hadronization of the outgoing hard parton. The second term on the *r.h.s.* indicates corrections to the factorization theorem that are suppressed by powers of the hard scale  $Q^2$ . The quantity  $\Lambda$  represents the scale of soft processes in the collision. This contribution becomes negligible as  $Q^2 \rightarrow \infty$ . Even in this asymptotic limit, the only term in the equation above that can be completely calculated within pQCD is the hard partonic cross section; the PDFs and the FF are non-perturbative objects which represent physics at softer scales.

The primary utility of factorization is based on the lack of interference between the hard and the soft scale, i.e., the PDFs and the FF (as well as the partonic cross section) are all squares of amplitudes. Eq. (4) contains only a convolution in two parameters ( $x_a, x_b$ ) between these probabilities. To compute the hard cross section one proceeds order by order and calculates all the amplitudes that may contribute to the process of two incoming partons scattering to  $n$  outgoing partons [ $n = 2$  for Leading Order (LO),  $n = 3$  for Next-to-Leading Order (NLO)]. These are then summed and squared to obtain  $d\sigma/d\hat{t}$ . The non-perturbative quantities  $G(x, \mu)$  or  $D(z, \mu)$  cannot be calculated from first principles, however they have well defined operator expressions on the light-cone, e.g., the PDF to find a quark with momentum fraction  $x$ , in a proton state  $|p\rangle$  traveling with a large light-cone momentum  $p^+$ , is defined as,

$$G(x) = \int \frac{dy^-}{2\pi} e^{-ixp^+y^-} \langle p | \bar{\psi}(y^-) \gamma^+ \psi(0) | p \rangle. \quad (5)$$

Given the operator expression, one may calculate higher order corrections. These tend to have collinear divergences which are absorbed into a renormalization of the operator product (or non-perturbative expectation values in the case of the FF). Such a redefinition introduces a scale dependence of the expectation. Divergent contributions up to this scale, denoted as the factorization scale  $\mu_f$ , are absorbed into the definition of the PDF. If  $\mu_f$  is large compared to  $\Lambda_{QCD}$ , the change of the PDF and the FF can be calculated by means of the Dokshitzer-Gribov-Lipatov-Altarelli-Parisi (DGLAP) equation [16, 17, 18],

$$\frac{\partial G(x, \mu)}{\partial \log \mu} = \frac{\alpha_s}{2\pi} \int_x^1 \frac{dy}{y} P(y) G\left(\frac{x}{y}, \mu^2\right). \quad (6)$$

In the equation above,  $P(y)$  is the splitting function which represents the probability for a hard quark to radiate a gluon and still retain a momentum fraction  $y$ . The homogeneous DGLAP equation, as expressed in Eq. (6) applies only to the non-singlet quark distribution [ $G_{NS}(x) = G_Q(x) - G_{\bar{Q}}(x)$ ]. The singlet distributions ( $G_S(x) = [G_Q(x) + G_{\bar{Q}}(x)]/2$ ) have couplings that mix the quark and gluon distributions.

Equation (6) is a differential equation and thus requires an initial condition for its solution. This requires the experimental measurement of the non-perturbative distribution at one value of the scale. Herein lies the other advantage of factorization: Once the non-perturbative distributions are factorized from the hard cross section, they are independent of the process and become universal functions in the sense that they may be given an identical definition and measured in a completely different process. In the case of totally inclusive DIS, the factorization theorem yields,

$$\frac{d\sigma}{dQ^2} = \int dx G(x, \mu^2) \frac{d\hat{\sigma}(\mu_R, \mu, Q, xP)}{dQ^2} \quad (7)$$

The operator expression for the PDF as well as its evolution equation, derived in this case, is identical to that in Eq. (4). Thus, the PDF measured in DIS (7), may be directly substituted in Eq. (4) to compute single particle inclusive cross section in  $p$ - $p$  collisions.

To summarize, the applicability of pQCD to vacuum processes, such as in Eqs. (4,7), consists of the ability to calculate the hard partonic cross section order by order, as well as to compute the scale dependence of the non-perturbative distributions. While these non-perturbative distributions need to be measured at one scale in experiment, they have rigorous operator definitions which are identical in all processes where they can be factorized and thus are universal functions. Even though the discussion above was focused on the PDF, an almost identical factorization theorem and DGLAP evolution equation may be written down for the FF. Most of the remaining review will deal with the vacuum and in-medium modification of the FF.

### 1.3 Hard jets in Semi-inclusive DIS on a nucleus and heavy-ion collisions

The preceding subsection briefly described the factorized formalism of high energy pQCD as applied to hard processes. The underlying assumption of factorization has been rigorously proven in all the examples mentioned above. In this subsection, we outline the extension of this factorized formalism to the modification of hard jets in a dense medium. Unlike the case of hard processes in vacuum, the factorization theorems which are the underlying assumptions in these calculations, though widely expected to hold, have not been proven to the same degree of rigor. So far there have only been a handful of attempts in this direction both in pQCD [19, 20, 21] as well as in an effective-field theory approach [22]. These factorization theorems will not be discussed further; we will assume their applicability. In this review we will focus on the application of the factorized theory to jet propagation in dense extended media and the ensuing phenomenology.

Imagine the single-inclusive DIS of a hard lepton on a proton in the Breit frame. This is illustrated in Fig. 1. The virtual photon with large negative light-cone momentum  $q \equiv [Q^2/2q^-, q^-, 0, 0]$  strikes a hard quark which carries a momentum fraction  $x_B$  of the Lorentz contracted proton with large positive light-cone momentum  $P^+$ . The quark is turned around and then exits the proton. Being considerably off-shell from the hard collision, it begins to shower gluons. The initial radiations have large transverse momentum  $l_\perp$  (due to the large virtuality), and thus have shorter formation times:

$$\tau_f \sim \frac{2q^-y(1-y)}{l_\perp^2}. \quad (8)$$

Where  $y$  is the momentum fraction of the parent parton carried away by the radiated gluon. Later radiations (those with larger formation times) have smaller transverse momentum. While not illustrated in the figure, the radiated gluons are also off-shell and tend to radiate gluons with smaller off-shellness. Eventually the local virtualities of the partons is so low that one cannot apply a perturbative partonic picture and hadronization begins to set in. As a result, the collection of hard collinear partons turns into a collimated jet of hadrons. The leading hadron in this picture is the one with the largest longitudinal momentum and, given some form of localized momentum conservation, is the result of hadronization of the highest longitudinal momentum part or the largest formation time part of the jet.

The picture in  $p$ - $p$  is somewhat similar except that one has at least 2 back-to-back jets being produced. Both of these jets are produced considerably off-shell and tend to lose this virtuality by successive emissions. Unlike the case of DIS, jets which arise from the produced hard partons in large  $Q^2$   $p$ - $p$  collisions have a large momentum transverse to the incoming hard partons. We will always denote the momentum in this direction as  $p_T$ , differentiating it from the momentum of gluons transverse to the produced jet which will be indicated with a  $\perp$ , as in  $l_\perp$ . The factorized formula to obtain the cross section of single hadrons is given by the first term on the right hand side of Eq. (4). At leading order, this formula simplifies to,

$$\frac{d^2\sigma^h}{dyd^2p_T} = \int dx_a dx_b G_a(x_a, Q) G_b(x_b, Q) \frac{d\sigma_{ab \rightarrow cX}(Q, x_a P, x_b P, p_T/z)}{d\hat{t}} \frac{D_c^h(z, Q)}{\pi z}. \quad (9)$$

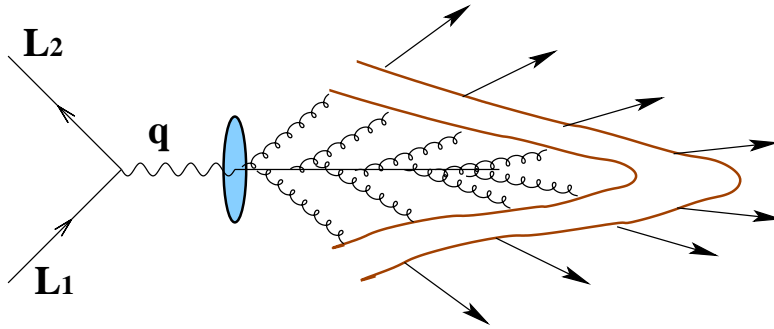


Figure 1: DIS on a nucleon leading to the formation of a quark jet which showers gluons in vacuum leading to the formation of a collimated jet of hadrons.

The reader will note that we have chosen all factorization and renormalization scales to be  $Q$  which is the hard scale in the problem. At leading order all hard scales that appear in the calculation are equivalent; in most cases one simply picks  $Q = p_T$ .

We now consider the process of DIS on a large nucleus. This will often be referred to as A-DIS (A referring to a nucleus). In the Breit frame, one may neglect the soft interactions between the various nucleons as these occur over a long time scale. The nucleus may then be modeled as a weakly interacting gas of nucleons traveling in the positive light-cone direction. The virtual photon strikes a hard quark in one of the nucleons and turns it backwards as in the case of the DIS on a single proton. The quark then propagates through the nucleons directly behind the one that is struck, as illustrated in Fig. 2, where we draw the struck quark as propagating outside the line of nucleons for clarity. The quark is virtual at production and radiates a shower of gluons with progressively longer formation times, similar to the case of DIS on a proton. In this case however, both the quark and the radiated gluons tend to scatter off the soft gluon field in the nucleons. This is indicated by the zig-zag lines. Note, the zig-zag lines do not indicate a pomeron or double gluon exchange, but rather are single-gluon exchanges which are distinct from the gluons in the shower of the jet. Diffractive exchanges with the nucleons may be neglected in the case of very large nuclei. This will be justified in the next chapter.

The multiple scattering of the partons in the shower changes their momentum distributions and as a result the final hadronization pattern is modified. In the case of a jet produced in a heavy ion collision, the picture is qualitatively similar except for the absence of nucleons. The different components of the jet now scatter off the quark-gluon substructure of the degrees of freedom in the hot deconfined matter. The leading effect of the multiple scattering on the shower profile is a broadening of the distribution in transverse momentum (recently this has been experimentally observed in cold nuclear matter [23]). Besides transferring transverse momentum, the medium also exchanges energy and longitudinal momentum with the jet (in the language of light-cone momentum, both (+) and (-) components are exchanged between the jet and the medium). While energy and momentum exchange (including transverse momentum) in the right proportion may cause minimal change in the virtuality of a given jet parton, arbitrary momentum exchanges may noticeably change the virtuality leading to induced radiation. In the case that the energy (and longitudinal momentum) of the jet partons far exceeds that of any constituent in the medium, such exchanges lead to a depletion of the light-cone momentum in the forward part of the jet. This is often referred to as radiative energy loss and results in a suppressed yield of leading particles [24, 25, 26, 27, 28, 29, 30]. This suppression has been quantitatively established in both DIS on a large nucleus [31] and in jets in heavy ion collisions [2, 3]. The primary difference between the two cases is the fact that a heavy-ion collision is not a static environment and evolves rapidly with time and then finally disintegrates into a cascade of hadrons.

The calculation of the modification of the hadronization pattern due to the multiple scattering in-



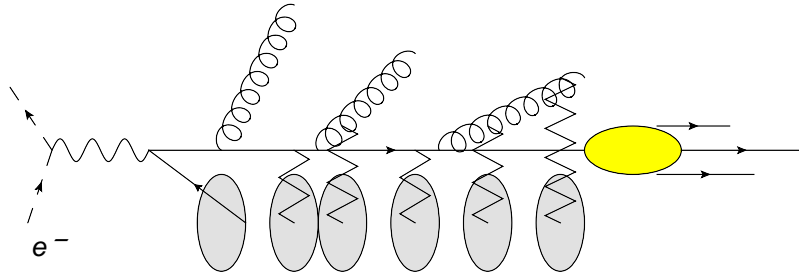


Figure 2: DIS on a large nucleus. A quark in a nucleon on the front side is struck and then propagates through the nucleons behind the struck nucleon. In the process both the quark and the ensuing shower gluons scatter off the soft glue field inside the nucleons. This modifies the shower pattern.

duced radiation will be the subject of the next two chapters. Until recently, experiments have only been able to measure the modification of the yield of the leading hadron or the correlation between the leading and next-to-leading hadrons. The basic theoretical object required to describe this aspect of jet modification is called the medium modified fragmentation function. Along with the perturbative calculation of the evolution of the fragmentation function in vacuum, one computes the change in the fragmentation function due to the broadening and stimulated emission that occurs as the jet passes through matter. The medium modified fragmentation function is now a function of not just the momentum fraction and the scale  $Q^2$ , but also of the energy of the jet and the distance travelled in the medium. While it has become conventional to call this a “medium modified” fragmentation function, it should be pointed out that in all pQCD based calculations, the fragmentation is assumed to occur once the jet has escaped the medium.

We should point out that while this review will describe jet modification in dense matter as an extension of the factorized processes in vacuum pQCD [this is often referred to as the Higher-Twist (HT) scheme [32, 33, 34]], there are other approaches to this problem. An entirely orthogonal approach is that based on finite temperature field theory based on the work of Arnold, Moore, Yaffe and collaborators [35, 36, 37, 38, 39, 40]. Referred to as the AMY scheme, this formalism considers the effective Hard Thermal Loop (HTL) effective theory of dense matter and considers the hard jet to have the same virtuality or mass scale as a thermal plasma particle but with energy  $E \gg T$ . Following this, one identifies and resums the collinear enhanced contributions emanating from the scattering and induced radiation off the hard parton. The entire calculation is carried out at the scale of the temperature  $T$  which is assumed to be large ( $T \rightarrow \infty$ ) so that the effective coupling  $g(T)$  is small [ $g(T) \rightarrow 0$ ]. Another approach developed by Armesto, Salgado, Wiedemann and collaborators models the medium as a series of Debye-screened, heavy, colored scattering centers. In this approach, referred to as the ASW scheme, the hard parton radiates a virtual gluon which is then progressively brought on shell by a large number of soft scatterings off these heavy centers [41, 42, 43, 44, 45]. Yet another approach developed by Gyulassy, Levai, Vitev and their collaborators considers the same medium as ASW, however both the hard parton and the radiated gluon undergo a few but hard interactions with the centers leading to the emission of the gluon [46, 47, 48, 49, 50, 51]. After the calculation of the single gluon emission kernel, the AMY scheme uses rate equations to incorporate multiple emissions whereas the GLV and the ASW use a Poisson emission *Ansatz*.

The comparison of the yield of leading particles between the case with and without a medium is a measure of the properties of the medium as felt by the jet. In DIS, one measures the fragmentation function to produce a hadron with a momentum fraction  $z$  of the original quark momentum immediately after being struck. For the case where the virtual photon carries a momentum,  $q \equiv [-Q^2/(2q^-), q^-, \mathbf{0}]$

and the incoming struck quark has  $p \equiv [Q^2/2q^-, 0, \mathbf{0}]$ , the outgoing quark has a momentum  $[0, q^-, \mathbf{0}]$ . Thus the hadron momentum is  $p_h \simeq zq^-$ . The fragmentation function for DIS on a proton (nucleus  $A$ ) and the ratio  $R$  are defined as,

$$D_{p(A)}(z) = \frac{1}{\sigma_{p(A)}} \frac{d\sigma_{p(A)}}{dz}, \quad \text{and} \quad R = \frac{\sigma_p}{\sigma_A} \frac{d\sigma_A/dz}{d\sigma_p/dz}. \quad (10)$$

In the equation above,  $\sigma_{p(A)}$  is the differential DIS cross section off a proton  $p$  (nucleus  $A$ ) integrated over a limited range of  $Q^2$  and energy imparted from the electron  $\nu = q^-$ . In order to compare with theoretical calculations, the fragmentation function in the case of DIS on a large nucleus  $D_A(z)$  should be identified with the medium modified fragmentation function  $\tilde{D}(z)$ .

In the case of  $p$ - $p$  or heavy-ion collisions, the jets span a range of momentum depending on the momenta of the two partons that undergo the hard scattering. In this case one cannot isolate separate bins in the final state momentum fraction  $z$  and thus cannot measure the fragmentation function directly. Instead one measures the ratio of the binary scaled differential yield to produce a high  $p_T$  hadron in a heavy-ion collision to that in a  $p$ - $p$  collision referred to as the nuclear modification factor  $R_{AA}$ . The  $R_{AA}$  may be measured both differentially as a function of angle with the reaction plane and the transverse distance between the centers of the colliding nuclei, the impact parameter  $b$ , or integrated. The angle integrated  $R_{AA}$  [also integrated over a small range of impact parameter ( $b_{min}$  to  $b_{max}$ )], is defined as

$$R_{AA} = \frac{\frac{dN^{AA}(b_{min}, b_{max})}{dyd^2p_T}}{\langle N_{bin}(b) \rangle \frac{dN^{pp}(p_T, y)}{dyd^2p_T}}, \quad (11)$$

where,  $\langle N_{bin}(b) \rangle$  is the mean number of binary nucleon nucleon encounters per ion-ion collision in the range of impact parameters chosen. The invariant yield in a heavy-ion collision and in a  $p$ - $p$  collision are related to the the invariant differential cross section by the relation,  $dN = d\sigma/\sigma$ , where the total cross section for a heavy-ion collision may be estimated as the geometrical cross section in that range of impact parameter selected. The relation between  $N_{bin}$  and the nuclear density profile will be discussed in Chapter 5.

The calculation of the nuclear cross section to produce a hard hadron may be expressed as the convolution of the nuclear PDFs, the hard partonic cross sections and the medium modified fragmentation function. The jets may be produced at various locations in the hot matter and propagate in any direction in the transverse plane. The location of the production point and the direction determine the extent and intensity of the medium as felt by the jet. One thus needs to integrate over all allowed production points and directions. This procedure will be described in Chapter 5.

## 1.4 Medium transport properties: what can be learnt from jets

As described in the preceding subsections, a jet is essentially a collection of high momentum particles which are somewhat collimated in a given direction. In the partonic part of the jet, these are virtual partons. To make this explicit we ascribe a virtuality  $\mu^2 \ll Q^2$  to the hard jet, where  $Q^2$  describes the scale of the hard interaction which produces the jet. In effective field theory approaches to hard jets such as that of Soft Collinear Effective Theory (SCET) [52, 53] one introduces a small parameter  $\lambda$  with  $\lambda \ll 1$ ; collinear radiations have a transverse momentum of  $l_\perp \sim \lambda Q$  and the virtuality of the jet may then be surmised as  $\lambda^2 Q^2$ . Thus  $\mu^2 \sim (\lambda Q)^2$ ; the two terminologies will often be used interchangeably in this review.

As the jet passes through matter each of these particles will scatter off the various constituents that it encounters. In the Breit frame (or infinite momentum frame) the nucleus has a large boost in

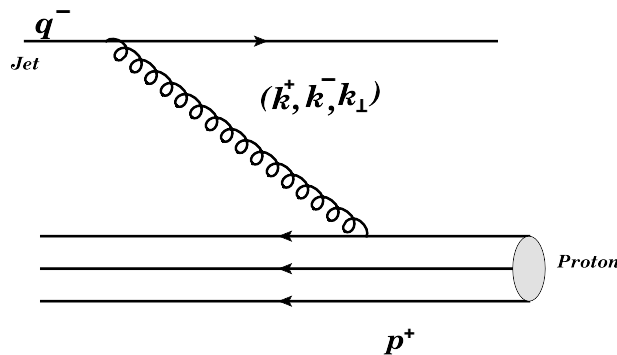


Figure 3: A single Coulomb (or Glauber) gluon interaction between a hard jet and a proton in the nucleus.

the direction opposed to that of the jet. As we pointed out earlier, one may consider each nucleon within the nucleus to be traveling in almost straight lines independent of each other. At sufficiently high energies, the “large- $x$ ” partons in the nucleons may also be considered to be traveling in straight lines independently of each other (see Fig. 3). The hard virtual partons in the jet with virtuality  $\mu^2$  will resolve this sub-structure down to transverse sizes of order  $1/\mu^2 \sim (\lambda Q)^{-2}$ . The hard partons in the jet will scatter off these partons by exchanging gluons with transverse momenta  $k_\perp \sim \mu \sim \lambda Q$ . As a result, the hard partons in the jet will undergo a transverse diffusion as they propagate through the extended matter.

Along with the exchanged transverse momentum there may also be a certain amount of negative light-cone momentum ( $k^-$ ) which may be exchanged between the partons in the jet and those from the medium. In this review, we will refer to this as “elastic energy loss” or “drag”, even though the incoming parton from the medium is not on-shell, is not a quasi-particle of the medium and may not go back on shell after the scattering. This is primarily done to distinguish this type of light-cone momentum loss from the light-cone momentum loss that occurs due to radiation. This is somewhat different from what is traditionally referred to as elastic energy loss, which involves a certain energy and momentum transfer to an in-medium quasi-particle which remains as one quasi-particle after the interaction, but with larger energy. The remaining component of the transferred momentum  $k^+$  is completely determined by insisting on the criterion that the jet parton virtuality does not change too much after the momentum transfer. Thus if the original off-shellness is  $2q^+q^- \simeq \mu^2$ , then after the transfer, one obtains the virtuality as,

$$2(q^+ + k^+)(q^- + k^-) - k_\perp^2 = \mu^2 + 2\frac{\mu^2}{q^-}k^- + k^+(q^- + k^-) - k_\perp^2. \quad (12)$$

Thus, for  $k^- \ll q^-$  we obtain that the virtuality of the parton will remain more or less unchanged if  $k^+ = k_\perp^2/[2(q^- + k^-)]$ . For cases where  $k^+$  exceeds this value, the hard parton from the jet is taken further off-shell leading to an induced radiation.

Treating the case of momentum change of the hard parton due to induced radiation separately, we obtain three separate components of momentum being exchanged between the jet and the medium: two components of transverse momentum and one component of negative light-cone momentum. At every exchange there is a distribution in transverse and light-cone momentum being imparted between the jet and the medium. Given the large number of exchanges, we invoke the Gaussian approximation, i.e., we approximate these distributions to be Gaussian and consider only the mean and the variance. The

Gaussian approximation based on the central limit theorem is not completely unjustified. Each parton interacts multiple times with the medium and the shower distributions contain several hard partons. Along with this, one should also consider that except for the highest  $p_T$  (or highest energy) hadrons, each bin in hadron momentum (or momentum fraction) contains several events that need to be summed over.

Given cylindrical symmetry around the jet axis, one may further argue that the imparted  $k_{x\perp}^2 = k_{y\perp}^2$ , and the mean of the transverse momentum distribution is vanishing. Thus the first transport coefficient may be defined as the variance of the distribution of imparted transverse momentum per unit length traversed. This is referred to as  $\hat{q}$ ,

$$\hat{q} = \frac{|k_{x\perp}|_L^2 + |k_{y\perp}|_L^2}{L}. \quad (13)$$

Where  $|k_{x,y\perp}|_L^2$  is the total transverse momentum gained in traversing a length  $L$ . In the case of negative light-cone momentum exchange, the mean of the distribution yields the drag per unit length ( $\hat{e}$ ), whereas the variance is the fluctuation in light cone momentum transfer per unit length ( $\hat{e}_2$ ):

$$\hat{e} = \frac{k^-}{L}, \quad \text{and} \quad \hat{e}_2 = \frac{(\Delta k^-)^2}{L} \quad (14)$$

Given these two quantities, the Gaussian distribution of the negative light-cone momentum transfer is completely specified.

Thus the modification of hard jets will reveal at most these three quantities. Due to the large number of scatterings that need to be summed over in order to obtain measurements with small error bars, access to higher moments in these distributions is somewhat limited. These transport coefficients can in principle be calculated given a model of the medium, e.g., in the asymptotically high temperature limit, the system can be described in the weakly coupled quasi-particle picture afforded by leading order Hard Thermal Loop (HTL) effective theory. This derivation will be described in some detail in the remaining review. Even in this case, the value of the transport coefficients are unknown unless the value of the coupling is specified. The relevant coupling is the in-medium coupling between thermal quasi-particles which is *a priori* unknown and is therefore set by fitting calculations to at least one data point. It should be pointed out that if the medium is determined to not be weakly coupled, the HTL formulae cannot be applied and some other model will have to be used. The value of the transport coefficient, in principle, will have to be evolved up to the scale of the hard jet prior to use in a jet quenching calculation.

## 1.5 Other approaches and medium response observables

In this review, we will primarily address the question of how a hard jet can be used as a weakly coupled probe to study the properties of a dense QCD medium. As such we will solely be interested in how different properties of the medium, codified as a set of transport coefficients will modify the shower pattern of the jet. As the medium modifies the jet, the jet in turn modifies the medium. There is a growing consensus that part of the energy radiated by a jet is deposited in the medium and this modifies the evolution of the soft medium at that location [54, 55]. Given the ‘‘supersonic’’ velocity of the hard jet, this may lead to the production of a Mach Cone [56] which trails the hard jet and may be observable as an excess in the hadronic yield at a large angle to the associated away side jet in the final soft hadronic spectra that is associated with a hard jet trigger [57, 58].

While the response of a soft medium to a hard jet may not be completely calculable in pQCD, in recent years an alternate theory based on the Anti-DeSitter space Conformal Field Theory (AdS/CFT) conjecture [59] has been used to compute both the drag experienced by a heavy quark [60, 61] and the Mach cone left in a wake of of a hard jet [62, 63]. Unlike calculations based on pQCD, these

theories assume that the hard jet is strongly coupled with the dense medium. In the absence of a pQCD based picture it is not clear if the final hadronization process or the initial production process may be consistently factorized from the energy loss calculation. Both these topics of medium response of a hard jet and the alternate theories of energy loss based on the AdS/CFT conjecture will not be covered in this review.

## 2 Scattering induced single gluon radiation.

In order to compute the energy loss of hard jets and the medium modified fragmentation function, one needs to compute a series of multiple scattering and multiple emission diagrams. In all formalisms, the means to achieve this is to first compute the single gluon emission kernel due to multiple scattering. This is then iterated to include the effect of multiple emissions. The methodology of iteration is somewhat related to the approximations made in the underlying calculation of the single gluon emission kernel. In this chapter, we will describe this calculation in some detail. The iteration of the kernel will be dealt with in the next chapter. As stated in the introduction, our description of the single gluon emission kernel will follow that of the higher-twist approach. The differences with the other approaches will be pointed out at the end of this chapter.

We present the formalism in the Breit frame. In the case of DIS on a large nucleus this is characterized by the frame where the absolute magnitude of the (+) and (-) components of the photon momentum  $q$  and the large (+) component of the initial momentum  $p$  of the struck quark are equal:

$$q \equiv \left( -\frac{Q}{\sqrt{2}}, \frac{Q}{\sqrt{2}}, \mathbf{0} \right) \quad \text{and} \quad p^+ = x_B P^+ = \frac{Q}{\sqrt{2}}, \quad p^- \simeq |\vec{p}_\perp| \rightarrow 0. \quad (15)$$

$P^+$  is the momentum of a proton. The struck quark has a final (-) momentum  $\simeq q^- = Q/\sqrt{2}$  and travels in the negative  $z$  direction. It now scatters off the gluons in the nucleons which follow the struck nucleon. The picture is similar to that in Fig. 3.

We will present the calculations in negative light-cone gauge  $A^- = 0$ . This makes the discussion of gluons emitted collinear to the outgoing quark particularly simple. The first step is to quantify the magnitude of the different components of the gluons being exchanged between the outgoing quark and the incoming nucleons. The final outgoing quark has a negative light-cone momentum of  $q_f^- \sim Q$ . Being close to on-shell, it has a virtuality  $q_f^2 \sim \lambda^2 Q^2$ , which is built up from some combination of a  $q_f^+ \sim \lambda^2 Q$  and a small transverse momentum  $q_{f\perp} \sim \lambda Q$ .

### 2.1 DIS on a proton and vacuum radiation

To familiarize the reader with the notation, we compute the simple process of vacuum gluon radiation from a quark struck by a hard photon. This constitutes the primary contribution to the scale evolution of fragmentation functions in vacuum. With this process we will also demonstrate an elementary example of factorization at leading order, where we factorize the parton distribution function (PDF) from the hard cross section. The basic quantity to be computed is the differential cross section for an electron with an initial momentum  $L_1$  to scatter off a proton (with momentum  $P^+$ ) with final electron momentum  $L_2$  and producing an outgoing quark with momentum  $l_q = [|l_{q\perp}|^2/\{2q^-(1-y)\}, q^-(1-y), l_{q\perp}]$  and a gluon with momentum  $l = [|l_\perp|^2/(2q^-y), q^-y, l_\perp]$ :

$$\mathcal{L}(L_1) + p(P^+) \longrightarrow \mathcal{L}(L_2) + Q(l_{q\perp}) + G(l_\perp) + X. \quad (16)$$

The complete cross section for the process is represented by Fig. 4. The rectangular blob at the bottom of the diagram represents the contents of the proton after the hard quark  $q$  is struck by the photon and removed from the proton.

The matrix element that needs to be evaluated may be represented as

$$\mathcal{M} = \langle X, l, l_q; L_2 | \mathcal{T} \exp \left[ -i \int_{-\infty}^{\infty} dt H_I(t) \right] | P; L_1 \rangle. \quad (17)$$

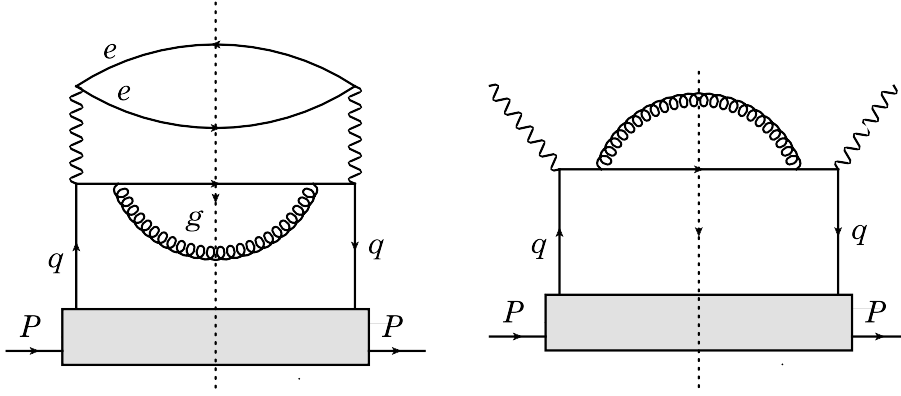


Figure 4: DIS on a nucleon leading to the formation of a quark and a radiated gluon. Left panel represents the complete diagram whereas the right panel represents the hadronic tensor. The dangling photon lines do not represent photon propagators, but rather the scattering of the quark off a photon. The photon propagator is not contained in the hadronic tensor, see text for details.

The state  $|X\rangle$  represents an arbitrary hadronic state. For the case of interest,  $|L_2, l, l_q, X\rangle$  represents a state with at least a quark and a gluon endowed with the requisite momenta and an outgoing electron with momentum  $L_2$ . At lowest order  $|X\rangle$  is simply the vacuum state. In the equation above,  $H_I(t)$  represents the interaction Hamiltonian in the interaction picture for QCD and QED. The eventual evaluation of the exponent will involve two orders of the electro-magnetic (EM) interaction and all orders of the strong interaction. For the case of one gluon emission in this section we will only have to expand the exponent to one order of the strong interaction (and two orders of the EM interaction) i.e.,

$$\begin{aligned} \mathcal{M} &= \langle X, l, l_q; L_2 | \frac{1}{3!} \int_{-\infty}^{\infty} d^4 y_e \bar{\psi}_e(y_e) e \gamma^\mu A_\mu(y_e) \psi_e(y_e) \int_{-\infty}^{\infty} d^4 y_0 \bar{\psi}(y_0) e \gamma^\mu A_\mu(y_0) \psi(y_0) \\ &\times \int d^4 y_1 \bar{\psi}(y_1) g \gamma^\nu t^a A_\nu^a(y_1) \psi(y_1) | P; L_1 \rangle. \end{aligned} \quad (18)$$

In the equation above,  $\psi_e$  is the wave function of the lepton, while  $\psi$  is that for a quark. The restriction to only two orders of the EM interaction, constrains the calculation to the one photon approximation. Squaring the matrix element one may calculate the cross section for this process. It may be straightforwardly demonstrated, in the one photon limit, that the process can be decomposed into a purely leptonic part and a partonic (or hadronic) part connected by a single photon propagator. The leptonic part will involve the trace over the Dirac matrix structure of the electron momenta; we will simply write this down without proof. The hadronic part will be somewhat more complicated as it will contain both a perturbative component describing the scattering of a quark off the virtual photon followed by the emission of a hard gluon and a non-perturbative component which describes the probability to find a quark with a particular momentum fraction in the incoming nucleon. This component will be described in some detail.

The quadruple differential cross section for the process in Eq. (16), in terms of  $L_2, l_\perp, l_{q\perp}, y$  can be decomposed, as stated above, into a purely leptonic part and a hadronic part in the one photon exchange approximation. This is symbolically represented as,

$$\frac{E_{L_2} d\sigma}{d^3 L_2 d^2 l_{q\perp} d^2 l_\perp dy} = \frac{\alpha_{em}^2}{2\pi s Q^4} L^{\alpha\beta} g_{\alpha\mu} g_{\beta\nu} \frac{dW^{\mu\nu}}{d^2 l_{q\perp} d^2 l_\perp dy}, \quad (19)$$

where  $L^{\alpha\beta}$  and  $W^{\mu\nu}$  are the leptonic and hadronic tensors respectively. The Mandelstam variable

$s = (p + L_1)^2$ . Each of the factors of  $g_{\alpha\mu}/Q^2$  and  $g_{\beta\nu}/Q^2$  represents a photon propagator, one from the amplitude and one from the complex conjugate.

The leptonic tensor has the straightforward definition,  $L^{\alpha\beta} = \mathbf{Tr}[\mathcal{L}_1\gamma^\alpha \mathcal{L}_2\gamma^\beta]/2$ , while the hadronic tensor, at leading order in the strong coupling, may be decomposed as

$$W_1^{\mu\nu} = \int d^4y_0 \langle P | \bar{\psi}(y_0) \gamma^\mu \widehat{\mathcal{O}}^{00} \gamma^\nu \psi(0) | P \rangle = \int d^4y_0 \mathbf{Tr} \left[ \frac{\gamma^-}{2} \gamma^\mu \frac{\gamma^+}{2} \gamma^\nu \right] F(y_0) \mathcal{O}^{00}(y_0). \quad (20)$$

This expression requires some explanation. The interaction terms in  $H_I$  are those contained in the QCD [Eq. (1)] and QED Lagrangians. These are composed of solely quarks, gluons, leptons and photons. While we have, somewhat artificially, constrained the final state to be a quark and a gluon, the initial state is a proton. In the Breit frame, the high energy proton can be approximated as a weakly interacting gas of collinear quarks and gluons. The distribution of these partons in bins of light-cone momentum fraction  $x$  depends on the transverse size of these partons (i.e., resolution of the probe). In this high energy limit, the projection of the product of  $\psi|X\rangle$  and its complex conjugate ( $\langle X|\bar{\psi}$ ) along the large momentum direction may be viewed as an annihilation and creation of a near on-shell quark in the proton's wave function. The Fourier transformation of the expectation of this operator product is referred to as the parton distribution function (PDF),

$$f(x) = \int dy_0^- e^{-ixP^+y_0^-} F(y_0^-) = \int dy_0^- e^{-ixP^+y_0^-} \langle P | \bar{\psi}(y_0^-, 0) \frac{\gamma^+}{2} \psi(0, 0) | P \rangle. \quad (21)$$

Unlike the parton distribution function in Eq. (21) above, the function  $F(y_0^0)$  that appears in Eq. (20) is not yet on the light-cone. Note that in the equation above only  $y_0^-$  appears. This happens after the invocation of the high energy or collinear approximation. The incoming parton is assumed to be endowed with very high forward momentum ( $p_0^+ = x_0 p^+, p_0^- \rightarrow 0$ ) with negligible transverse momentum  $p_{0\perp} \ll p_0^+$ . Within the kinematics chosen, the incoming virtual photon also has no transverse momentum. As a result, the produced final state parton also has a vanishingly small transverse momentum (i.e., with a distribution that may be approximated as  $\delta^2(\vec{p}_\perp)$  up to corrections suppressed by powers of the hard scale). In this limit, the leading spin projection of the pieces which represent the initial state and final state may be taken. The factors,

$$\gamma^+ = \frac{\gamma^0 + \gamma^3}{\sqrt{2}} ; \quad \gamma^- = \frac{\gamma^0 - \gamma^3}{\sqrt{2}}, \quad (22)$$

are used to obtain the spin projections along the leading momenta of the outgoing state and the incoming state. See Refs. [34, 64] for precise details of how this is done.

The other function in Eq. (20) is  $\mathcal{O}^{00}$  which represents the physics of the final state after the hard scattering with the photon. The superscript on the operator  $\mathcal{O}^{00}$  implies that the quark undergoes no scattering in the final state. Taking the leading projection in Dirac matrix structure we obtain

$$\begin{aligned} \mathcal{O}^{00} &= \mathbf{Tr} \left[ \frac{\gamma^-}{2} \widehat{\mathcal{O}}^{00} \right] = \int \frac{d^4l}{(2\pi)^4} d^4z d^4z' \frac{d^4l_q}{(2\pi)^4} \frac{d^4p_0}{(2\pi)^4} \frac{d^4p'_0}{(2\pi)^4} e^{iq \cdot y_0} e^{-i(p_0+q) \cdot (y_0-z)} e^{-il \cdot (z-z')} e^{-il_q \cdot (z-z')} e^{-i(p'_0+q) \cdot z} \\ &\times g^2 \mathbf{Tr} \left[ \frac{\gamma^-}{2} \frac{-i(\not{p}_0 + \not{q})}{(p_0+q)^2 - i\epsilon} i\gamma^\alpha \not{v}_q 2\pi\delta(l_q^2) G_{\alpha\beta}(l) 2\pi\delta(l^2) (-i\gamma^\beta) \frac{i(\not{p}'_0 + \not{q})}{(p'_0+q)^2 + i\epsilon} \right] \mathbf{Tr}[t^a t^b]. \end{aligned} \quad (23)$$

In the equation above,  $G_{\alpha\beta}(l)$  is the sum over the product of polarization vectors of the radiated gluon with momentum  $l$ . In light cone gauge  $A \cdot n = A^- = 0$  (with  $n = (1, 0, 0, 0)$ ) this is given as,

$$G_{\alpha\beta}(l) = -g_{\alpha\beta} + \frac{l_\alpha n_\beta + l_\beta n_\alpha}{l \cdot n}. \quad (24)$$



To evaluate the above Feynman integral one integrates over the internal locations  $z, z'$ , which will yield the momentum conserving delta functions. This will set  $p_0 = p'_0$ . Then one approximates the numerators of the fermion propagators as  $\gamma^+ q^-$ . The denominators may be expressed as  $2P^+ q^-(x_0 - x_B \pm i\epsilon)$  where  $x_0 = p^+/P^+$ . The  $\delta(l^2)$  sets  $l^+ = l_\perp^2/2l^-$ . The other  $\delta$ -function over  $l_{q\perp}$  sets  $x_0 = x_B + x_L$  where  $x_L = l_\perp^2/[2P^+ q^- y(1-y)]$ . The remaining steps involve carrying out the simplifications associated with the  $\gamma$  matrices and carrying out the integrations over the momenta that do not appear in the integrand. This yields

$$\mathcal{O}^{00} = \delta(y_0^+) \delta^2(y_{0\perp}) e^{-i(x_B + x_L)p^+ y_0^-} \frac{\alpha_s C_F}{2\pi} \int \frac{dy dl_\perp^2}{l_\perp^2} \frac{2 - 2y + y^2}{y}. \quad (25)$$

The resulting phase factors constrain  $F(y^0)$  to the light cone and convert it into the PDF. The factor  $(2 - 2y + y^2)/y$  is the splitting function  $P(y)$  which expresses the probability for the hard quark to radiate a gluon. Re-incorporating this expression back into Eq. (20), we obtain the differential hadronic tensor for a quark in a proton, struck by a hard virtual photon, to radiate a gluon with momentum  $[q^- y, l_\perp]$  and itself have a momentum  $[q^-(1-y), l_{q\perp}]$ :

$$\frac{dW_1^{\mu\nu}}{dy dl_\perp^2 d^2 l_{q\perp}} = \sum_q 2\pi Q_q^2 f_q(x_B + x_L) \frac{\alpha_s C_F}{2\pi l_\perp^2} P(y) \delta^2(\vec{l}_{q\perp} + \vec{l}_\perp). \quad (26)$$

The above result should be compared with the simpler result of DIS without any radiation in the final state. The derivation is similar to that presented for the case of a produced radiation, we here simply state the result (referring the interested reader to Ref. [33]). The differential hadronic tensor for a quark in a proton, struck by a hard photon, to have a momentum  $[q^-, l_{q\perp}]$  is

$$\frac{dW_0^{\mu\nu}}{d^2 l_{q\perp}} = \sum_q 2\pi Q_q^2 f_q(x_B) \delta^2(\vec{l}_{q\perp}). \quad (27)$$

In the equation above,  $f_q(x)$  is the quark PDF defined in Eq. (21). Note that the arguments  $x$  in Eqs.(26,27) are slightly different. They differ by the quantity  $x_L = l_\perp^2/[2P^+ q^- y(1-y)]$ . This should be understood as the ratio of the off-shellness of the outgoing quark to  $Q^2/x_B = s$ , i.e.,

$$x_L s = \frac{x_L}{x_B} Q^2 = x_L 2P^+ q^- = \frac{l_\perp^2}{y(1-y)} = 2(l_q^+ + l^+)(l_q^- + l^-) - \left| \vec{l}_\perp + \vec{l}_{q\perp} \right|^2. \quad (28)$$

The momentum component  $p^+ = x_L P^+$  is the extra (+)-component of the momentum that must be brought in by the incoming quark such that the quark after being struck should be off-shell enough to radiate the gluon with momentum  $[l_\perp^2/(2q^- y), q^- y, \vec{l}_\perp]$ . We work in the limit where a collinear jet is produced in the hard interaction, so that the off-shellness is very small compared to the hard scale  $Q^2$ :

$$x_L 2P^+ q^- = \frac{l_\perp^2}{2P^+ q^-} \ll Q^2 = x_B 2P^+ q^- \implies x_L \ll x_B. \quad (29)$$

As mentioned in the introduction, this ratio of the off-shellness of the produced quark to  $Q^2$  is used to qualify the small parameter  $\lambda$ , i.e.,  $l_\perp \sim \lambda Q$ . In this limit of transverse momenta,  $x_L = \lambda^2 x_B (\lambda x_B)$  if  $y \sim 1(\lambda)$ . In either case, this small correction to  $x_B$  in Eq. (26) can be neglected.

In both equations (26,27), the distribution of the final outgoing quark involves a  $\delta$ -function. This is meant to be a simplification. A better expression is to use a narrow, normalized Gaussian distribution. The width is of order  $\sim \lambda Q$ , i.e., small compared to the hard scale but still perturbatively large. The width of this outgoing quark distribution is related to the transverse momentum and off-shellness of the incoming quark; this controls the virtuality of outgoing quark and thus the virtualities involved in

all final state processes. This also controls the scale at which the coupling constant is evaluated in the case of final state gluon emissions.

In the limit of small  $x_L$ , the ratio of the cross sections for both processes, computed using Eq. (19), assumes a rather simple form. Integrating out the transverse momentum of the produced quark gives the differential number of gluons radiated,

$$\frac{dN_g}{dydl_{\perp}^2} = \frac{1}{\sigma_{[q+\gamma\rightarrow q+g+X]}} \frac{d\sigma_{[q+\gamma\rightarrow q+g+X]}}{dydl_{\perp}^2} = \frac{\alpha_s(l_{\perp}^2)C_F}{2\pi l_{\perp}^2} P(y). \quad (30)$$

In the subsequent section, we will derive the cross section for a hard quark to radiate a single gluon while undergoing multiple scattering in the medium. This will involve modifying a related version of Eqs. (26,27,30).

We close with a comment regarding Eq. (30). The reader will note that the expression for the differential number of gluons in  $y, l_{\perp}$  possesses both an infra-red  $y \rightarrow 0$  [ $P(y) \rightarrow 2/y$  as  $y \rightarrow 0$ ] and a collinear singularity  $l_{\perp} \rightarrow 0$ . The infrared singularity is cancelled by virtual diagrams which convert the splitting function into the well known (+)-functions [18]. The collinear divergence remains and makes even the differential number of gluons radiated from a struck quark  $\frac{dN_g}{dy} \rightarrow \infty$ . The source of this divergence are gluons with  $l_{\perp} \rightarrow 0$ , and thus those with formation times  $\tau_f \rightarrow \infty$ . In a factorized approach such long distance effects are absorbed into a renormalization of the final fragmentation function to produce hadrons  $D$ . In the case of single hadron inclusive DIS, absorbing gluons with transverse momenta up to the final factorization scale  $l_{\perp} = \mu \ll Q$  yields the scale dependent fragmentation function to produce a hadron with momentum fraction  $z = p_h/q^-$ . Including the effect of multiple emissions yields the DGLAP evolution equation for the fragmentation function:

$$\frac{\partial D(z, \mu^2)}{\partial \log(\mu^2)} = \frac{\alpha_s C_F}{2\pi} \int_z^1 \frac{dy}{y} P(y) D\left(\frac{z}{y}, \mu^2\right). \quad (31)$$

In the in-medium version of Eq. (30), Landau-Pomeranchuk-Migdal (LPM) interference tends to cancel the collinear divergence making the differential yield of gluons finite at  $l_{\perp} \rightarrow 0$ . As a result, one obtains a finite energy of gluons emitted on integrating over  $l_{\perp}$ . Two of the formalisms use this value to construct an iterative formalism, thus ignoring the fact that a fraction of the number of gluons are produced much later in time and should not be included in the calculation. This will be further discussed in Chapter 3.

## 2.2 Multiple scattering induced single gluon radiation

In this section, we compute the cross section for single gluon emission induced by multiple scattering. Iterating this process and convoluting with the fragmentation function will produce the medium modified fragmentation function. We will approximate each scattering to only transfer a small transverse momentum  $k_{\perp} \sim \lambda Q$  and a (+)-component  $\sim \lambda^2 Q$  between the jet and the medium partons. There can also be an exchange of a small (-)-component; this leads to elastic energy loss and will be discussed separately in Chapter 4.

### 2.2.1 Multiple scattering without gluon radiation

We begin by considering the case of a hard quark produced in a DIS on a large nucleus, which produces a hard quark propagating through the nucleus encountering multiple scattering without radiation. The virtual photon strikes a hard quark in one of the nucleons and turns it back towards

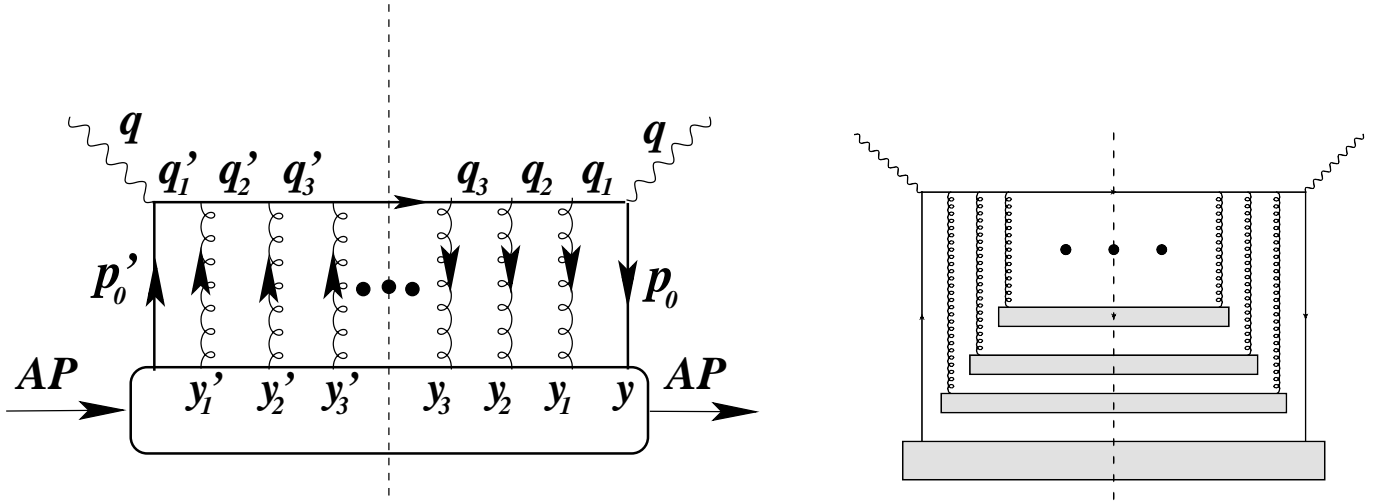


Figure 5: Left panel: DIS on a nucleus leading to the formation of a quark jet which is constrained to propagate through the nucleus without radiating. Its only interactions are scatterings. Right panel: The dominant length enhancement arises from nested scattering diagrams, where the blobs represent individual nucleons, see text for details.

the nucleus. The quark then propagates through the nucleus without radiating. In this process the hard quark scatters  $n$  times in the amplitude and in the complex conjugate. This is represented by the diagram in the left panel of Fig. 5. The diagram represents a quark in one of the incoming nucleons with momentum  $p'_0$ , being struck with the photon with momentum  $q = [-x_B P^+, q^-, 0, 0]$ . The outgoing quark has momentum  $q'_1 = p'_0 + q$ . After encountering the  $j^{\text{th}}$  scattering, its momentum is  $q'_{j+1} = p_0 + q + \sum_{i=1}^j k'_i$ .

In the case of the higher-twist scheme, these gluon lines represent the gluon field at the point at which scattering takes place. Thus there is no meaning to crossing of gluon lines. The sources of the gluon lines are the nucleons in the nucleus (or rather the partons within these nucleons). The only assumption made regarding the gluon momenta are simple scaling relations regarding the momentum of the exchanged gluons and the magnitude of the corresponding components of the vector potentials. This is somewhat different in the other schemes. Under the assumption that the gluons transfer a transverse momentum of  $k_\perp \sim \lambda Q$ , and the incoming and outgoing quark lines remain close to on-shell, the  $k^+$  component is constrained with the leading contribution given by the equation,

$$(q + k)^2 = 2q^- k^+ - k_\perp^2 = 0 \implies k^+ = \frac{k_\perp^2}{2q^-} \sim \lambda^2 Q. \quad (32)$$

Ascribing the same criteria to the hard quark or gluon in the nucleons from which the exchanged gluon originates, implies that  $k^- \simeq k_\perp^2/2p^+$  (where  $p^+$  here is the momentum of some hard parton) also scales as  $\sim \lambda^2 Q$ . Exchanged gluons with transverse momenta much larger than their longitudinal components are referred to as Glauber gluons or Coulomb gluons. If the (+)-component were to become larger than  $k_\perp^2/2q^-$ , it would drive the jet parton to go off-shell and radiate a hard gluon. If the  $k^-$  component were to become larger, this will lead to energy loss from the jet parton but the parton in the nucleon will then go off shell and may radiate. As jet quenching measurements do not concern themselves with the fate of the target, the latter sort of momentum transfer is often referred to as elastic energy loss for the jet.

Given these approximations we may now compute the scaling of the different components of the gauge field. To remind the reader we are calculating in the Breit frame where the hard quark moves in

the  $-z$  direction with a large light cone momentum  $q^- \sim Q$  and the valence quarks inside the nucleon are moving in the  $+z$  direction with a large  $p^+ \sim Q$ . We use the linear response formula to ascertain the power counting of the  $A^+$  field. Suppressing the color superscripts we obtain,

$$A^\mu(x_1) = \int d^4 y_1 \mathcal{D}^{\mu\nu}(x_1 - y_1) J_\nu(y_1). \quad (33)$$

In the equation above,  $\mathcal{D}$  is the gluon propagator and at leading order in the light cone gauge  $A^- = 0$  is given as,

$$\mathcal{D}^{\mu\nu}(x_1 - y_1) = \int \frac{d^4 k}{(2\pi)^4} \frac{i \left( -g^{\mu\nu} + \frac{k^\mu n^\nu + k^\nu n^\mu}{k \cdot n} \right) e^{-ik \cdot (x_1 - y_1)}}{k^2 + i\epsilon}. \quad (34)$$

In Eq. (33),  $J^\nu(y_1) = \bar{\psi}(y_1) \gamma^\nu \psi(y_1)$  is the current of partons in the target which generates the gluon field. The fermionic operator may be decomposed as,

$$\psi(y_1) = \int \frac{dp^+ d^2 p_\perp}{(2\pi)^3 \sqrt{p^+ + \frac{p_\perp^2}{2p^+}}} \sum_s u^s(p) a_p^s e^{-ip \cdot y_1} + \dots \quad (35)$$

The scaling of the fermionic operator depends on the range of momentum which are selected from the in-state by the annihilation operator. Note that this influences both the scaling of the annihilation operator  $a_p$  as well as the bispinor  $u(p)$ . The power counting of the annihilation operator may be surmised from the standard anti-commutation relation,  $\{a_p^r, a_{p'}^s\} = (2\pi)^3 \delta^3(\vec{p} - \vec{p}') \delta^{rs}$ . The power counting of the bispinor can be obtained from the completeness relation,  $\sum_s u_p^s \bar{u}_p^s = \not{p} = \gamma^- p^+ + \gamma^+ p^- - \gamma_\perp \cdot p_\perp$ . Substituting the equation for the current in Eq. (33), and integrating out  $y$ , we obtain,

$$A^+ \simeq \int \frac{d^3 p d^3 q}{(2\pi)^6 \sqrt{p^+} \sqrt{q^+}} \frac{i \left( -g^{+-} + \frac{n^+(p^- - q^-)}{(p^- - q^-)} \right) e^{-i(p-q) \cdot x_1}}{(p-q)^2} a_q^\dagger a_p \bar{u}(q) \gamma^+ u(p). \quad (36)$$

If the incoming and outgoing momenta  $p$  and  $q$  scale as collinear momenta in the (+)-direction, i.e.,  $p \sim Q(1, \lambda^2, \lambda)$ , then we get,  $\delta^3(\vec{p} - \vec{p}') \sim [\lambda^2 Q^3]^{-1}$ , as one of the momenta will involve the large (+)-component and the remaining are the small transverse components. Thus the annihilation (and creation) operator scales as  $\lambda^{-1} Q^{-3/2}$ . Also in the spin sum  $\not{p} \sim Q$  and thus  $u(p) \sim u(q) \sim Q^{1/2}$ ; one can check that the  $\gamma^+$  projects out the large components in  $u$  and  $\bar{u}$  in the expression  $\bar{u}(q) \gamma^+ u(p)$ . We also institute the Glauber condition that  $p^+ - q^+ \sim \lambda^2 Q$ ,  $p^- - q^- \sim \lambda^2 Q$  and  $p_\perp - q_\perp \sim \lambda Q$ .

Using these scaling relations we correctly find that the bispinor scales as  $\lambda Q^{3/2}$ . However, to obtain the correct scaling of the gauge field  $A^+$  one needs to institute the approximation that  $q^+ = p^+ + k^+$  where  $k^+ \sim \lambda^2 Q$ . This condition is introduced by insisting that the (+) momentum of the incoming and outgoing state, which control the scaling of  $a_q^\dagger$  and  $a_p$ , are separated by  $k^+ \sim \lambda^2 Q$ . This is used to shift the  $dq^+ \rightarrow dk^+$  and as a result we obtain the scaling of the  $A^+$  field as  $\lambda^2 Q$ . Following a similar derivation, with the replacement  $\gamma^+ \rightarrow \gamma_\perp$  we obtain the scaling of the  $A_\perp \sim \lambda^3 Q$ . Thus in the Breit frame and  $A^- = 0$  gauge, the  $A^+$  field is dominant over the  $A_\perp$  components which may be neglected.

The evaluation of the right panel of Fig. 5 is straightforward within the approximations outlined above. The numerator of every propagator is replaced with  $\gamma^+ q^-$  and every vertex with  $\gamma^- A^+$ . The denominators are simplified by contour integration, e.g., for the simple case of the first propagator, we would get,

$$\int \frac{dk_1^+}{2\pi} \frac{e^{-ik_1^+(x_1^- - x_0^-)}}{(q^- + k_1^+)^2} \simeq \int \frac{dk_1^+}{2\pi} \frac{e^{-ik_1^+(x_1^- - x_0^-)}}{q^- k_1^+ - (k_1^+)^2 + i\epsilon} = -i\theta(x_1^- - x_0^-) e^{-i \frac{|k_1^+|^2}{2q^-} (x_1^- - x_0^-)}. \quad (37)$$

Thus carrying out the contour integrations, simply orders the locations of the scatterings and sets the (+) components of the momentum to be  $k_{\perp}^2/2q^-$ . Carrying out these integrations on both sides of the cut we obtain an expression which is a modification of Eq. (27),

$$\begin{aligned}
\frac{dW^{\mu\nu}}{dl_{q\perp}^2} &= \frac{-g_{\perp}^{\mu\nu} g^{n+n'}}{(2\pi)^2} \int \prod_{i=0}^n dy_i^- d^2 y_{\perp}^i \prod_{j=1}^{n'} dy_j'^- d^2 y_{\perp}^j \int \prod_{i=0}^n \frac{d^2 p_{\perp}^i}{(2\pi)^2} \prod_{j=0}^{n'-1} \frac{d^2 p_{\perp}^j}{(2\pi)^2} (2\pi)^2 \delta^2(\vec{l}_{q\perp} - \sum_i \vec{k}_{\perp}^i) \\
&\times e^{-ix_B P^+ y^-} \prod_{i=0}^n e^{-ix_D^i P^+ y_i^-} e^{ip_{\perp}^i \cdot y_{\perp}^i} \prod_{j=0}^{n'} e^{ix_D^j P^+ y_j'^-} e^{-ip_{\perp}^j \cdot y_{\perp}^j} \prod_{i=n}^1 \theta(y_i^- - y_{i-1}^-) \prod_{j=n'}^1 \theta(y_j'^- - y_{j-1}'^-) \\
&\times \langle A; p | \bar{\psi}(y^-, y_{\perp}) \frac{\gamma^+}{2} \psi(0) \mathbf{Tr} \left[ \prod_{i=1}^n t^{a_i} A_{a_i}^+(y_i^-, y_{\perp}^i) \prod_{j=n'}^1 t^{a_j} A_{a_j}^+(y_j'^-, y_{\perp}^j) \right] | A; p \rangle. \quad (38)
\end{aligned}$$

In the equation above, we use the short hand  $x_D^i = \left[ \sum_{k=0}^i 2p_{\perp}^k \cdot p_{\perp}^k + |p_{\perp}^i|^2 \right] / 2P^+ q^-$  to save writing, and similarly for the complex conjugate.

Further evaluation requires two sets of approximations. The first arises from the large length limit of a large nucleus. Each of the  $dy_i^-$  or  $dy_j'^-$  integrals may be extended up to the light-cone length of the nucleus  $L^-$ . The largest factor of  $L^-$  is obtained in the limit that the gluon operators  $A^+(y_i)$  are distributed over the largest number of nucleons. The color singlet nature of nucleons requires that the extraction of a gluon in the amplitude from a particular nucleon be matched by an identical gluon being extracted from the same nucleon in the complex conjugate. This along with the strong ordering of positions of the scatterings restricts the calculation to the set of nested scattering diagrams where the locations  $y_i$  and  $y_j'$  are within the same nucleon. These diagrams are represented by the right panel of Fig. 5. Diagrams with more gluons per nucleon have smaller length enhancement factors, this is the reason that pomeron like exchanges which include at least four gluons per nucleon are suppressed in the large nucleus limit. Since the transverse size of a nucleon is much larger than the inverse transverse momentum carried by either exchanged gluon, one may integrate over the mean transverse location of the two insertions. This equates the transverse momentum that is exchanged between the jet and the nucleon, in the amplitude and the complex conjugate. For the  $i^{\text{th}}$  scattering, this may be expressed as

$$\begin{aligned}
&\int dy_i^- dy_j'^- d^2 y_{\perp}^i d^2 y_{\perp}^j \langle p | A^+(\vec{y}_{\perp}^i) A^+(\vec{y}_{\perp}^j) | p \rangle e^{-ix_D^i P^+ y_i^-} e^{ip_{\perp}^i \cdot y_{\perp}^i} e^{ix_D^j P^+ y_j'^-} e^{-ip_{\perp}^j \cdot y_{\perp}^j} \\
&= (2\pi)^2 \delta^2(\vec{p}_{\perp}^i - \vec{p}_{\perp}^j) \int d^2 y_{\perp} e^{-ix_D^i P^+ (y_i^- - y_j'^-)} \times e^{ip_{\perp} \cdot y_{\perp}} \langle p | A^+(\vec{y}_{\perp}/2) A^+(-\vec{y}_{\perp}/2) | p \rangle. \quad (39)
\end{aligned}$$

Given this pairing of interactions, the largest length enhancement that may be obtained is  $L^n$  for  $n$  scatterings in the amplitude and complex conjugate.

The other approximation is that the scatterings transfer small amounts of transverse momentum compared to the transverse momentum of the original quark, though both are at the same scale  $\lambda Q$ . The possibility of scattering over  $n$  nucleons, greatly enhances the transverse momentum exchanged between the jet and the medium. Thus the transverse momenta from these scatterings cannot be ignored. However, since each is small compared to the transverse momentum of the jet, we may Taylor expand in them. In the case of spin independent cross sections, the leading term in the Taylor expansion is the second derivative of the  $\delta$ -function in terms of each of the small momenta  $k_{\perp}^i$ :

$$\delta^2(\vec{l}_{q\perp} - \sum_i \vec{k}_{\perp}^i) \simeq \prod_{i=1}^n \frac{(k_{\perp}^i \cdot \nabla_{l_{q\perp}})^2}{2} \delta^2(\vec{l}_{q\perp}) \quad (40)$$

The two factors of  $k_{\perp}^i$  can be combined with the two gluon vector potentials in Eq. (39) to convert them into the correlator of field strengths  $\langle p | F^{+\perp}(y_i^-) F_{\perp}^+(y_j'^-) | p \rangle$ . Higher transverse momentum derivatives

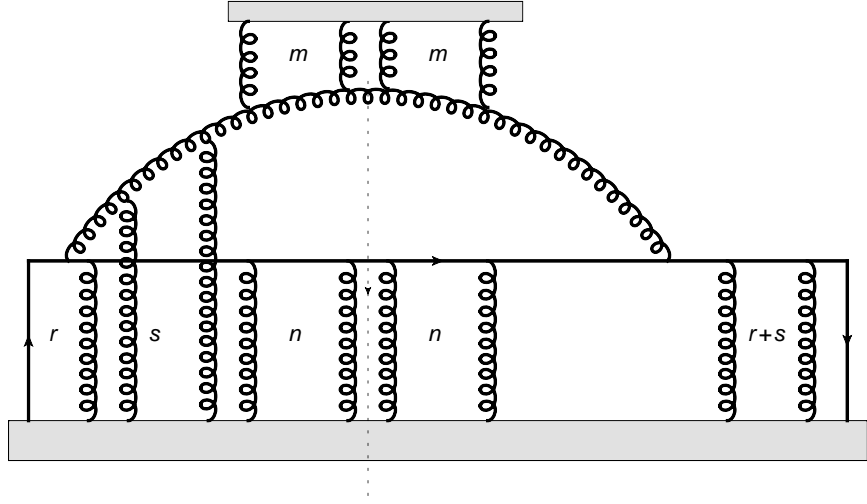


Figure 6: DIS on a nucleus leading to the formation of a quark jet with a radiated gluon.

will involve more factors of  $k_{\perp}$  which may be converted through by-parts integration into derivatives of the field strength. Thus these are further suppressed without any extra length integration to enhance them. Thus we stop at just the double derivative in the Taylor expansion of the  $\delta$ -function in terms of the transverse momentum.

Incorporating these approximations, one obtains the differential hadronic tensor as,

$$\frac{d^2 W_n^{\mu\nu}}{d^2 l_{\perp}} = W_0^{\mu\nu} \frac{1}{n!} \left[ \{ \nabla_{l_{\perp}}^2 \}^n \delta^2(\vec{l}_{\perp}) \right] \left[ \frac{\pi^2 \alpha_s}{N_c} L^- \int \frac{dy^-}{2\pi} \frac{d^2 y_{\perp}}{(2\pi)^2} e^{-i \left( \frac{k_{\perp}^2}{2q^-} + k_{\perp} \cdot y_{\perp} \right)} \langle p | F^{a+\alpha}(y^-, y_{\perp}) F^{a-}_{\alpha} | p \rangle \right]^n. \quad (41)$$

The latter quantity in square brackets is referred to as  $D$ . This series may be resummed by noting that  $\phi(l_{q\perp}) = dW^{\mu\nu}/d^2 l_{q\perp}$  obeys the diffusion equation,

$$\frac{\partial \phi}{\partial L^-} = D \nabla_{l_{q\perp}}^2 \phi, \quad (42)$$

which has a normalized solution given as

$$\phi(L^-, \vec{l}_{q\perp}) = \frac{1}{4\pi D L^-} \exp \left\{ -\frac{l_{q\perp}^2}{4 D L^-} \right\}. \quad (43)$$

The transverse momentum squared gained by a parton as it traverses a length  $L^-$  is given as  $|l_{q\perp}|_{L^-}^2 = 4 D L^- = \hat{q} L^-$ . Thus the jet quenching transport coefficient  $\hat{q} = 4 D$ .

### 2.2.2 Multiple scattering of quark and radiated gluon

With the derivation of the single gluon emission cross section and the multiple scattering cross section for a single quark without radiation, we can surmise the form of the multiple scattering single gluon emission cross section. Consider the general process depicted in Fig. 6. A quark is produced in the DIS on a large nucleus at location  $y_0$ . We consider the process where, in the amplitude, this quark will radiate a gluon without a re-scattering before the vertex at which the hard gluon is radiated. The produced quark and gluon will then scatter  $r$  and  $s$  times, respectively, on the incoming nucleons. The first location where the gluon scatters will be denoted as  $\zeta_C$ . The first location where the quark scatters

will be denoted as  $y_C$ . There will be additional scatterings but the  $q = r + s$  scatterings are special as they represent the interference contributions. On the complex conjugate side, the produced quark will itself scatter  $r + s = q$  times on the same nucleons and then radiate the gluon. The location of the last such scattering which occurs on the parent quark in the complex conjugate and on either the produced quark or radiated gluon in the amplitude will be denoted as  $y_E$ . Thus the radiated gluon is produced at two separate points: it is just after  $y_0^-$  in the amplitude and just after  $y_E^-$  in the complex conjugate. After this cross scattering, the gluon will scatter  $m$  times and the quark  $n$  times in both the amplitude and the complex conjugate. The location of the first independent scattering on the gluon is at location  $\zeta_I^-$  and that on the quark at location  $y_I^-$ .

The Feynman integral for this process may be expressed as (see Ref. [34] for a detailed derivation of this equation),

$$\begin{aligned}
\mathcal{O} = & \int \frac{dy d^2 l_\perp d^2 l_{q\perp}}{2\pi^2} \frac{\alpha_s C_F P(y)}{y} C_A^m C_F^n (C_F - C_A/2)^r (C_A/2)^s \delta^2 \left( l_{q\perp} - \sum_{i=1}^s k_\perp^i - \sum_{j=1}^r p_\perp^j - \sum_{l=1}^m k_\perp^l - \sum_{k=1}^n p_\perp^k \right) \\
& \times \frac{l_\perp - \sum_{i=1}^s k_\perp^i - \sum_{l=1}^m k_\perp^l}{\left( l_\perp - \sum_{i=1}^s k_\perp^i - \sum_{l=1}^m k_\perp^l \right)^2} \cdot \frac{l_\perp - y \sum_{i=1}^{r+s} k_\perp^i - \sum_{l=1}^m k_\perp^l}{\left( l_\perp - y \sum_{i=1}^s k_\perp^i - \sum_{l=1}^m k_\perp^l \right)^2} \\
& \times \prod_{i=1}^q \int dy_i^- \frac{\int d^3 \delta y_i \rho \langle p | A^+(y_i^- + \delta y_i^-, 0) A^+(y_i^-, -\delta y_\perp^i) | p \rangle}{2p^+(N_c^2 - 1)} e^{ik_\perp^i \delta y_\perp^i} \\
& \times \prod_{j=1}^n \int dy_j^- \frac{\int d^3 \delta y_j \rho \langle p | A^+(y_j^- + \delta y_j^-, 0) A^+(y_j^-, -\delta y_\perp^j) | p \rangle}{2p^+(N_c^2 - 1)} e^{ik_\perp^j \delta y_\perp^j} \\
& \times \prod_{l=1}^m \int d\zeta_l^- \frac{\int d^3 \delta \zeta_l \langle p | A^+(\zeta_l^- + \delta \zeta_l^-, 0) A^+(\zeta_l^-, -\delta \zeta_\perp^l) | p \rangle}{(N_c^2 - 1)} e^{ik_\perp^l \delta \zeta_\perp^l} \\
& \times \left[ \theta(\zeta_I^- - y_E^-) \left\{ e^{-ip^+ x_L y_E^-} - e^{-ip^+ x_L \zeta_I^-} \right\} - \theta(\zeta_I^- - y_I^-) e^{-ip^+ x_L y_I^-} - \theta(y_I^- - \zeta_I^-) e^{-ip^+ x_L \zeta_I^-} \right] \\
& \times \left[ \theta(\zeta_C^- - y_0^-) \left\{ e^{ip^+ x_L y_0^-} - e^{ip^+ x_L \zeta_C^-} \right\} - \theta(\zeta_C^- - y_C^-) e^{ip^+ x_L y_C^-} - \theta(y_C^- - \zeta_C^-) e^{ip^+ x_L \zeta_C^-} \right]. \tag{44}
\end{aligned}$$

In the equation above  $q = r + s$ . While not explicitly mentioned, all scattering points on the same line (quark or gluon) are strongly ordered. The only unspecified orderings are scatterings on the gluon versus those on the quark after emission. This expression may be easily generalized from Eqs. (26,25,38) The  $\delta$ -function  $\delta(l_\perp + l_{q\perp})$  is shifted to  $\delta(l_{q\perp})$  and is then broadened by multiple scattering as in Eq. (38). There are now  $r + s + m + n$  two gluon matrix elements corresponding to the number of scatterings.

While there is no simple means to derive the second line of Eq. (44), it can be qualitatively understood as follows. Consider the case of gluon radiation without scattering as described in Sect. 2.1. The factor of  $1/l_\perp^2$  in Eqs. (25,26) may be more naturally expressed as

$$\frac{1}{l_\perp^2} = \sum_\lambda \left( \frac{l_\perp \cdot \varepsilon_\lambda^*}{l_\perp^2} \right) \left( \frac{\varepsilon_\lambda \cdot l_\perp}{l_\perp^2} \right), \tag{45}$$

where  $l_\perp$  is the transverse momentum of the gluon just after emission and  $\varepsilon$  is the polarization vector of the produced gluon. This expression naturally arises in the case of one gluon bremsstrahlung from a hard quark by evaluating the square of the matrix element  $\mathcal{M} \sim J^{\mu a} A_\mu^a$ . This will be modified in the multiple scattering case. In  $A^- = 0$  gauge with the gluon moving in the  $(-)$ -direction, the dominant components of the projection vectors are the transverse components. In the case of no scattering the transverse momentum at emission is identical in the amplitude and complex conjugate. In the case

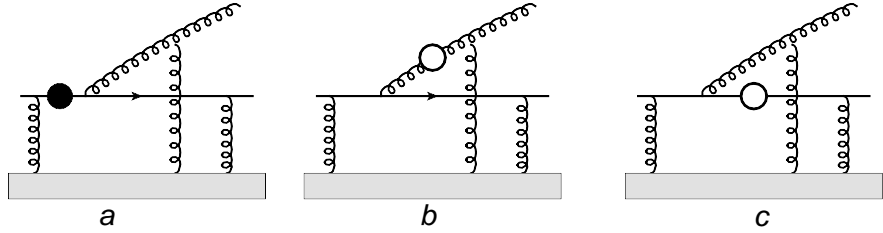


Figure 7: Diagrams which lead to LPM interference.

of multiple scattering, the transverse momentum of the radiated gluon in the amplitude and complex conjugate is identical at the cut line but not at the point of emission. Thus, at the point of emission, the factor is modified as,

$$\sum_{\lambda} \frac{\left( l_{\perp} - \sum_{i=1}^s k_{\perp}^i - \sum_{l=1}^m k_{\perp}^l \right) \cdot \varepsilon_{\lambda}^* \varepsilon_{\lambda} \cdot \left( l_{\perp} - y \sum_{i=1}^{r+s} k_{\perp}^i - \sum_{l=1}^m k_{\perp}^l \right)}{\left( l_{\perp} - \sum_{i=1}^s k_{\perp}^i - \sum_{l=1}^m k_{\perp}^l \right)^2 \left( l_{\perp} - y \sum_{i=1}^s k_{\perp}^i - \sum_{l=1}^m k_{\perp}^l \right)^2}. \quad (46)$$

Summing over the projections of the radiated gluons, yields the second line of Eq. (44). In the amplitude part (the right side of the expression), the gluon is radiated after the  $r + s$  scattering on the original quark. Of the transverse momenta gained by the parent quark in the  $r + s$  scattering, only a fraction  $y$  is transferred to the radiated gluon. This is the reason for the factor of  $y$  in the amplitude terms in Eq. (46).

The third, fourth and fifth line of Eq. (44) contain the products of the two-gluon matrix elements at the locations of the various scatterings. The first set on the third line contains the collection of correlated scatterings where the parent quark scatters in the amplitude at the locations  $i = 1$  to  $q$  and the produced quark and gluon scatter off these same locations in the complex conjugate. The next set of scatterings on the fourth line at locations  $j = 1$  to  $n$  represent the scatterings of the final produced quark in both amplitude and complex conjugate, i.e., there is no interference in these scatterings. The last set on the fifth line represent the independent scatterings on the final outgoing gluon line.

The last two lines of Eq. (44) contain the phase factors that arise from the interference between the gluon emission from different locations in the amplitude and complex conjugate. The phase factors may be somewhat more straightforwardly motivated. There are in principle three types of vertices that will lead to the radiation of a hard gluon. These are illustrated in Fig. 7. The left-most diagram represents the case where the incoming quark is taken time-like off-shell, indicated by the filled dot. In the first term of the phase factors in Eq. (44) [sixth line of Eq. (44)] the quark in the complex conjugate is taken time-like off-shell by the scattering at  $y_E^-$ . This immediately introduces a phase factor of  $\exp(-ip^+ x_L y_E^-)$ ; the quark goes off-shell and immediately radiates a gluon. The  $\theta$ -function expresses the fact the the other propagators are all on shell and thus the location  $\zeta_I$  is far ahead of  $y_E^-$ .

The second diagram in Fig. 7 expresses the possibility that the quark after the scattering remains on shell and radiates a space-like gluon which is then brought on-shell by the first independent scattering on the gluon. In the second term of the phase factor of Eq. (44), this occurs in the complex conjugate at location  $\zeta_I$ . The exponential factor is  $\exp(-ip^+ x_L y_E^-)$ . The negative sign is due to the fact that the propagator goes space-like. This is indicated by the hollow blob in the figure. Such a contribution occurs twice in the calculation: it occurs in the case where the initial quark propagator is taken on shell first or when the final quark propagator is taken on shell first. The fourth exponential factor is the instance of the latter pole in the complex conjugate. The third phase factor corresponds to the case



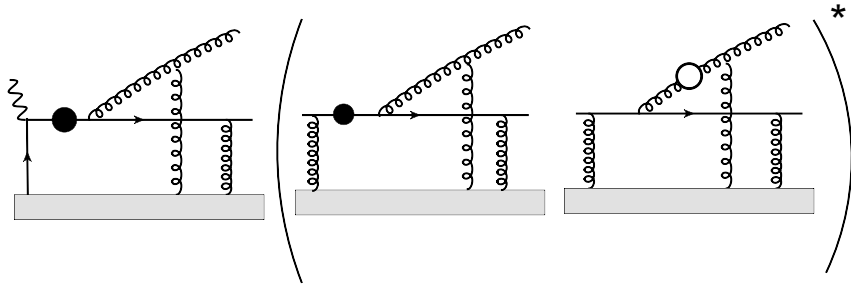


Figure 8: Diagrams which are leading in the higher twist approach.

where the on-shell quark radiates an on-shell gluon and goes off-shell. It is brought back on-shell by a hard scattering. In the case of the quark in the complex conjugate in Eq. (44), this occurs at location  $y_I^-$  and has the corresponding exponential factor. The remaining phase factors for the gluon emission in the amplitude have similar explanations and thus similar phase factors.

In the higher twist formalism, one takes the hard scattering hierarchy, in the sense that the hard scattering scale  $Q$  is assumed to be much larger than the medium scale  $\sim T$  or the scale of Debye screening. Thus, one tries to isolate terms which are minimally suppressed by the hard scale  $Q$ . This is obtained, as in the case of no emission, by Taylor expanding the small transverse momenta  $k_\perp^i$ . The expansion of the  $\delta$ -function can be shown to yield a similar diffusion equation as for the case of no emission. The emission yields a factor of the splitting function  $P(y)$  and phase factors which appear in the last line of Eq. (44). Of these, the phase factor which is dependent on the origin ( $e^{ip^+x_L y_0^-}$ ) represents the terms where the jet exits the hard interaction off-shell and immediately radiates a hard gluon. This is represented by the leftmost diagram in Fig. 8. Terms containing this factor in a product with the complex conjugates of similar diagrams as well as those where the hard parton is driven off shell later in its history are representative of vacuum like emission and vacuum medium interference. These are the leading contributions in the higher twist formalism. A subset of these are represented by the diagrams of Fig. 8. One also has to include contributions where the quark propagator after emission becomes space-like off-shell.

Including these contributions along with the contributions where all three types of scattering may not be present and then Taylor expanding in  $k_\perp^i$ , we obtain the next-to-leading power suppressed contributions, i.e., those suppressed by one extra power of  $Q^2$  (or rather  $l_\perp^2$ ) as a sum of three terms each with a different power of the gluon momentum fraction  $y$ . The leading contribution to the radiated gluon spectrum in  $y$  arises from purely gluon scattering, and is given as

$$\frac{dN_1}{dy dl_\perp^2} = \frac{\alpha_s C_F}{2\pi l_\perp^4} P(y) \int_0^{L^-} d\zeta^- \hat{q}(\zeta^-) [2 - 2 \cos(p^+ x_L \zeta^-)]. \quad (47)$$

We have dropped the subscript  $I$  from the position  $\zeta_I^-$  in writing the above equation. The next contribution is proportional to  $y$  and includes the cross-scattering terms between the final radiated gluon and the quark before the split. This contribution to the radiated gluon spectrum is given as

$$\frac{dN_2}{dy dl_\perp^2} = -\frac{\alpha_s C_F}{2\pi l_\perp^4} y P(y) \int_0^{L^-} d\zeta^- \frac{\hat{q}(\zeta^-)}{2} [2 - 2 \cos(p^+ x_L \zeta^-)]. \quad (48)$$

The last contribution at this level of power suppression, suppressed by two powers of  $y$ , is the set of diagrams where the initial quark scatters in the amplitude and the complex conjugate. These diagrams were not included in the Eq. (44) or in the corresponding diagrams in Fig. 6. The contributions from

these are

$$\frac{dN_3}{dydl_\perp^2} = \frac{\alpha_s C_F}{2\pi l_\perp^4} y^2 P(y) \int_0^{L^-} d\zeta^- C_F \hat{q}(\zeta^-) [2 - 2 \cos(p^+ x_L \zeta^-)]. \quad (49)$$

Summing the above three equations yields the next-to-leading power correction due the single gluon emission cross section due to multiple scattering of the parent quark, radiated gluon as well as the produced quark. The argument for terminating at this order of power correction is the hard factorization limit of  $Q^2 \gg \hat{q}L^-$ , i.e., higher power corrections are further suppressed.

### 2.2.3 Length dependence of energy loss and extensions to heavy-ion reactions

In general, the application of Eqs. (47,48,49) to the computation of a medium modified fragmentation function tends to yield a complicated dependence of the length  $L^-$  of the medium. However one may deduce a simple and approximate relation for the fractional energy lost in the small  $y$  limit which illustrates the length dependence of the energy loss.

In the small  $y$  limit, one may focus solely on the first term of the differential gluon radiation spectrum, i.e., Eq. (47). The fractional energy loss may then be estimated as,

$$\frac{\langle \Delta E \rangle}{E} = \langle y \rangle = \int_{y_{\min}}^{y_{\max}} dy \int_0^{Q^2} dl_\perp^2 \int_0^{L^-} d\zeta^- y \frac{dN_g}{dy dl_\perp^2}. \quad (50)$$

We say “estimated” as the integral over  $l_\perp$  is taken to zero which is never done in realistic HT calculations. Carrying out the  $l_\perp$  integration first and retaining only the leading term in  $y$  we obtain,

$$\langle y \rangle = \int_{y_{\min}}^{y_{\max}} dy \frac{\alpha_s C_F P(y)}{4q^-} \int_0^{L^-} d\zeta^- \hat{q} \zeta^- \quad (51)$$

In a medium the range of  $y$  is limit by the fact that the momentum fraction  $x_L = \frac{Q^2}{2q^- p^+ y(1-y)} < 1$ , i.e., a proton can at most impart its entire light-cone momentum to the jet in a single gluon exchange. Thus the  $y$  integration is not divergent. Assuming that  $\hat{q}$  is independent of the location  $\zeta^-$  we obtain the simple and well known relation that,

$$\langle \Delta E \rangle \propto \hat{q} L^{-2}, \quad (52)$$

with the constant of proportionality depending on the range of  $y$  integration. This, in turn, depends on the maximum of  $l_\perp^2 = Q^2$  and on the energy  $q^-$  of the hard jet. We should point out that this relation is quite approximate and the modification of the fragmentation function has a much more involved length dependence that what is suggested by the above equation.

As pointed out in the previously, the HT approach is cast in the framework of DIS on a large nucleus. The medium in this case is confined. However the basic formalism may be straightforwardly extended to the case of a jet propagating through a deconfined medium. This extension is illustrated with the case of transverse broadening as in Eq. (41). In this case the part of the hadronic tensor (or cross section) where the virtual photon strikes an incoming quark and sends it into the nucleus is entirely contained within  $W_0^{\mu\nu}$ . This part, which is specific to DIS, has been factorized from the remaining process which represents the multiple scattering of the hard quark in the medium.

Extending this formalism to the case of jet propagation in a hot deconfined medium consists of replacing the hard cross section to produce a hard quark in DIS:

$$\frac{E_{L_2} d\sigma_0}{d^3 L_2 d^2 l_{q\perp} d^2 l_\perp dy} = \frac{\alpha_{em}^2}{2\pi s Q^4} \frac{L_{\mu\nu} dW_0^{\mu\nu}}{d^2 l_{q\perp} d^2 l_\perp dy} = \frac{\alpha_{em}^2}{2\pi s Q^4} \frac{L_{\mu\nu} (-g_\perp^{\mu\nu}) \sum_q 2\pi Q_q^2 f_q(x_B) \delta^2(\vec{l}_{q\perp})}{d^2 l_{q\perp} d^2 l_\perp dy}, \quad (53)$$

with the cross section to produce a hard quark or gluon in a heavy-ion collision with a momentum  $\hat{p}_T$ ,

$$\frac{d^2\sigma^h}{dyd^2\hat{p}_T} = \frac{1}{\pi} \int dx_a G_a(x_a, Q) G_b(x_b, Q) \frac{d\sigma_{ab \rightarrow cX}(Q, x_a P, x_b P, \hat{p}_T)}{d\hat{t}}. \quad (54)$$

What remains is the final state multiple scattering of the produced quark. This is assumed to be formally identical to the case of jet propagation in cold matter. The only change is that the expectation of the two gluon operator which is an input in the expression for the transport coefficient  $\hat{q}$  Eq. (41) will now be evaluated in a hot deconfined medium, i.e.,

$$\hat{q}_{QGP} = \frac{4\pi^2\alpha_s C_R}{N_c^2 - 1} \int \frac{dy^- d^2y_\perp}{2\pi} e^{-i\left(\frac{k_\perp^2}{2q} y^- - k_\perp \cdot y_\perp\right)} \sum \langle n | e^{-\beta\mathcal{H}} F^{a+\mu}(y^-, y_\perp) F^{a+\mu}(0, 0) | n \rangle \quad (55)$$

In the equation above,  $|n\rangle$  represents a state in a thermal ensemble and  $\mathcal{H}$  is the hamiltonian operator and  $\beta$  is the inverse temperature. The exact value of  $\hat{q}$  obtained depends on the methodology used in modeling the medium. For example, assuming that the medium can be represented as a weakly coupled plasma of quarks and gluons in the Hard Thermal Loop (HTL) approximation yields the expression in Eq. (73).

## 2.3 Other approaches and pictures of the medium

### 2.3.1 AMY approach: Hard Thermal Loop field theory

Unlike the HT approach, the formalism of jet modification based on the work of Arnold, Moore and Yaffe (AMY) starts with a rather precise definition of the medium. The medium is assumed to be composed of quark gluon quasi-particles with dispersion relations and interactions given by the HTL effective theory. Thus all quasi-particles in the medium have thermal masses  $\sim gT$  and their scattering is dominated by soft scattering. The hard jet is assumed to have a virtuality scale comparable to the Debye mass or thermal mass. Thus there is no jet-like hard scale in the problem. One constructs a consistent perturbation theory at the  $T \rightarrow \infty$  limit and applies it to a realistic temperature.

In spite of these differences, at the diagram by diagram level, the AMY approach evaluates diagrams which are topologically equivalent to those evaluated by the higher twist (HT) approach. To illustrate this we consider a generic diagram in the HT approach and convert it to a diagram similar to those evaluated in the AMY scheme. In the left top panel of Fig. 9, we consider the case that a hard quark produced in a hard scattering then radiates a hard gluon and both final partons scatter once off the medium. While in the case of HT, the dominant contribution contains the case where the initial quark could be quite off-shell and radiates immediately, this is not the case in AMY. The incoming parton is close to on-shell and will radiate a hard gluon only on being stimulated by scattering. As a result, the transverse momentum of the radiated gluon is always of the the order of  $gT$ .

As a result of the initial quark being on-shell, the momentum of the quark in the amplitude and the complex conjugate is identical, indicated by the double notches on these lines in the left top diagram of Fig. 9. In this limit, the final state scattering part can be factorized from the initial structure function, as indicated by the right top diagram. The final state scattering part now contains an incoming quark which is on-shell and then is driven off shell by the scattering experienced by the remnant quark and the radiated gluon. The complex conjugate also contains the same process. The blobs which connect to the scattering gluons can be replaced by the imaginary parts of the HTL self-energies. Given that the initial quark in the amplitude and the complex conjugate are identical, we can consider these to also arise from a cut diagram as shown in the bottom right panel. This final diagram corresponds to the type of self energy diagrams evaluated by the AMY scheme.

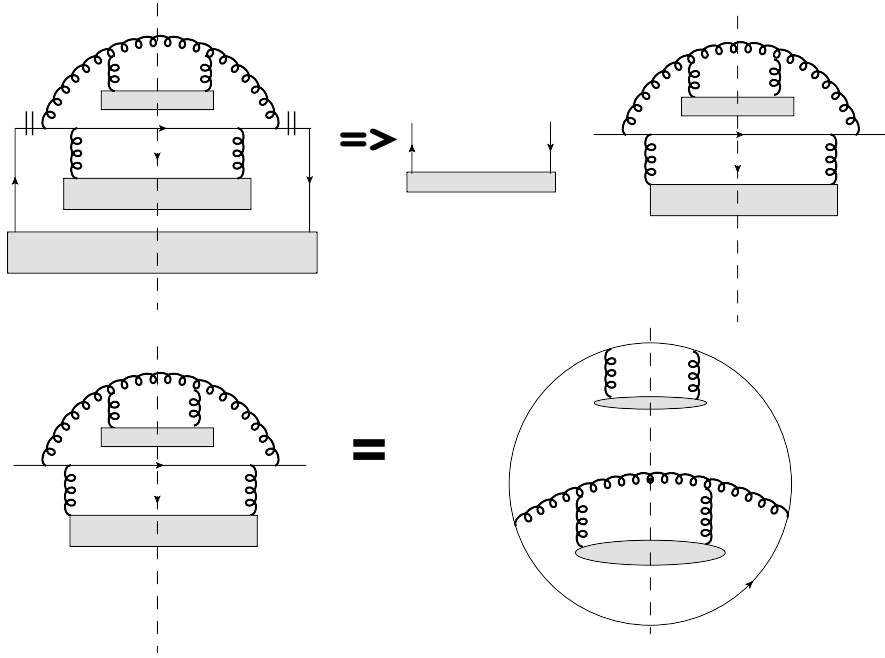


Figure 9: Starting with a higher twist diagram and obtaining the equivalent AMY diagram.

While the diagrams considered by AMY and HT are topologically similar, the limit in which these are evaluated, as well as the pole structure, is quite different. As pointed out in the previous section, the leading contribution in the higher twist always contains, either in the amplitude or in the complex conjugate, a term which represents the quark being produced far off-shell in the initial hard scattering and immediately radiating a gluon. This is missing in the AMY approach. The dominant contributions in the AMY approach consist of interferences between different medium stimulated emissions along with the squares of the amplitudes themselves. As the single gluon emission cross section is evaluated in a different limit in the AMY approach, the formalism used to iterate this is also different and will be discussed in the next chapter.

### 2.3.2 GLV approach: Opacity expansion

This scheme named after Gyulassy, Levai and Vitev is very closely related to the HT approach. The primary difference is that the GLV scheme makes a very specific assumption regarding the structure of the medium. The medium is modeled as separated heavy static scattering centers with color screened Yukawa potentials. This model of the medium was originally introduced in the seminal work of Gyulassy and Wang [24, 25, 26] and is often referred to as the Gyulassy-Wang model. The cross section for the interaction of the jet parton with one of these heavy medium partons is

$$\frac{d\sigma_{el}}{d^2k_{\perp}} = \frac{C_R C_2}{(2\pi)^2 (N_c^2 - 1)} \left| \frac{4\pi\alpha_s}{k_{\perp}^2 + \mu^2} \right|^2. \quad (56)$$

Where,  $C_R$  is the Casimir for the jet parton and  $C_2$  is for the medium parton. Alternatively, one may think of this as a specific model to evaluate the gluon field strength correlator of Eq. (55). The quantity  $\mu$  represents the Debye mass which screens the potential of the scattering centers and represents one of the parameters of the model. The other parameter is the mean free path of the jet  $\lambda = (\rho\sigma)^{-1}$ , where  $\sigma$  can be obtained from integrating Eq. (56) and  $\rho$ , the density of scattering centers in the medium can be obtained from entropy considerations.

Beyond this, the assumptions regarding the hierarchy of scales where the forward light-cone momentum of the jet  $q^- \gg l_\perp$  the transverse momentum of the radiated gluon [which in turn is much larger than the  $(-)$ -components] are the same as in HT. However, unlike the HT, there is no concept of scale evolution, thus the model of the medium as incoherent scattering centers is meant at the momentum scale of the medium. The first term to be considered is the vacuum radiation term as in the HT scheme. This is followed by terms that involve the interference of medium induced radiation and vacuum radiation. As in the HT scheme, the leading contribution in the GLV approach also involves one scattering with the medium and is proportional to the number of scattering centers as seen by the jet. This is expressed as  $L/\lambda$ , where  $L$  is the path length of the hard jet and  $\lambda$  is the mean free path for a scattering. The former quantity depends on the medium in question while the latter is a parameter of the calculation. The ratio of  $L/\lambda$ , called the opacity, is similar to the length enhancement factor in the HT approach and, combined with the cross section for a scattering, represents the expansion parameter for this calculation.

Thus calculations which include only the vacuum radiation and one scattering, which are proportional to one power of  $L/\lambda$  and are called up to first order in opacity. The additive term in the cross section to produce a single gluon at first order in opacity is

$$\frac{d\sigma}{dy dl_\perp^2} = \frac{\alpha_s C_F}{2\pi l_\perp^2} P(y) \frac{L}{\lambda} \int_0^{q_{MAX}^2} d^2 k_\perp^2 \frac{\mu^2}{\pi(k_\perp^2 + \mu^2)^2} \int_0^\infty d\zeta n(\zeta) [2 - 2 \cos((l_\perp - k_\perp)^2 / 2q^- y)]. \quad (57)$$

The major difference with the next to leading twist term in the HT expansion is the integral over the exchanged gluon transverse momentum  $k_\perp$  and the explicit appearance of the the Yukawa cross section to scatter off a heavy scattering center. In the equation above,  $n(\zeta) = \theta(L - \zeta)/L$  is the longitudinal profile.

Terms with two scatterings are proportional to  $(L/\lambda)^2$  and so on. Note that leading order in opacity does not mean that the jet has scattered only once in the dense medium. Rather, it represents the case that at most one scattering was involved in a single gluon radiation. The basic methodology of the GLV approach is to compute the single gluon emission kernel, order by order in opacity. For dilute media or short path lengths one uses only the leading order in opacity, while denser or more extended media require higher orders. Higher orders in opacity have been explored analytically [49], but it has, so far, not been possible to analytically resum the full series in opacity.

### 2.3.3 ASW approach: Multiple-soft gluon exchange

Similar to the GLV scheme, the ASW approach named after Armesto, Salgado and Wiedemann also assumes that the medium may be modeled as a collection of heavy static scattering centers with Debye screened potentials. In the calculation of the single gluon spectrum, the ASW scheme also invokes the small  $y$  limit where  $y$  is the longitudinal momentum fraction of the radiated gluon. As in the case of the HT scheme, it also finds that the leading contributions in this limit consist of diagrams where primarily the gluon scatters or diagrams with cross scatterings where the quark in the amplitude scatters and interferes with gluon scattering in the complex conjugate.

In the ASW approach, the multiple scattering analysis is carried out in impact parameter space. The square of the amplitude where the gluon scatters  $m$  times in both amplitude and complex conjugate, is at a transverse position  $u_\perp$  in the amplitude and at a transverse position  $\bar{y}_\perp$  in the complex conjugate is given as

$$\propto \frac{1}{m!} \left( -\frac{1}{2} \int_{\zeta_I}^{\zeta_F} d\zeta n(\zeta) \sigma(u_\perp - \bar{y}_\perp) \right)^m e^{-ik_\perp \cdot (u_\perp - \bar{y}_\perp)}, \quad (58)$$

where,  $\zeta_I$  and  $\zeta_F$  indicate the longitudinal positions over which the scatterings occur. The quantity  $n(\zeta)$  is the opacity at the location  $\zeta$  and  $\sigma$  is the dipole cross section of two gluons separated by a transverse

distance  $u_\perp - y_\perp$ . The gluon propagation from  $\zeta_I$  to  $\zeta_F$  in the amplitude represents one part of the dipole, where as the propagation of the gluon in the complex conjugate is the other part of the dipole. The case of multiple scattering is obtained by summing over  $m$  to obtain the obvious exponential with the argument in parenthesis in Eq. (58).

In the region before  $\zeta_I$  there is cross scattering with scattering on the incoming quark in the amplitude matched with scattering on the gluon in the complex conjugate and vice versa. This case is more complicated; starting at the location  $\bar{\zeta}_I$ , the quark propagates in the amplitude and a quark gluon pair in complex conjugate. The result is given by a path integral where the dipole moves in the two dimensional space of relative transverse location. The diagrams involved in this part are near identical to those of the AMY scheme. However, in the AMY case, the entire calculation is carried out in momentum space, as a result all positions are integrated from  $-\infty$  to  $\infty$ . As the calculation here is carried out in position space, the numerator factor of  $l_\perp \cdot l'_\perp$  in Eq. (46) is replaced by the appropriate derivatives over transverse position. The final expression for the cross section to radiate a gluon with transverse momentum  $l_\perp$  and energy  $\omega$  and momentum fraction  $y$  (or alternatively the distribution of radiated gluons in transverse momentum and energy), is given as

$$x \frac{d^3 I}{dx dl_\perp^2} = \frac{\alpha_s C_F}{2\pi^2 \omega^2} 2Re \int_{\zeta_0^-}^{\infty} dy_l^- \int_{y_l^-}^{\infty} dy_l'^- \int d^2 u_\perp e^{-i l_\perp \cdot u_\perp} e^{\left[ \frac{-i}{2} \int_{y_l'^-}^{\infty} d\zeta n(\zeta) \sigma(u_\perp) \right]} \frac{\partial^2}{\partial u_\perp \partial y_\perp} \int_{y_\perp=0}^{u_\perp} \mathcal{D} r_\perp e^{y_l^- \int_{y_l^-}^{y_l'^-} d\zeta -i \frac{\omega r_\perp^2}{2} - \frac{n(\zeta^-) \sigma(r_\perp)}{2}}. \quad (59)$$

For a short range potential one may take the saddle point approximation around the  $r_\perp \rightarrow 0$  limit by replacing,

$$n(\zeta) \sigma(r_\perp) \simeq \frac{\hat{q}(\zeta)}{2} r_\perp^2. \quad (60)$$

This approximation allows the above path integral to be carried out. While introduced in this way, the one transport coefficient  $\hat{q}$  has the standard meaning as in any other formalism: the transverse momentum gained by a hard parton (in this case a gluon) per unit length.

Unlike the HT or the GLV approach, there is no explicit introduction of the vacuum contribution or vacuum medium interference. The fact that a hard jet in DIS or a heavy-ion collision is not created at  $y_l^- = -\infty$  is incorporated by introducing a finite starting point to the longitudinal integrals. In this case starting  $y_l^-$  integral at  $\zeta_0^-$  usually set to be the origin. There is no systematic insistence that the off-shellness from the vacuum contribution be much larger than that from the medium scatterings. Given all these approximations, the single gluon cross section from multiple scattering is found to be dependent on only one parameter:  $w_c = \int d\zeta \zeta \hat{q}(\zeta) = \frac{1}{2} \hat{q} L^2$ , as (in the  $\omega_c L \rightarrow \infty$  limit),

$$\frac{d\sigma}{d\omega} = \frac{\alpha_s C_F P(y)}{\pi} \ln \left[ \cos \left[ (1+i) \sqrt{\frac{\omega_c}{2\omega}} \right] \right]. \quad (61)$$

## 2.4 Parametrizing the effect of the medium: $\hat{q}$ , $dN/dy$ , $T$ and $\alpha_s$

All the different schemes above depend on one or two parameters. In the case of the HT, the unknown quantity is the two gluon field strength correlation in the medium in question:

$$\int dy^- d^2 y_\perp e^{-i \frac{k_\perp^2}{2q} y^- + k_\perp \cdot y_\perp} \langle F^{+\mu}(y^-, y_\perp) F_\mu^+(0) \rangle. \quad (62)$$

Expressing  $F^{+\mu} = F^{\nu\mu} v_\nu$  where  $v_\nu$  is the light-like velocity of the hard parton we note that the above quantity is simply the Lorentz force correlator in the system. Since this quantifies the transverse

force experienced by a jet as it passes through a medium, it may be straightforwardly related to the transport coefficient  $\hat{q}$  as in Eq. (55). Since  $k_\perp \gg \Lambda_{QCD}$ , the integrals over transverse location  $y_\perp$  are rather limited. On the other hand  $k^+ = k_\perp^2/2q^-$  may well be non-perturbative, so that the  $y^-$  integral is limited by non-perturbative effects, such as the confinement length in cold nuclear matter and the screening length in hot deconfined matter.

To obtain some form for the two-gluon field strength correlator in Eq. (62), one requires a microscopic model of the medium. The situation in the ASW approach is similar. Although a specific medium model of static scattering centers is used in the derivation, the final result depends only on the transport coefficient  $\hat{q}$ , suggesting that the energy loss within the multiple soft scattering approximation (i.e. when the saddle point approximation of Eq. (60) is valid) does not depend on the specific details of the medium, but measures directly the mean transverse momentum exchange per unit path length.

In the AMY scheme, which is cast completely within the HTL formalism of finite temperature field theory, the scattering is not factorized from the gluon emission process. Since HTL perturbation theory is cast in the limit that there exist separate scales  $T, gT$ , the two obvious parameters of the theory are  $T$  and  $g$  (or rather  $\alpha_s$ ). Note that this formalism may only be applied to hot deconfined matter. The coupling constant  $\alpha_s$  is the same for the jet and for the medium. It is allowed to vary as a fit parameter and set by fitting one data point.

Since the AMY formalism makes a precise assumption regarding the microscopic structure of the produced matter, it provides a well-defined way to calculate the transport coefficient  $\hat{q}$ , given a  $T$  and an  $\alpha_s$ . Following Ref. [65] we note that  $\hat{q}$  may be defined as,

$$\hat{q} = \int d^2k_\perp \frac{d\Gamma}{d^2k_\perp}, \quad (63)$$

where,  $d\Gamma/d^2k_\perp$  is the differential rate for elastic collisions of a hard parton with quasi-particles from the medium. While the expression for the differential rate has slightly different forms depending on whether the exchanged gluon is soft or hard, we will approximate the rate with the expression for soft momentum transfer:

$$\frac{d\Gamma}{d^2k_\perp} \simeq \frac{C_R}{(2\pi)^2} \frac{g^2 T m_D^2}{k_\perp^2 (k_\perp^2 + m_D^2)}, \quad (64)$$

where  $m_D$  is the Debye mass,  $m_D^2 = \frac{4\pi\alpha_s T^2}{3} \left( N_c + \frac{N_f}{2} \right)$ . Substituting the expression for the differential rate in Eq. (63), one may easily calculate  $\hat{q}$  given the range of integration of the exchanged momentum.

One notes immediately that the expression for  $\hat{q}$  is bounded from below and thus the lower limit of integration may be taken to zero. This is often done in many different approaches. The upper limit is bounded by kinematics of the process, i.e, the outgoing two partons may not carry more energy than the incoming partons. This constrains the upper limit to  $q_\perp^{MAX} \sim \sqrt{4ET}$  where  $E$  is the energy of the hard parton. The energy loss calculation in the AMY is based on rate equations similar to Eq. (64) and thus uses the same transport properties, but without explicitly calculating the transport coefficient  $\hat{q}$ .

In the case of the GLV approach, one needs to set two parameters: the Debye screening mass and the mean free path of the radiated gluon  $\lambda$ . The mean free path may be obtained using  $\lambda = 1/(\rho\sigma)$ , where  $\rho$  is the density of scattering centers and  $\sigma$  is the integrated cross section for a gluon to scatter off these. Because of the dependence on  $\rho$ , the total number of gluons at mid-rapidity  $dN/dy$  has often been quoted as a measure of the medium density in GLV calculations [66]. However, it should be noted that the Debye screening mass and thus the temperature also enters in the GLV formalism via the scattering potential Eq. (56) and the cross section  $\sigma$ .

In conclusion, this means that in all four formalisms, a microscopic model of the medium is needed to set the input parameters for the energy loss calculation, be it the two gluon field strength correlator, the transport coefficient  $\hat{q}$ , or  $m_D$  and  $\lambda$ . The AMY approach makes a specific choice for a HTL plasma.

Given such a model, the local medium parameters can be related to single quantity in the medium, such as the temperature  $T$  in HTL. It is, however, worth to keep in mind that the radiative energy loss in all models is driven by transverse momentum exchanges, so that the energy loss is governed by the transport coefficient  $\hat{q}$  or a closely related quantity. In addition to the microscopic model of the medium, a realistic calculation of energy loss in heavy collisions also requires a macroscopic model of the medium, specifying the space-time dependence of the local properties of the plasma. This aspect will be further discussed in Chapter 5.



### 3 Incorporating Multiple radiations

In the preceding chapter we described the calculation of medium induced single gluon radiation from a hard parton traversing a dense medium. Imagine a gluon radiated with a transverse momentum  $l_\perp$  and a forward momentum  $l^-$ , its formation time is given as,  $\tau = l^-/l_\perp^2$ . For realistic values of  $l_\perp^2 = 3 \text{ GeV}^2$  and  $l^- = 6 \text{ GeV}$  say from a jet with forward momentum  $q^- \sim 20 \text{ GeV}$ , we obtain a formation time of  $\tau \sim 0.4 \text{ fm}$ . Thus in almost any medium with a length  $L > 1/2 \text{ fm}$  there will be more than one such radiation. In this chapter we describe the different ways in which the single gluon emission is iterated in different jet modification schemes.

The incorporation of multiple emissions completes the theoretical calculation of radiative energy loss for light partons. The final form of the result depends on the observable in question. For the computation of the single hadron inclusive cross section one computes the medium modified fragmentation function  $\tilde{D}^h(z)$ , where  $z$  is the momentum fraction of the hadron  $h$  with respect to the momentum of the originating hard parton. We should point out that, unlike the case in vacuum where the hard parton produced in a hard collision continues to monotonously lose virtuality till the onset of the non-perturbative process of hadronization, the process of multiple radiation in a medium may be far more complicated, including a series of both virtuality increasing collisions and virtuality decreasing emissions. To date, the space-time structure of this process has not been completely elucidated. The different approaches of the various schemes represent approximations to the actual mechanism.

#### 3.1 Higher twist: In medium DGLAP

A hard parton from a large  $Q^2$  collision is considerably off-shell when it is produced. This parton then proceeds to lose this virtuality by a series of gluon emissions ordered in virtuality or transverse momentum. The radiated gluons are themselves virtual and continue to radiate lower virtuality gluons. The progress of this shower may be described using pQCD as long as the virtuality  $\mu$  is large compared to  $\Lambda_{QCD}$ . Beyond this, one describes the process with a phenomenologically fitted fragmentation function  $D^h(z, \mu^2)$  which contains all processes up to the scale  $\mu^2$  which produce at least one hadron with momentum fraction  $z$ . The effect of multiple gluon emissions from the scale  $\mu^2$  up to some predefined virtuality or scale  $Q^2$  is incorporated by evolving the fragmentation function using the Dokshitzer-Gribov-Lipatov-Altarelli-Parisi (DGLAP) evolution equation from  $\mu^2$  up to  $Q^2$ .

The DGLAP evolution equation may be understood as the resummation of an arbitrary number of ordered emissions which connect a hard parton with a virtuality  $Q^2$  with a parton with lower virtuality  $\mu^2$ . For the non-singlet fragmentation function  $D_{NS} = D^h - D^{\bar{h}}$ , which is always vanishing when the fragmenting parton is a gluon, this process may be straightforwardly expressed as,

$$\begin{aligned}
 D(z, Q^2) &= D(z, \mu^2) + \frac{\alpha_s}{2\pi} \int_{\mu^2}^{Q^2} dl_\perp^2 \frac{dy}{y} \frac{C_F P(y)}{l_\perp^2} D\left(\frac{z}{y}, \mu^2\right) \\
 &+ \frac{\alpha_s}{2\pi} \int_{\mu^2}^{Q^2} dl_\perp^2 \frac{dy}{y} \frac{C_F P(y)}{l_\perp^2} \frac{\alpha_s}{2\pi} \int_{\mu^2}^{l_\perp^2} dl_\perp^{12} \frac{dy^1}{y^1} \frac{C_F P(y^1)}{l_\perp^{12}} D\left(\frac{z}{yy^1}, \mu^2\right) + \dots
 \end{aligned} \tag{65}$$

We have ignored the ordering in the momentum fraction  $y$  and have only written the first three terms in a series where each term contains a product of integrals over transverse momenta where the transverse momenta at each emission is limited by the preceding radiation. The factor  $P(y)$  represents the  $q \rightarrow qg$  splitting function, i.e., the probability for a quark to radiate a gluon and retain a fraction  $y$  of its momentum. This series can be resummed by noting that differentiating with respect to  $\log(Q^2)$  yields an identical series as above for the shifted fragmentation function  $D(z/y)$ , convoluted with the splitting function  $P(y)$ :

$$\frac{\partial D(z, Q^2)}{\partial \log Q^2} = \frac{\alpha_s}{2\pi} \int_z^1 dy C_F P(y) D\left(\frac{z}{y}, Q^2\right). \tag{66}$$

For an arbitrary fragmentation function, the evolution equation for the quark-to-hadron fragmentation function is coupled with the evolution equation for the gluon-to-hadron fragmentation function.

The jet modification formalism which is closest to this line of argument is the HT formalism. It assumes that while scattering processes may raise the intermediate virtuality in a given amplitude prior to or just after a gluon emission, there is an overall drop in the average virtuality between the incoming parton and the outgoing pair of radiated gluon and remnant parton in the single gluon emission cross section. Note that multiple scattering tends to progressively raise the virtuality of the propagating partons. Thus the above assumption is valid in the regime of densities and incoming virtualities where the formation time of the gluon is so short that the drop in virtuality from the emission dominates over the rise due to multiple scattering over the same time, i.e.,

$$\hat{q}\tau = \frac{\hat{q}2l^-}{l_\perp^2} \lesssim l_\perp^2 \implies l_\perp^2 \gtrsim \sqrt{2\hat{q}l^-}. \quad (67)$$

We also note that gluons with a formation time  $\tau$  longer than the length of the medium  $L$  are not influenced by energy loss, which sets a minimum virtuality:  $\tau \leq L \implies l_\perp^2 \gtrsim 2l^-/L$ . Thus for the formalism to remain consistent till the exit of the jet from the medium we require the minimal condition,

$$\sqrt{2\hat{q}l^-} = \frac{2l^-}{L} \implies \Delta E = \frac{1}{2}\hat{q}L^2. \quad (68)$$

The last equality is obtained by relating the light-cone momentum of the radiated gluon with the light-cone loss and thus the energy loss.

Calculationally one simply replaces the vacuum splitting in Eq. (66) with the in-medium splitting function derived in the section above. It is assumed that the hard parton exits the medium with a virtuality (related to the transverse momentum of its radiations)  $\mu^2 \simeq 2Ey/L \sim E/L$ , where  $E$  is the energy of the initial hard parton,  $L$  is the length of the medium and  $y$  is a representative momentum fraction carried by the radiated gluon; this is approximated as  $y \sim 1/2$  in the second part of the equality. As pointed out earlier, a dynamical calculation of the loss of virtuality with emission as a function of the distance travelled by a hard parton is still lacking.

Given the measured fragmentation function at the scale  $\mu^2$ , this is evolved up to the hard scale  $Q^2$  of the process which represents the largest possible initial virtuality. Results of such an evolution in a hot QGP-brick will be presented at the end of this chapter. The result of the evolution is not very sensitive to the choice of the upper limit of the evolution; for instance, using  $Q^2/4$  will yield very similar results as long as  $Q^2 \gg \mu^2$ .

### 3.2 ASW and GLV: Poisson convolution

The ASW and the GLV schemes share a common microscopic picture of the medium: that of heavy static scattering centers. They also use an almost identical methodology for iterating the single gluon emission. Unlike the HT which computes the change in the distribution of hadrons (or the AMY scheme which computes the change in the distribution of partons), the central quantity that is calculated in these formalisms is the probability distribution  $P(\Delta E)$  for a hard parton to lose an energy  $\Delta E$ , via an arbitrary number of gluon emissions. This probability is then used to shift the fragmentation momentum fraction  $z$  and define a medium modified fragmentation function.

Contrary to the HT approach, in these formalisms, the virtuality evolution of the parton is not taken into account. A hard jet propagating through the medium will progressively gain virtuality by collision and lose it by emission. Each of these emission processes makes a minimal shift in the energy of the jet and to leading order one may ignore this shift, this is often referred to as the eikonal limit. Thus all these emissions may be considered as independent of each other. The fate of these emitted gluons is also not considered, the focus is solely on the emitting hard parton.

In either formalism, one calculates the differential distributions of radiated gluons, e.g., in Eq. (59). To obtain the differential energy distribution of radiated gluons, these expressions have to be integrated over the transverse momentum  $l_{\perp}$ . The formalism does not have a natural cut-off for transverse momentum integration, but instead uses kinematic considerations to limit these integrations, e.g.,  $l_{\perp}^{Max} \leq \min\{y, 1 - y\}E$  as used by the GLV scheme or in the small  $y$  limit  $l_{\perp}^{Max} \leq yE$  as used by the ASW scheme. The different choices of kinematic bounds, along with slightly different definitions of  $y$  (light-cone momentum fraction in GLV and energy fraction in ASW) lead to somewhat different results [67].

Having limited the transverse momentum integrations, the differential energy or momentum fraction distribution  $dI/d\omega, dI/dx$  is well defined. The integral over this quantity yields the mean number of gluons radiated from the jet:

$$N_g = \int dx \frac{dI}{dx} = \int d\omega \frac{dI}{d\omega}. \quad (69)$$

Given that each of these emissions are independent, the number of radiated gluons  $n$  is assumed to follow a Poisson distribution, giving the following probability distribution for energy loss:

$$P(\Delta E) = \sum_{n=0}^{\infty} \frac{1}{n!} \left[ \prod_{i=1}^n \int d\omega_i \frac{dI(\omega_i)}{d\omega_i} \right] \delta \left( \Delta E - \sum_{i=1}^n \omega_i \right) e^{-N_g}. \quad (70)$$

Using the expression for  $dI/d\omega$  the above probability distribution may be numerically calculated. Having lost energy  $\Delta E$ , the jet now fragments a hadrons with momentum  $p_h$  off a hard parton with energy  $E - \Delta E$ . The shifted or medium modified fragmentation function is defined as,

$$\tilde{D}(z, Q^2) = \int_0^E d\Delta E P(\Delta E) \frac{D\left(\frac{z}{1-\Delta E/E}, Q^2\right)}{1 - \Delta E/E}. \quad (71)$$

Under the assumption that the virtuality gain from the medium is comparable to that brought in by the hard parton, the scale used in the final fragmentation function is the same as the hard scale of the process.

### 3.3 AMY: rate equations.

In the AMY formalism, the hard jet is treated similar to a hard parton in the medium. The virtuality is assumed to be the same as that for any hard thermal parton in the medium  $\sim gT$ . In this sense it is similar to the assumption made in the ASW and GLV calculations. The rates for a quark to decay into a quark and gluon, a gluon to decay into a quark anti-quark pair etc., are now used to set up a Fokker-Planck equation which describes the change in the distribution of hard partons with time. There are two sets of equations which describe the change of the distribution of the sum of quarks with anti-quarks and gluons. For example the  $q + \bar{q}$  distribution may be described as

$$\frac{dP_{q\bar{q}}(p)}{dt} = \int_{\infty}^{\infty} dl P_{q\bar{q}}(p+l) \frac{d\Gamma_{qg}^q(p+l, l)}{dl dt} - P_{q\bar{q}}(p) \frac{d\Gamma_{qg}^q(p, l)}{dl dt} + 2P_g(p+l) \frac{d\Gamma_{q\bar{q}}^g(p+l, l)}{dl dt}. \quad (72)$$

In the equation above, the first term on the *r.h.s.* describes the process where a hard quark (antiquark) with a momentum  $p+l$  decays in to a quark (anti-quark) with momentum  $p$  and a gluon with momentum  $l$ . Hence, its contribution to the Fokker-Planck equation is proportional to the distribution of  $q + \bar{q}$  at a momentum  $p+l$ . The second term on the *r.h.s.* represents the decay of the quark (antiquark) with momentum  $p$  into lower momentum quarks and gluons and thus represents a depletion of the

distribution at that momentum. The last term proportional to the population of hard gluons with momentum  $p + l$  represents the process where the gluon decays into a quark anti-quark pair where one has a momentum  $p$  and the other has a momentum  $l$ . The factor of 2 accounts for the case where the momenta of the two fermions are reversed.

The integrals over  $l$  run from  $-\infty$  to  $\infty$ . When the momentum of the outgoing gluon or quark ( $l$  or  $p - l$ ) becomes soft, of the order of  $T$ , they will encounter Bose enhancement or Pauli blocking from the medium. These factors of distribution are already included in the expression for the rate  $d\Gamma/dl dt$ . Negative values of  $l$  indicate absorption of thermal gluons from the medium, the distributions for these arise simply from the sign change in the functions which lead to Pauli blocking or Bose enhancement. The AMY formalism is different from the other three approaches as it naturally incorporates feedback from the medium which is missing from all other approaches. A similar, but slightly more complicated equation may be written down for the gluon distribution [68]. These two equations are solved in tandem.

In this set-up one represents an incoming quark jet by setting the distribution at  $t = 0$  to be a  $\delta$ -function,  $P_{q+\bar{q}}(p, t = 0) = \delta(p - E_{jet})$ . The gluon distribution at this time is set to zero. These distributions are then evolved up to the time of exit by means of the coupled Fokker-Planck equations. In spite of the completeness of this approach, it does suffer from the rates being computed at a fixed temperature. Which implies that the medium remains static during the formation time of the radiated gluons. As a result, the application of this formalism to short or rapidly varying media is somewhat tenuous.

The final medium modified fragmentation function is obtained by convoluting the final distribution of hard quarks, anti-quarks and gluons with the respective shifted fragmentation functions, using Eq. (71) with the probability of energy loss replaced by the distribution of hard partons. In most applications so far the scale at which the fragmentation functions are evaluated is chosen to be the hard scale of the process.

### 3.4 Comparison of the different energy loss formalisms

In the previous sections, we have outlined the calculation of the medium modified fragmentation functions within the four different schemes that are currently in use. We now attempt a standard comparison between these different formalisms in an identical medium. In a recent effort by the TECHQM collaboration [69] this problem has been formulated as a computation of the modification of a single quark jet propagating through a homogeneous static medium of fixed length held at a constant temperature. This medium is often referred to as the ‘‘QGP brick’’, as temperatures are usually chosen to be high enough that deconfinement has set in.

In order to carry out computations in all four formalisms, their medium parameters have been defined in this standardized medium. We present our own particular prescription of a standardized medium in this review. One starts out by setting the temperature  $T$  and a value of the in-medium coupling  $\alpha_s = 0.33$ . Given these two parameters, calculations of jet modification may be carried out in the AMY formalism. Given these two parameters,  $\hat{q}$  can be computed using Eq. (63). Carrying out calculations for a quark-gluon plasma with 3 flavors of quarks ( $N_f = 3$ ) using the HTL approximation for small  $k_\perp$ , Eq. (64), we obtain,

$$\hat{q} = \frac{C_A g^2 m_D^2 T}{2\pi} \ln \left( \frac{q_\perp^{\text{MAX}}}{m_D} \right), \quad (73)$$

with  $q_\perp^{\text{MAX}} = \sqrt{ET}$ .

The value of  $\hat{q}$  obtained by the prescription above for the AMY scheme may now be directly substituted in the HT and the ASW approach. This will in some sense place these three calculations on the same footing, by using the  $\hat{q}$  for a weakly coupled plasma of quark gluon quasiparticles in all three formalisms.

The GLV formalism requires the specification of the Debye mass  $m_D$  and the mean free path  $\lambda$ . The Debye mass is taken directly from HTL field theory  $m_D^2 = \frac{4\pi\alpha_s T^2}{3} \left( N_c + \frac{N_f}{2} \right)$ . The mean free path  $\lambda$  is calculated from the scattering rate

$$\frac{1}{\lambda} = \int d^2k_\perp \frac{d^2\Gamma}{d^2k_\perp}, \quad (74)$$

using the same HTL approximation for small  $k_\perp$ , Eq. (64). Unlike the calculation for  $\hat{q}$ , the equation above has an infra-red divergence. This is controlled by restricting the lower limit to  $m_D$ , with the result:

$$\frac{1}{\lambda} = \int_{m_D}^{q_\perp^{\text{MAX}}} d^2k_\perp \frac{d\Gamma^2}{d^2k_\perp} \approx 3\alpha_s T \ln(2),$$

with the further approximation  $q_\perp^{\text{MAX}} \gg m_D$ .

Figure 10 shows a comparison of quark fragmentation function ratios using four different formalisms to calculate energy loss (HT, AMY, WHDG radiative and ASW) for a uniform medium with 2 different path lengths  $L$  and temperatures  $T$  in the regime relevant to RHIC. The Higher Twist (HT) uses  $\hat{q}$  and  $L$  as input to calculate a fragmentation function in the medium. The Figure shows the ratio between the medium-modified fragmentation function and the fragmentation function in the vacuum.

In the AMY formalism, the Fokker-Planck equations are solved to calculate the distribution of outgoing quarks and gluons starting from a mono-energetic distribution of quarks, the incoming quark with  $E = 20$  GeV. The outgoing quarks are then convoluted with the KKP fragmentation function to give a medium-modified fragmentation function. Gluon fragments were not included in this calculation for the purpose of comparison to the opacity expansion and multiple soft scattering approximations.

For the multiple soft scattering approach, ASW, the publicly available quenching weights code was used to calculate the energy loss probability distribution  $P(\Delta E)$  given the transport coefficient  $\hat{q}$  and medium length  $L$ . The medium modified fragmentation function is calculated by convoluting the energy loss probability distribution with KKP fragmentation functions using Eq. (71). Note that only quark fragments are taken into account, fragmentation of the radiated gluons is not calculated.

For the opacity expansion, we used the DGLV expressions from Appendix B of Ref. [66], with an in-medium gluon mass of  $m_g = m_D/\sqrt{2}$  and a quark mass  $m_q = m_D/2$ . The Debye screening mass  $m_D$  and  $1/\lambda$  are defined above. Multi-gluon emission is treated using a Poisson convolution for multi-gluon emission. The medium modified fragmentation function was calculated using Eq. (71).

Comparing the fragmentation functions in Fig. 10, we see a characteristic rise in the ratio at low  $z$  for the HT calculation that can be identified with gluon fragments, which are not included in the other calculations. Because of the steeply falling parton spectrum, the large  $z$  behaviour is most important for high- $p_T$  hadron production. For short path length  $L = 2$  fm, HT, GLV and ASW give very similar results at high  $z > 0.5$ , for both  $T = 250$  MeV and  $T = 350$  MeV. The AMY calculation shows a much larger suppression. This may be due to the absence of vacuum-medium interference in AMY.

At larger  $L = 5$  fm (bottom panels of Fig. 10), larger differences between the various formalism are seen. The magnitude of the suppression in the GLV opacity expansion and the ASW multiple-soft gluon emission formalisms are similar, but the  $z$  dependence is different between the two. The HT result approaches the AMY result for  $L = 5$  fm and  $T = 350$  MeV. It should be noted, however, that in this case, the suppression becomes very large, more than a factor 10 at  $z > 0.5$ , thus violating the  $\Delta E \ll E$  limit in which all the formalisms have been derived.

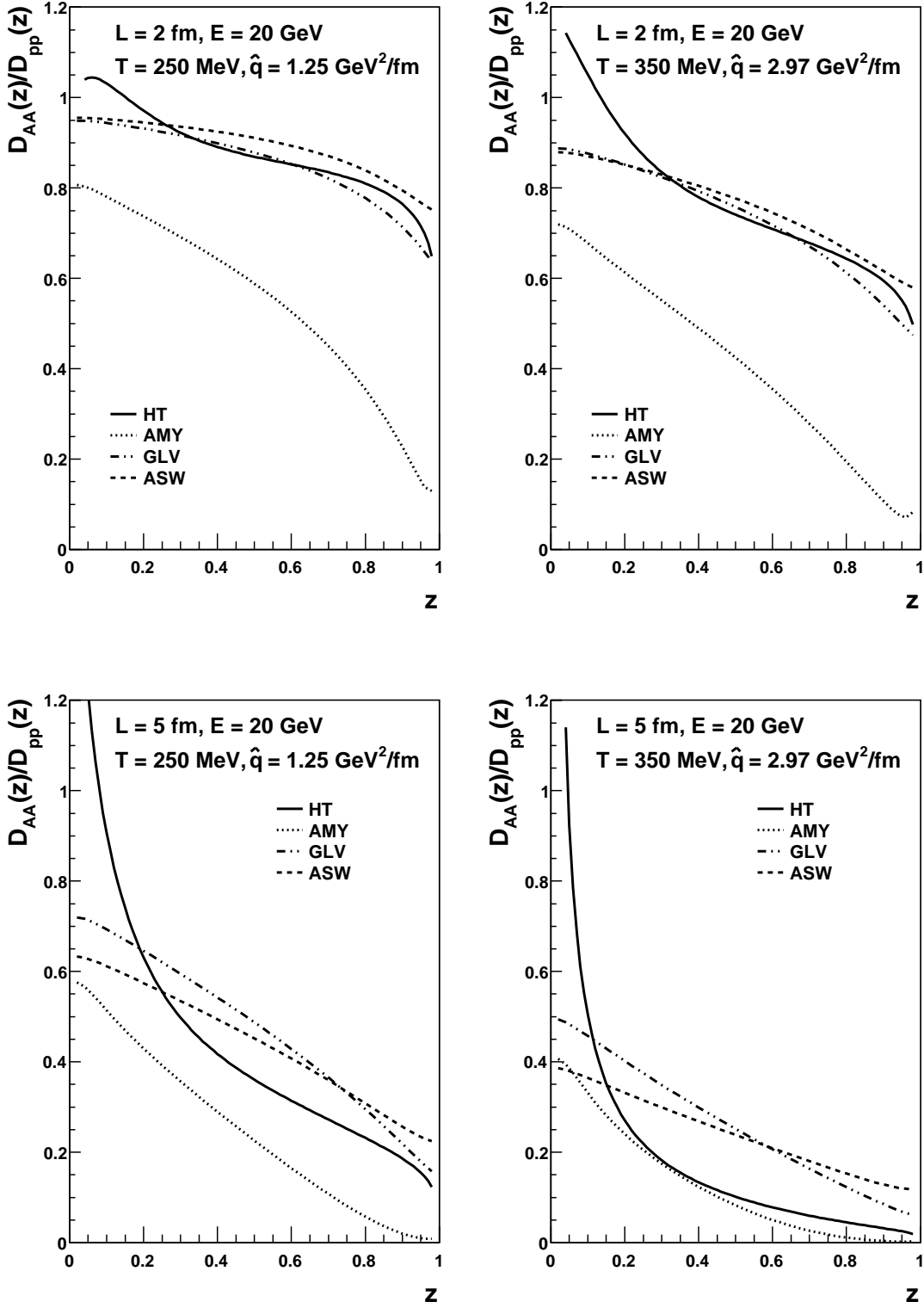


Figure 10: Comparison of quark fragmentation function ratios using four different formalisms for a uniform medium with  $L = 2$  fm (upper panels) and  $L = 5$  fm (lower panels). For both upper and lower panels the left plot is at  $T = 250$  MeV and the right plot is at  $T = 350$  MeV. For details, see text.

## 4 Heavy flavors and elastic energy loss

In the preceding chapters we explicitly discussed the case of light quark and gluon energy loss. It is now almost established that for light partons, transverse scattering induced radiative energy loss, plays a dominant role (see Section 6.4.5). There is, however, an entirely orthogonal mechanism: elastic energy loss. While the nomenclature is somewhat confusing, this refers to a process where the jet transferred energy and momentum to a constituent of the medium and the interaction with the medium did not stimulate the jet to radiate a hard gluon, i.e., it was not inelastic for the jet. On the medium side, the effect may be both elastic or inelastic. We should point out that existing calculations of elastic energy loss [70, 71, 72, 39] have focused specifically on 2-to-2 scattering, where the medium parton also stays more or less on shell.

For heavy quarks, radiative energy loss is much reduced, due to the dead cone effect, which suppresses collinear radiation. As a result, elastic energy loss may be more important for heavy quarks than for light quarks. In the remaining part of this chapter we will review the dead cone effect and how it reduces the energy lost by a hard heavy quark. Following this we will consider the inclusion of elastic energy loss within the jet modification formalism.

### 4.1 Dead cone effect in radiative energy loss

Imagine a hard heavy quark produced in a DIS event about to radiate a hard gluon. Physically this will occur in a process where a hard heavy quark in the nucleon (produced in large  $Q^2$  fluctuation) is struck by the virtual photon. An alternative to this process is when the incoming electron encounters a charge current interaction via a  $W^-$  exchange which converts a  $u$  quark in the nucleon to a  $b$  quark. In the interest of simplicity and given the factorization of final state effects from the hard cross section and the initial PDF, we ignore the specifics of the charge current interaction and only focus on the final state radiation of a hard gluon from the produced heavy quark.

The simplest means to see the effect of the mass of the heavy quark is to introduce a mass  $M$  in the fermion propagators in Eq. (23). This converts the equation to

$$\begin{aligned} \mathcal{O}^{00} = \text{Tr} \left[ \frac{\gamma^-}{2} \widehat{\mathcal{O}}^{00} \right] &= \int \frac{d^4 l}{(2\pi)^4} d^4 z d^4 z' \frac{d^4 l_q}{(2\pi)^4} \frac{d^4 p_0}{(2\pi)^4} \frac{d^4 p'_0}{(2\pi)^4} e^{iq \cdot y_0} e^{-i(p_0+q) \cdot (y_0-z)} e^{-il \cdot (z-z')} e^{-il_q \cdot (z-z')} e^{-i(p'_0+q) \cdot z'} \quad (75) \\ &\times g^2 \text{Tr} \left[ \frac{\gamma^-}{2} \frac{-i(\not{p}_0 + \not{q} + M)}{(p_0 + q)^2 - M^2 - i\epsilon} i\gamma^\alpha (\not{l}_q + M) 2\pi \delta(l_q^2 - M^2) G_{\alpha\beta}(l) 2\pi \delta(l^2) (-i\gamma^\beta) \frac{i(\not{p}'_0 + \not{q} + M)}{(p'_0 + q)^2 - M^2 + i\epsilon} \right]. \end{aligned}$$

Carrying out the integrations over  $z$  and  $z'$  yields the usual constraints,  $l_q = p_0 + q - l$  and  $p_0 = p'_0$ . These are used to perform the  $p'_0$  and  $l_q$  integrals. The difference with the case of the light quarks are essentially the factors of  $M$  that appear in the denominators, in the Dirac matrix structure and in the on-shell constraint  $\delta(l_q^2 - M^2)$ . The argument of the  $\delta$ -function may be simplified as (using  $l_q = p_0 + q - l$  and  $l$  is on-shell),

$$\begin{aligned} 2p_0^+ q^- + 2q^+ q^- + 2p^+ l^- + 2q^+ l^- + 2q^- l^+ - M^2 &= 0 \\ \Rightarrow 2P^+ q^- \left( x_0(1-y) - x_B(1-y) - \frac{l_\perp^2}{y} - M^2 \right) &= 2P^+ q^- (1-y) [x_0 - x_B - x_L - x_M]. \quad (76) \end{aligned}$$

Where,  $x_L = l_\perp^2 / 2P^+ q^- y(1-y)$  has the usual definition, while,  $x_M = M^2 / 2q^- P^+(1-y)$ .

To simplify the trace, we take the small  $y$  limit i.e., the soft gluon limit, which reduces this expression to a form similar to that of Eq. (19). In this limit, the only projection of the gluon propagator that has

to be retained is  $G^{++} = l_{\perp}^2/(q_{\perp}^2)$ . As a result, one only needs to retain the terms proportional to  $\gamma^-$  in the gluon emission vertices. This simplifies the trace over Dirac matrices:

$$\text{Tr} \left[ \frac{\gamma^-}{2} q^+ q^- \gamma^- \gamma^+ q^- \gamma^- \gamma^+ q^- \right] = 8q^{-3}. \quad (77)$$

With these simplifications, the operator  $\mathcal{O}^{00}$  [defined for the case of light quarks in Eq. (23)] which is directly proportional to the cross section may be expressed as,

$$\mathcal{O}^{00} = \frac{\alpha_s C_F}{2\pi} \int dy \frac{2}{y} \frac{l_{\perp}^2}{(l_{\perp}^2 + y^2 M^2)^2} \quad (78)$$

Defining the angle of radiation as  $\theta = l_{\perp}/\omega^-$  where  $\omega^- = q^- y$ , and the mass dependent angle  $M/\omega^-$  as  $\theta_0$  we obtain the gluon radiation distribution to be

$$\frac{dN_{Q \rightarrow Qg}}{d\theta^2} = \frac{\alpha_s C_F}{\pi} \frac{d\omega^-}{\omega^-} \frac{\theta^2}{(\theta^2 + \theta_0^2)^2} = \frac{dN_{q \rightarrow qg}}{d\theta^2} \left( 1 + \frac{\theta_0^2}{\theta^2} \right)^{-2}, \quad (79)$$

where  $dN_{q \rightarrow qg}/d\theta^2$  is the angular distribution from a light quark which has a logarithmic divergence as  $\theta \rightarrow 0$ . The angular distribution of gluon radiation from the heavy quark is cut off at small angles. This is called the dead cone effect [73]. The origin of this effect is essentially the shielding of the collinear singularity by the large mass of the quark. Since gluon radiation from quarks occurs dominantly at smaller values of  $l_{\perp}$ , the suppression of radiation in this region by the mass of the quark, leads to a smaller amount of radiative energy loss from a heavy quark compared with a light quark.

In the case of gluon radiation from multiple scattering there will be multiple instances of the heavy quark mass as there will be multiple quark propagators. So far, the calculation of medium induced gluon radiation from a heavy quark has only been performed up to one scattering per radiation in the HT formalism [74, 75], up to 1<sup>st</sup> order in opacity in a variant of the GLV approach (called the DGLV) [50] and in the multiple soft scattering approximation of the ASW approach [45]. As in the case of light flavors we will follow the derivation in the higher twist approach. The expression for the radiated gluon distribution from a massive quark is given, following Ref. [74] as a shift in the formation time  $\tau_f$  of the radiated gluon and an overall multiplicative factor  $f$  as,

$$\tau_f = \frac{2q^- y(1-y)}{l_{\perp}^2 + y^2 M^2}, \quad \text{and} \quad f = \frac{l_{\perp}^8}{[l_{\perp}^2 + y^2 M^2]^4}. \quad (80)$$

In both the GLV and the HT calculations, the above factors lead to a considerable reduction in the amount of energy loss by radiation of gluons. This has led to the realization that other sources of energy loss, such as elastic energy loss, which is a smaller effect for light partons, may be more important in the case of heavy quarks.

While the radiative energy loss calculations in the GLV, HT and ASW schemes have all been modified to incorporate the effect of the heavy quark's mass, it was found that in all three cases, purely radiative processes cannot describe the observed suppression in the yield of non-photonic electrons from  $D$  and  $B$  meson decay (see also Section 6.4.7. Attempts to incorporate elastic energy loss within the energy loss formalism and describe the heavy flavor suppression have been carried out by the DGLV and the HT schemes. In the last section of this chapter we will describe the inclusion of elastic energy loss in jet modification calculations.

## 4.2 Longitudinal drag and diffusion: other transport coefficients



In the derivation of the multiple scattering of a hard parton and the ensuing gluon radiation in Chapter 2, we specialized to the case where the negative light-cone momentum of the exchanged gluon was assumed to be vanishingly small, i.e.,  $k^- \rightarrow 0$ . All factors of the exchanged negative light-cone momenta  $k_i^-$  were ignored from the expressions and this led to the restriction of the entire process to the  $y^+ = 0$  plane. In reality, depending on the structure of the dense medium with which the jet interacts, one can have a non-vanishing amount of  $k^-$  exchanged. This is true not only for a massive quark but also for light partons. In this section we derive the leading correction to the differential cross section for a hard light quark travelling through a large nucleus encountering multiple scattering which may change both its transverse as well as its longitudinal momentum. These may then be easily extended to the case of a heavy quark. The final expression will be written in a factorized form where the hard dynamics of the quark propagation will be separated from the in-medium expectation of gluonic operators which will codify the respective in-medium transport coefficients. Once defined in such a factorized form, the results may be immediately extended to the case of jets in a heavy ion collision by replacing the hard production cross section in DIS with that in  $A$ - $A$  and replacing the transport coefficients with those calculated in a hot deconfined environment. In real comparisons to date, these are often fitted to light hadron production data points.

The reader may wonder about the focus on light cone loss as opposed to actual energy loss. This emanated from our insistence on defining as boost invariant a quantity as possible. For a large magnitude of energy loss in an extended time  $\Delta t$ , the measure  $\Delta E/\Delta t$  changes with boost, but the light cone ratio is boost invariant:

$$\frac{\Delta q^-}{\Delta L^-} = \frac{\Delta E - \Delta p_z}{\Delta t - \Delta z} \xrightarrow{\text{boost}} \frac{\gamma(1 - \beta)(\Delta E - \Delta p_z)}{\gamma(1 - \beta)(\Delta t - \Delta z)}. \quad (81)$$

Starting again from the case of DIS on a large nucleus, we now define the triple differential distribution for the hadronic tensor for the case of no rescattering and no final state radiation where a quark with  $x_B$  momentum fraction is struck by a hard virtual photon and sent back through the nucleus as

$$\frac{d^3 W_0^{\mu\nu}}{d^2 l_{q\perp} dl_q^-} = W_0^{\mu\nu} \delta^2(\vec{l}_{q\perp}) \delta(l_q^- - q^-), \quad (82)$$

where  $W_0^{\mu\nu} = -g^{\mu\nu} 2\pi \sum_q Q_q^2 f_q^A(x_B)$ . The two  $\delta$ -functions indicate that the three momentum components of the outgoing quark have a narrow distribution around  $l_q^- \sim q^-$ , the large light cone momentum of the incoming photon, and  $l_{q\perp} \sim 0$ . Being close to onshell,  $l^+ \simeq l_{\perp}^2/2l^-$

Considering the case of one scattering, the modified differential distribution may be expressed as

$$\begin{aligned} W^{\mu\nu} &= W_0^{\mu\nu} g^2 \int \frac{dl^- d^2 l_{\perp}}{(2\pi)^3} dY^- dy^- dy^+ d^2 y_{\perp} \frac{dk^- d^2 k_{\perp} (2\pi)^3 \delta(l^- - q^- - k^-) \delta^2(\vec{l}_{\perp} - \vec{k}_{\perp})}{(2\pi)^3} \frac{\mathbf{Tr}[t^a t^b]}{N_c} \\ &\times \frac{\mathbf{Tr}}{4} \left[ \gamma^+ \gamma^\alpha \left\{ (\not{q} + \not{k}^-) + \frac{\gamma^- k_{\perp}^2}{2(q^- + k^-)} - \not{k}_{\perp} \right\} \gamma^\beta \right] \exp \left[ -i \frac{k_{\perp}^2}{2q^-} (y^-) + i y_{\perp} \cdot k_{\perp} - i y^+ k^- \right] \\ &\times \langle P | A_\alpha^a(Y^- + y) A_\beta^b(Y^-) | P \rangle. \end{aligned} \quad (83)$$

One immediately notices the shifts in the three  $\delta$ -functions which describe the final outgoing quark distribution. These are, as expected, proportional to the expectation of the two gluon operator in the nucleus. The Dirac structure is obvious from the fact that the quark immediately after the hard scattering on the virtual photon is almost on shell in both the amplitude and the complex conjugate and has a magnitude only in the negative light cone direction  $l = (0, q^-, 0)$ . The cut line emanates after the scattering and has a momentum  $[k^+, q^- + k^-, k_{\perp}]$  with  $k^+ = k_{\perp}^2/2(q^- + k^-)$ . We make the same set of approximations on the gauge fields as for the case of transverse broadening, i.e.,  $A^+ \gg A_{\perp}$  (recall that we are calculating in  $A^- = 0$  gauge) as in Section 2.2.

Given the scaling of the  $A^{a\mu}$  field, we obtain that the dominant contribution in the Dirac trace as given by

$$\mathbf{Tr} [\gamma^+ \gamma^- \gamma^+ (q^- - k^-) \gamma^-]. \quad (84)$$

In the case of transverse broadening, one Taylor expands in  $k_\perp$ ; to obtain the distribution in light cone momentum one Taylor expands in  $k^-$ . In the interest of simplicity, we will ignore the factors of transverse momentum and simply focus on the light cone components. Taylor expanding the hard part, we obtain that the leading terms emanate from the expansion of the  $\delta$ -function,

$$\delta(l^- - q^- - k^-) = \delta(l^- - q^-) - \frac{\partial \delta(l^- - q^-)}{\partial l^-} (k^-) + \frac{1}{2} \frac{\partial^2}{\partial l^{-2}} \delta(l^- - q^-) [k^-]^2 + \dots \quad (85)$$

Unlike the case of transverse broadening there is no cylindrical symmetry to insist that the term proportional to  $k^-$  is vanishing. One thus obtains two sets of terms involving derivatives of the  $\delta$ -function, one which involves single derivatives, which lead to a drag effect on the light-cone momentum distribution and the other which depend on double derivatives which lead to a diffusion in the light cone momentum. The coefficients of these terms will yield the elastic light-cone loss per unit light cone length  $\hat{e}$  and the diffusion in light-cone loss  $\hat{e}_2$ .

The coefficient of the the single derivative of the  $\delta$ -function may be simplified as,

$$C_1 = \int dY^- d^4 y \frac{dk^- d^2 k_\perp}{(2\pi)^3} e^{-i \frac{k_\perp^2}{2q} y^- - ik^- y^+ + ik_\perp \cdot y_\perp} \frac{4\pi\alpha}{2N_c} \langle P | [i\partial^- A^{a+}(y) A^{a+}(0)] | P \rangle. \quad (86)$$

In the equation above  $|P\rangle$  represents the nuclear state. We have dropped the  $Y^-$  in the arguments of the gluon field based on translation invariance in a large nucleus. Color confinement insists that the quark struck by the hard virtual photon emanate from the same nucleon in both the amplitude and complex conjugate. Similarly the gluon off which the outgoing quark scatters must also be restricted to the same nucleon in both the amplitude and complex conjugate. In the model of a nucleus made up of almost free nucleons (in the high energy limit), the correlation between these two nucleons is  $\rho(y^-)/2p^+$  where  $\rho$  is the nucleon density evaluated along the path of the propagating out-going quark and  $p^+$  is the mean light cone momentum of a nucleon in the nucleus  $p^+ = P^+/A$ .

Incorporating the above simplifications one obtains the light-cone loss per unit light cone path travelled by a struck quark without radiation in cold nuclear matter as  $\hat{e} \simeq C_1$ . In the case of hot deconfined matter the light-cone loss per unit path is obtained by generalizing the expression in cold matter as

$$\hat{e}_{hot} = \frac{4\pi\alpha_s \int dy^- \langle n | e^{-\beta \hat{H}} [i\partial^- A^{a+}(y^-) A^{a+}(0)] | n \rangle}{2N_c}. \quad (87)$$

Where  $|n\rangle$  is a state in the thermal ensemble. In writing the above equation, we have made use of the boost invariance of the derived expressions along the direction of the jet. Unlike the expression for  $C_1$  which is derived in the Breit frame, Eq. (87) is intended in the rest frame of the medium. In this frame, one relates the light cone loss to the energy lost by a hard jet per unit length, for a jet traveling in the  $-z$  direction

$$\frac{dq^-}{dL^-} \sim \frac{dE + |dp_z|}{dt + |dz|} = \frac{dE(1 + |v|^{-1})}{|dz|(|v|^{-1} + 1)} = \frac{dE}{|dz|}. \quad (88)$$

The other transport coefficient of importance to the light-cone or longitudinal propagation of a hard jet without radiation is obtained from the double derivative of the  $\delta$ -function in Eq. (85). This yields the diffusion in the light cone momentum per unit light cone path, denoted as the coefficient  $\hat{e}_2$ :

$$\hat{e}_2 = \frac{4\pi\alpha \int dy^- \langle n | e^{-\beta \hat{H}} [F^{a-+} F^{a-+}] | n \rangle}{2N_c}, \quad (89)$$

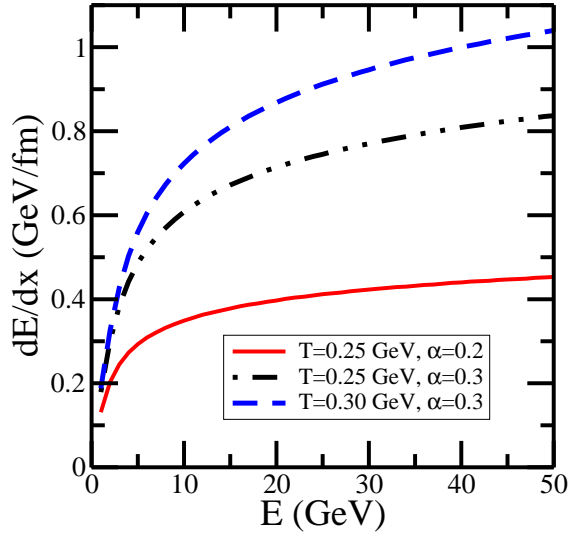


Figure 11: The drag experienced by a hard quark jet in an HTL plasma. Figure adopted from Ref. [76].

Calculating the change in the light-cone fraction of the leading parton due to only these two coefficients amounts to incorporating a drag and a diffusion term in the energy distribution of the hard parton. This is often referred to as the Gaussian approximation with the location of the peak of the Gaussian given by  $\hat{e}$  and the width given by  $\hat{e}_2$ .

While operator products, in general, are evaluated at the hard scale at which they interact with the jet, they may be calculated at the scale of the medium if there exists a well defined microscopic model of the medium. These may then be evolved up to the hard scale of the jet. For example, for an HTL plasma, the elastic loss coefficient may be evaluated as

$$\hat{e} = 4\pi\alpha_s \int_0^{Q_{MAX}^2} \frac{d|\vec{k}|^2}{2\pi} \int_0^1 \frac{dx |\vec{k}|^2 (-x)(1-x^2)(N_c^2 - 1)}{4N_c} \left[ \left\{ \rho_T(|\vec{k}|, k^0) - \rho_L(|\vec{k}|, k^0) \right\} \{1 + n_B(k^0)\} \right]_{k^0 = -|\vec{k}|_x} \quad (90)$$

The equation above is obtained by evaluating Eq. (87) in the HTL limit. The factors  $\rho_L$  and  $\rho_T$  are the longitudinal and transverse HTL spectral densities (see Ref.[76] for details). The limits of the integral  $Q_{MAX} = \sqrt{ET}$  is set identically as for the calculation of  $\hat{q}$  in an HTL medium. The elastic energy loss experienced by a hard jet with energy  $E$  propagating through an HTL plasma at a variety of temperatures and couplings are presented in Fig. 11.

With the discussion of elastic energy loss we complete the theoretical section of this review. In the remaining, we will outline the phenomenological modeling of the media encountered in jet modification experiments and review the main experimental measurements.

## 5 Parton energy loss in collisions: modeling of the medium

Experimental measurements of parton energy loss are performed in cold nuclear matter ( $eA$  and  $pA$  collisions) and in hot nuclear matter produced in heavy ion collisions. In the experiment, the matter density is not uniform. In heavy ion collisions, there is a strong longitudinal expansion which causes a rapid decrease of the medium density. In addition, the point of origin of the hard parton within the matter is not known and therefore has to be integrated over. Due to these effects, it is necessary to include some form of averaging over the collision geometry in parton energy loss calculations when comparing to experimental results.

We will first discuss the relevant aspects of the collision geometry, before turning to a more detailed discussion of the geometry averages used in the various calculations.

### 5.1 Nuclear overlap geometry

In central high-energy nuclear collisions, all of the incoming nucleons traverse the entire nucleus that moves in the opposite direction. The collision can be conveniently modeled in the approximation where the incoming nucleons travel along straight lines.

The density distribution of nucleons in the nucleus follows the Woods-Saxon density profile [77]:

$$\rho(\vec{r}) = \frac{\rho_0}{1 + \exp \frac{|\vec{r}| - R}{d}},$$

where  $R$  is the radius of the nucleus and  $d$  is the 'skin depth';  $\rho_0$  is a normalization constant, such that the integrated density is equal to the atomic number  $A$ . The density in the transverse plane, the thickness function  $T$ , is then

$$T(\mathbf{s}) = \int dz \rho(z, \mathbf{s}),$$

where  $z$  is along the longitudinal direction and  $\mathbf{s}$  is a vector in the transverse plane.

In a collision of two nuclei, the transverse distance between the centers of the nuclei is called the impact parameter  $b$ . Using the transverse impact vector  $\mathbf{b}$ , we define the thickness function for the overlapping nuclei  $T_{AB}$  and the collision density  $\rho_{coll}$ :

$$T_{AB}(\mathbf{s}) = T_A(\mathbf{s} - \frac{1}{2}\mathbf{b}) \times T_B(\mathbf{s} + \frac{1}{2}\mathbf{b}) \quad \text{and} \quad \rho_{coll} = T_{AB} \sigma. \quad (91)$$

Another measure of the overlap is the participant density

$$\rho_{part}(\mathbf{s}) = T_A(\mathbf{s} - \frac{1}{2}\mathbf{b}) \cdot \left( 1 - e^{-T_B(\mathbf{s} + \frac{1}{2}\mathbf{b}) \sigma} \right) + T_B(\mathbf{s} + \frac{1}{2}\mathbf{b}) \cdot \left( 1 - e^{-T_A(\mathbf{s} - \frac{1}{2}\mathbf{b}) \sigma} \right). \quad (92)$$

$T_A$  and  $T_B$  are thickness functions of the two colliding nuclei and  $\sigma$  is the cross section for the process one is interested in. By integrating these two densities over the transverse coordinate  $\mathbf{s}$  and taking  $\sigma$  as the total inelastic cross section we obtain the total number of binary (inelastic) collisions  $N_{coll}(b)$  and the total number of participants  $N_{part}(b)$ , the number of nucleons that had at least one (inelastic) collision at a given impact parameter  $b$ .

The number of participants and the number of binary collisions are the limiting cases of scaling of the particle production in heavy ion collisions, in a way that is related to the production cross section.

- *Participant scaling* occurs for large-cross section processes, where every nucleon can produce particles at most once. This is also called wounded nucleon scaling [78]. The multiplicity distribution in Au+Au collisions at RHIC follows this limit rather closely.

- *Collision scaling* occurs for small cross section processes, where every individual encounter between two nucleons contributes the same probability to the total production cross section. High- $p_T$  production of non-interacting probes at RHIC (photons) follows this limit (see Section 6.4).

In parton energy loss models,  $\rho_{part}$  or  $\rho_{coll}$  can be used as a first approximation for the medium density profile. Since the soft particle production scales more closely with the number of participants,  $\rho_{part}$  is the most intuitive choice for a medium density profile. The distribution of initial hard scatterings, which are the points of origin for the partons that traverse the medium, is expected to follow  $\rho_{coll}$ .

In the above, we have used a continuum approach, the ‘optical limit’, where the nuclei are modeled as smooth density profiles. Alternatively, one can model the collisions with localized nucleons leading to a non-uniform density. This leads to important fluctuations of the density profile in peripheral collisions. For more details we refer the reader to [79] and references therein.

The density profiles discussed above are suitable descriptions of the initial state geometry. The initial state density profile has pressure gradients that will lead to expansion, both in the transverse and longitudinal direction. In an expanding medium, the density decreases with time. The dominant effect is longitudinal expansion, which results in a density decreasing approximately as  $1/\tau$ , where  $\tau$  is the proper time. Transverse expansion also leads to a reduction of the local density, but at same time increases the system size, so that the overall effect on energy loss observables is smaller. Transverse and longitudinal expansion can be modeled using hydrodynamic evolution.

## 5.2 Modeling the produced matter: hydrodynamic evolution

Relativistic fluid dynamics at low viscosity has emerged as the leading theoretical setup with which to describe the space-time evolution of the soft produced matter at RHIC. Global fits of a number of simulations to the experimental data have placed an upper bound on ratio of the viscosity  $\eta$  to the entropy density  $s$  to be at most five times the absolute minimum allowed from quantum mechanics and predicted by the AdS/CFT conjecture [80]:

$$\frac{1}{4\pi} \leq \frac{\eta}{s} \leq \frac{5}{4\pi}. \quad (93)$$

Even ideal hydrodynamics where  $\eta = 0$  yields a more or less consistent description of the soft spectrum [81]. In these simulations, one solves the local differential equation,

$$\partial_\mu T^{\mu\nu}(x, y, z, t) = 0, \quad (94)$$

where,  $T^{\mu\nu}$  is the energy momentum tensor, for the ideal case:

$$T^{\mu\nu} = (\epsilon + p) u^\mu u^\nu - p g^{\mu\nu}. \quad (95)$$

In the equation above,  $\epsilon$  is the local energy density,  $p$  is the local pressure and  $u$  is the fluid four velocity. The energy density is related to the pressure by the equation of state which is usually obtained by parametrizing lattice results. The set of equations are solved with the additional constraint of local baryon number conservation,

$$\partial_\mu (n_B u^\mu) = 0. \quad (96)$$

A solution to the equations also requires a starting proper time  $\tau_0$ . Fits to data have placed this around  $\tau_0 = 0.6 \text{ fm}/c$ . One also requires an initial configuration for the energy density and the baryon number density as a function of both the transverse location as well as the longitudinal location or rapidity. In the calculations presented in this review,  $\epsilon$  and  $n_B$  were assumed to scale with each other

with an overall normalization fit from experimental data. For the energy density, one assumes the impact parameter dependent profile.

$$\epsilon(\tau_0, \mathbf{s}, \eta) = \epsilon_{MAX} \rho(\mathbf{s}; b) H(\eta). \quad (97)$$

Based on the equation of state and lattice data, the initial energy density can be related to the entropy density which may then be inferred from the produced multiplicity. The normalization of the the Baryon number density is also obtained by fitting to the final experimental data on  $p/\pi$  ratios. The transverse profile  $W(x, y; b)$  is obtained as a combination of the wounded nucleon density and the binary collision density. In 2+1 D hydrodynamics, the rapidity profile is assumed to be a constant while in 3+1 D simulations it is assumed to be a broad Gaussian, given by the form  $H(\eta) = \exp(-(\eta)^2/(2\sigma_\eta^2))$  with the width  $\sigma_\eta$  set from experimental data.

The solution of the fluid dynamical equations results in a space-time profile of the energy momentum tensor and, as a result, of the energy density and pressure. As the temperature drops below the transition temperature, one enters the hadronic phase, at this point either the fluid dynamical simulation is continued with the hadron gas equation of state or one may switch to a hadronic cascade such as URQMD [82]. Eventually as the temperature drops below the kinetic freezeout temperature the hadrons have to be decoupled from the calculation. In the case where hydrodynamics is continued into the hadronic phase, one uses a Cooper-Frye prescription [83] to convert the energy and momentum density in a unit cell into a distribution of free hadrons.

The various input parameters along with the initial thermalization time  $\tau_0$  and final freezeout time are dialed to obtain the best fit with experimental data on soft hadrons of various flavors and from various centralities. Once all these parameters have been set, the space-time profile of the energy density can be used to calculate the quenching of hard jets.

### 5.3 Energy loss in a non-uniform medium

Hard partons are produced at all locations in the transverse plane, with a probability distribution following  $\rho_{coll}$  and no preference in azimuthal angle, and then propagate through the dense matter undergoing energy loss. In order to take into account the non-uniform, dynamic medium, one has to integrate over all production points and azimuthal angles, taking into account the medium density profile that the partons experience along their path out of the medium.

All energy loss formalisms contain an integral over the scattering centers that the partons encounter along their paths. To obtain analytical results, the medium density profile is assumed to be either uniform or of a specific analytical shape (*e.g.* exponential decay in GLV). For a non-uniform medium, one can evaluate the full integral over the non-uniform medium density for every parton. This is what was done in the case of the HT formalism in [84].

For the ASW and GLV approaches, analytical results have been derived for a homogeneous expanding medium, where the density falls as  $1/\tau$  along the path length [30, 44, 85]. It has been shown in that in the infinite-energy regime those analytical results are well approximated by

$$\Delta E \propto \int dx x \hat{q}(x), \quad (98)$$

where  $\hat{q}(x)$  is a local transport coefficient and  $x$  is a coordinate along the path of the parton. Note that the integral is equal to  $\frac{1}{2}\hat{q}L^2$  for a uniform medium. In addition to the scaling of the average energy loss, it has also been shown that in the homogeneous expanding medium, the differential gluon emission spectrum can be approximated using the calculation for a homogeneous static medium with effective transport coefficient [44]

$$\hat{q}_{\text{eff}} = \frac{2}{L} \int_{x_0}^{x_0+L} dx x \hat{q}(x).$$

This is often referred to as the 'dynamical scaling law'. A more general version of this scaling law was recently derived in [86].

To calculate energy loss in a non-uniform, dynamical medium using the ASW formalism, it is assumed that the dynamical scaling law can be extended to this scenario. The first example of such a calculation is the Parton Quenching Model (PQM) by Dainese, Loizides and Paic [87], where  $\rho_{coll}$  was used based on saturation model arguments [88]. More recent calculations use a hydrodynamical medium and where the local  $\hat{q}(x)$  is proportional to the temperature  $T^3$ , energy density  $\epsilon^{3/4}$  or the entropy density  $s$  [84, 89, 90].

The AMY energy loss calculation is carried out in the finite temperature field theory approach and therefore directly relates the energy loss to the temperature  $T$ . In a hydrodynamical evolution, the local temperature  $T$  is known. The rates for a hard parton to decay into a quark or a gluon are then calculated using the local temperatures and the change in the distribution is computed using the Fokker-Planck equation over all paths [38, 84].

## 5.4 Calculating observables

Now we have all the ingredients for a calculation of parton energy loss that can be directly compared to experiment. For example, to calculate the nuclear modification factor  $R_{AA}$ , one starts from the factorised calculation in the vacuum, Eq. (4). Parton energy loss is then included by substituting the vacuum fragmentation function with the medium-modified fragmentation function, which is given in Section 3, averaged over the medium density profile, as explained in the previous section. In general, the average over the medium density profile involves integrating out the parton production point and direction.

In the next Chapter, we will compare energy loss calculations to experimental data on the nuclear modification factor  $R_{AA}$  for light and heavy hadrons, and di-hadron and  $\gamma$ -hadron measurements. The di-hadron measurements involved pairs of partons, which are produced at a single point in the medium and then propagate outward in opposite directions in the transverse plane (back-to-back). As a result, the pathlength and density profile that both partons see are not independent. For example, if the pair originates from the periphery of the collisions zone and travels outward, one parton is likely to see a long pathlength in the dense medium, while the other will see a short pathlength. These correlations have to be included in the model calculations as well.

Early comparisons of energy loss calculations to experimental data were based on a simplified medium geometry, using hard spheres or cylinders [91, 92, 93], instead of the Woods-Saxon geometry in Eq. (5.1) and no hydrodynamical evolution. There are also calculations using a Woods-Saxon overlap geometry, without hydrodynamical evolution [87, 66]. These are more realistic than the hard-sphere geometries in the sense that they include the low-density regions at the edge of the nuclei. In this review, we will focus on calculations which sample the space-time evolution using a hydrodynamical calculation for the medium density evolution [89, 84, 90].

## 6 Comparison to experiment

### 6.1 Choosing observables

In the following, we review a selected set of experimental data and compare to energy loss calculations to show how the measurements constrain the energy loss formalisms and the properties of the medium.

A wealth of different measurements have been performed to provide insight in the energy loss mechanism. In general, care should be taken to select observables that are sensitive to the process that one wants to investigate. This selection process requires a careful exchange of ideas between theory and experiment. For example, the first measurements at RHIC of the nuclear modification factor [2, 3] and di-hadron correlations (disappearance of the away-side jet) [94] have clearly shown that energy loss is large. It was subsequently realised, however, that a variety of models can describe the data, because these measurements are not very sensitive to the details of the energy loss distribution. It has been shown that it is in practice impossible to extract the energy loss probability distribution from such measurements [95] even if the experimental uncertainties would be exceedingly small. It is therefore key to identify observables that are sensitive to specific aspects of the energy loss process. For example, it has been argued that comparing the away-side suppression to the single hadron suppression allows to determine the path-length dependence of energy loss ( $L$  vs  $L^2$ ) [96].

In Figure 10 it was shown that the different formalisms for parton energy loss calculations predict different medium modified fragmentation functions. Such differences can only be determined from experiments if the initial parton energy can be controlled or measured. This technique has been used successfully in Deeply Inelastic Scattering experiments off nuclei to measure parton energy loss in cold nuclear matter (see Section 6.3.1). In heavy ion collisions, there are two basic ways in which one can control the initial parton energy. One is to use  $\gamma$ -jet events (or  $Z^0$ -jet at LHC) where the transverse momentum of the photon and the initial parton (jet) are equal (as long as initial state broadening and higher order large angle radiations are negligible). The alternative is to reconstruct jets in the final state. To what extent the reconstructed jet energy is equal to the initial parton energy depends both on the jet reconstruction algorithm and on the effect of medium modifications on the jet. Several measurements are likely needed to disentangle various effects (jet spectra, jet fragmentation functions and away-side jet rates have been discussed).

The primary consideration when selecting observables should be the intrinsic sensitivity: the larger the effect of a given model aspect on the observed quantity, the more promising the observable is. This type of optimization is performed based on theoretical insight and model calculations.

A secondary consideration is the experimental precision. Experimental uncertainties vary from observable to observable, depending mainly on the cross section and the amount of background. Experience at RHIC shows that for the least complicated measurement, such as pion spectra, an experimental uncertainty in the 5-10% range can be reached. More complicated measurements, with larger backgrounds that cannot always be accurately modeled in heavy ion events, have correspondingly larger uncertainties. Further reduction of the uncertainties often requires a large effort, often requiring dedicated detector construction and calibration for a specific measurement, and is therefore only pursued by experiments if there are compelling theoretical reasons to do so (*e.g.* precision tests of the electroweak sector of the standard model). A few specific examples of how the experimental precision may evolve at RHIC are given in Section 6.5.

### 6.2 Perturbative QCD in p+p collisions

---

<sup>1</sup>The systematic uncertainties in this figure represent a single standard deviation for both STAR and PHENIX. The values in the STAR publication are the quadrature sum of several full ‘100%’ confidence intervals. Those values have been divided by  $\sqrt{3}$  to represent approximate single standard deviation intervals. No conversion was needed for the PHENIX



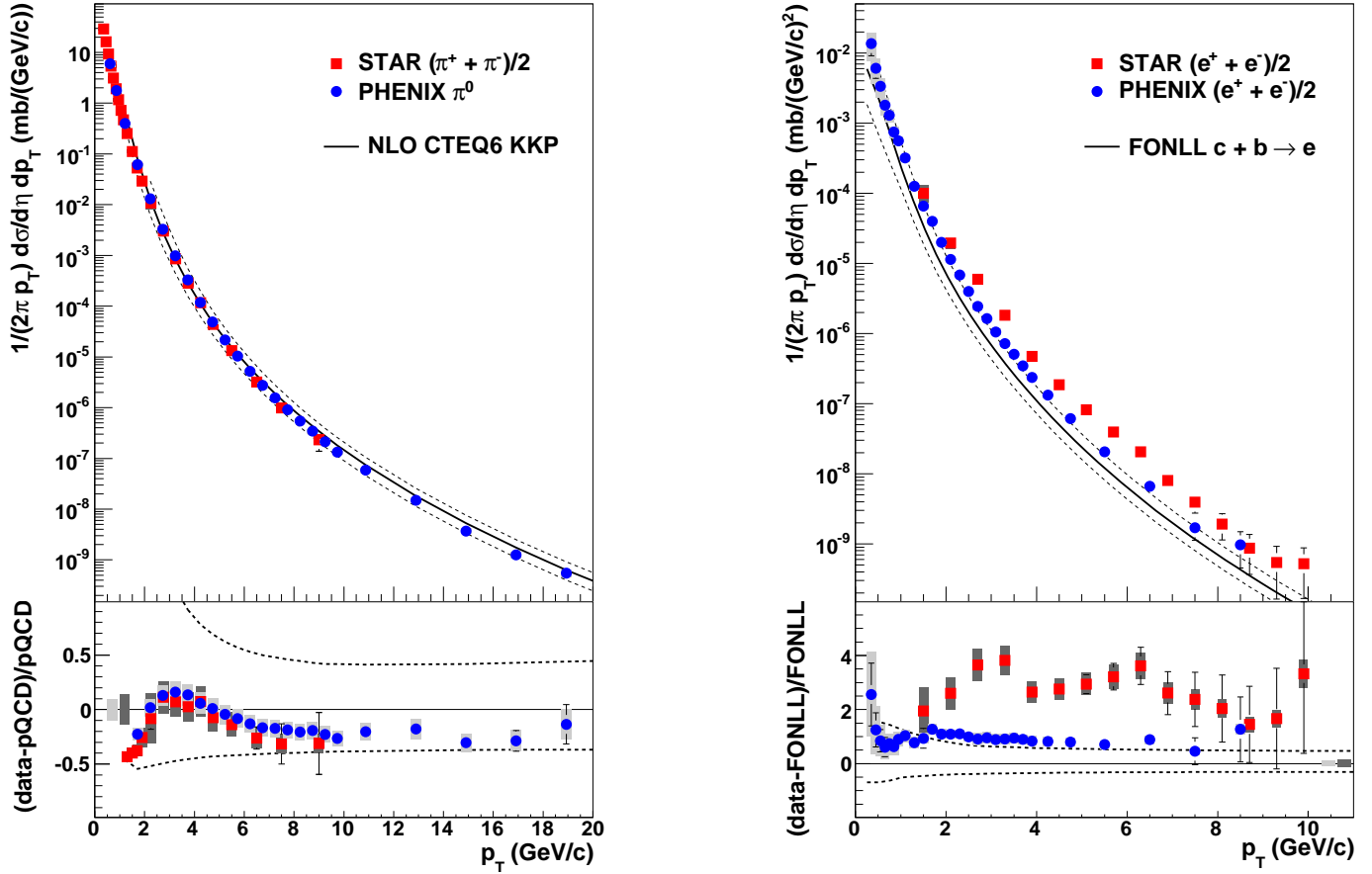


Figure 12: Left panel: Comparison of the  $\pi^0$   $p_T$ -spectrum in p+p collisions at  $\sqrt{s} = 200$  GeV as measured by PHENIX [97] and charged pions measured by STAR [98] to NLO pQCD calculations [11] at three scales  $\mu = p_T$  (solid line) and  $\mu = 0.5p_T$  and  $\mu = 2p_T$  (dashed lines). The uncertainty bars on the left side of the lower panel show the overall normalization uncertainty in the STAR (dark grey band) and PHENIX (light grey band) measurements. Right panel: Comparison of the  $p_T$ -spectrum of non-photonic electrons as measured by STAR [99] and PHENIX [100] <sup>1</sup> to a NLO pQCD calculation with resummed Next-to-leading logarithms (FONLL) [101]. The dashed lines indicate the uncertainty on the FONLL calculation, which is estimated by varying the factorization scale and the quark masses. The lower panels show the relative difference with the central curves. The normalisation uncertainty is indicated in the lower panel on the right.

Factorized perturbative QCD calculations have been compared extensively to experimental data on  $p$ - $p$  collisions at energies ranging from ISR  $\sqrt{s} \approx 60$  GeV to Tevatron energies  $\sqrt{s} = 1.9$  TeV [102, 103, 104, 105]. RHIC measurements at mid-rapidity generally agree well with perturbative QCD calculations. Two examples are shown in this section.

Figure 12 (left panel) shows a comparison of pion spectra measured by STAR and PHENIX, with STAR measuring charged pions in a Time Projection Chamber (TPC) [98] and PHENIX measuring neutral pions with an Electromagnetic Calorimeter (EMCal) [97]. The measurements are compared to Next-to-Leading Order (NLO) pQCD calculations by Jäger et al. [11], using the CTEQ6M parton density functions [9] and fragmentation functions by Kniehl, Kramer and Pötter (KKP) [106]. The measurements by STAR and PHENIX agree well with each other and with the NLO pQCD calculation. The uncertainties on the calculation are estimated by varying the factorization and renormalization scales between  $\mu = 0.5p_T$  and  $\mu = 2p_T$  and are indicated by dashed lines on the figure.

Heavy quark production is measured at RHIC via the semi-leptonic decays  $D \rightarrow e$  and  $B \rightarrow e$ . The inclusive electron distributions that are measured in the experiment contain substantial contributions from photon conversions and Dalitz decays of  $\pi^0$  and  $\eta$  mesons which are subtracted to obtain the ‘non-photon’ electron yield. The  $p_T$ -dependent inclusive cross section of non-photon electron production as measured by PHENIX [100] and STAR [99] in p+p collisions at  $\sqrt{s} = 200$  GeV are shown in the right panel of Fig. 12 and compared to NLO pQCD calculations including resummed Next-to-Leading Logarithms (FONLL) [101]. A large overall difference between the STAR and the PHENIX result is visible in the figure. The cause of this large difference is not yet known, but the effect is under active investigation by both experiments. The uncertainties on the theory expectation are estimated by varying the renormalization and factorization scale and the quark masses. The yields measured by PHENIX are larger than the nominal theory expectation, but close to the upper bound on the expectation. The STAR results are significantly above the theory expectation.

## 6.3 Cold nuclear matter effects

Before turning to nucleus-nucleus collisions to study parton energy loss in hot nuclear matter, we will briefly discuss the relevant effects in cold nuclear matter. We distinguish initial state and final state effects in cold nuclear matter. The dominant initial state effect is the modification of the parton density distribution in the nucleons, or the ‘EMC-effect’, named after the first experiment that measured this effect [107]. The most important final state effect is parton energy loss in cold nuclear matter, which has been found to be significant in the HERMES experiment [31]. Both effects are discussed below.

For completeness, we also mention here the ‘Cronin effect’, a possibly mass-dependent enhancement of hadron production at intermediate  $p_T$  in proton-nucleus collisions [108] which is generally attributed to transverse momentum broadening due to multiple scattering of partons on the nuclear target. For a recent review, see [109].

### 6.3.1 Energy loss in cold nuclear matter

Figure 13 shows a comparison the measured suppression of pions from fragmentation in cold nuclear matter in  $eA$  collisions by the HERMES experiment [31] with calculations using the BDMPS-ASW quenching weights (left panel) and the higher twist formalism (right panel). In deeply inelastic scattering experiments, the jet energy can be determined from the momentum vector of the scattered electron; the measurement is presented in terms of the momentum fraction  $z = E_h/\nu$  where  $E_h$  is the hadron energy and  $\nu$  the energy of the virtual photon. The extracted transport coefficient for the BDMPS quenching weights is  $\hat{q} = 0.6$  GeV<sup>2</sup>/fm in the center of the nucleus. Using the higher twist formalism, including the

---

data.

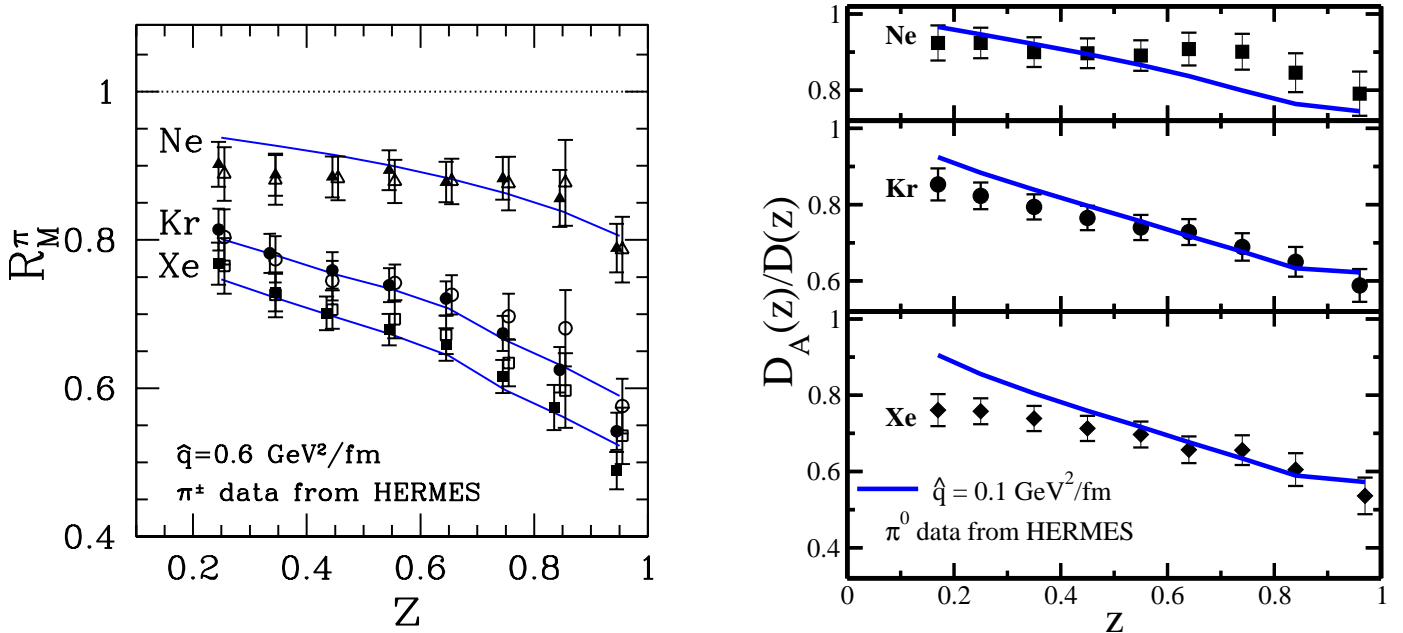


Figure 13: Comparison of the measured suppression of pion (full symbols  $\pi^+$ , open symbols  $\pi^-$ ) production in  $eA$  collisions by HERMES [31] with calculations using ASW-BDMPS quenching weights (left panel) and the higher twist formalism (right panel). Figures from [110] (©Societ Italiana di Fisica) and [111].

effect of multiple emissions, a quark  $\hat{q} \simeq 0.08 \text{ GeV}^2/\text{fm}$  is obtained. In an earlier calculation, involving only one emission in medium [91], a  $\hat{q} = 0.12 \text{ GeV}^2/\text{fm}$  was obtained [112].

### 6.3.2 Experimental study of initial state: d+Au

At RHIC, d+Au collisions are used to measure the effect of possible initial state effects on the pion and photon spectra. The left panel of Fig. 14 shows recent measurements of the nuclear modification factor  $R_{dAu}$  for  $\pi^0$  from PHENIX [115] and charged pions from STAR [116] and compares to calculations using a recent analysis of nuclear parton density functions (nPDF) (EPS09 [113] and HKN07 [117]). It should be noted that the DIS results do not fully constrain the nPDFs and the  $R_{dAu}$  measurement has been included in the determination of the nPDFs. The good agreement with the data therefore indicates that the measured values of  $R_{dAu}$  are consistent with the nuclear modification of PDFs which is measured in DIS off nuclei [107]. No significant final state interaction is apparent in the data.

The apparent absence of cold nuclear matter energy loss in the  $R_{dAu}$  in Fig. 14 at first sight is surprising, given the large suppression of hadron production at high momentum fraction  $z$  in the DIS data in Fig. 13. However, the  $d + Au$  results are at  $y = 0$  in the laboratory; in order to compare with the HERMES results, we boost to the rest frame of the nucleus where the jet with only a transverse momentum  $p_T$  at midrapidity has an extremely large energy due to the boost. The HERMES measurements show that the effect of energy loss reduces with jet energy [31] and is expected to vanish at the very high energy of the boosted jet. A detailed modeling of this effect is given in [109].

The right panel of Fig. 14 shows a comparison of the measured nuclear modification factor  $R_{dAu}$  for photons in d+Au collisions at RHIC ( $\sqrt{s_{NN}} = 200 \text{ GeV}$ ) with calculations including various cold nuclear matter effects [114]. The calculations show a modest enhancement at  $p_T < 5 \text{ GeV}/c$  due to the Cronin effect and modest suppression at higher  $p_T$  due to a combination of isospin effects and shadowing. The curves with energy loss (labeled  $\Delta E(IS)$ ) refer to energy loss of the incoming parton as it propagates through the nuclear matter before the hard scattering [118]. The total effect on the

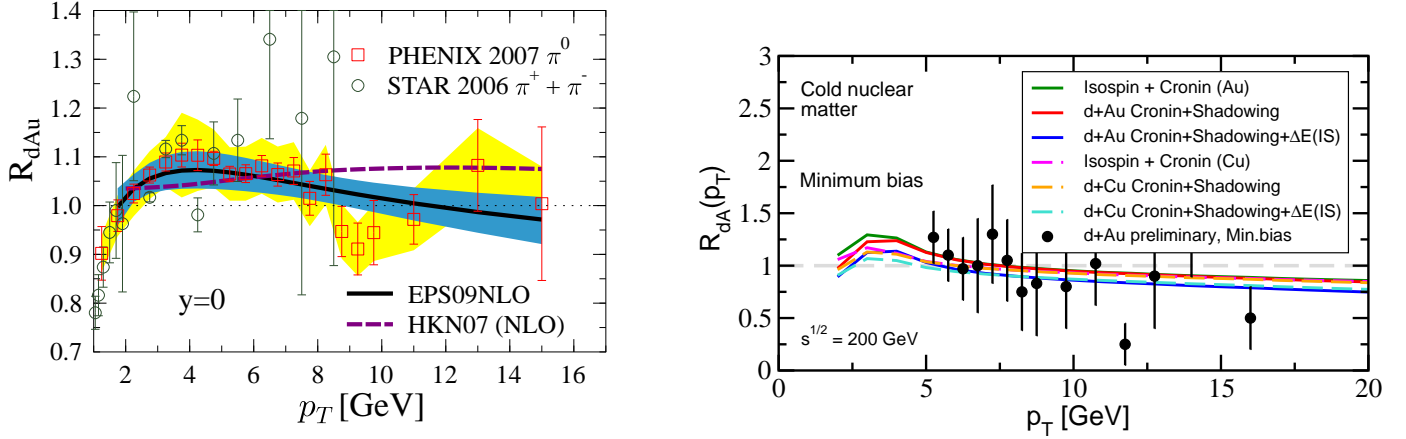


Figure 14: Nuclear modification factor  $R_{dAu}$  for pions (left panel) and photons (right panel) in d+Au collision at  $\sqrt{s_{NN}} = 200$  GeV, compared to calculations with nuclear parton density functions (left panel) and various other cold nuclear matter effects (right panel). Figures reproduced with permission from [113] and [114] (right panel ©American Physical Society).

photon spectrum is around 20%, which is slightly smaller than the current experimental uncertainties in the measurement.

## 6.4 Heavy ion collisions at RHIC

At RHIC, several types of measurements that are sensitive to parton energy loss in hot and dense QCD matter have been performed. In the following, we will discuss the results on inclusive hadron suppression, di-hadron suppression as well as results for heavy quarks. Comparisons to model calculations of energy loss are made where possible, with emphasis on calculations based on a full hydrodynamic evolution of the density and radiative energy loss according to the four formalisms discussed in Chapter 2.

We also focus on the region of high  $p_T$ , where perturbative QCD is most likely to be applicable. Experimental results at RHIC show anomalously large baryon to meson ratios at  $p_T \lesssim 6$  GeV/c [119, 120, 121], indicating that there are important contributions to hadron production beyond factorized perturbative QCD in that regime. We therefore limit the discussion to  $p_T > 6$  GeV/c where possible.

### 6.4.1 Verifying initial production rates: Photon production

Figure 15 shows the centrality dependence of the nuclear modification factor  $R_{AA}$  (Eq. 11) for prompt photons in central Au+Au collisions as measured by PHENIX at  $\sqrt{s_{NN}} = 200$  GeV, compared to various model curves. The measured  $R_{AA}$  for photons is close to unity, as expected for hard probes ( $N_{coll}$  scaling) without energy loss.

The model curves in Fig. 15 show the effect of initial state energy loss (left panel) and final state energy loss for fragmentation photons (right panel) and medium-induced photons, including medium induced QED bremsstrahlung and parton-photon conversion in scattering (right panel). These mechanisms, together with isospin effects, are expected to lead to a suppression of the photon yields by up to 25% at high  $p_T \gtrsim 10$  GeV, with the exact value depending on details of the modeling. The model predictions are in agreement with the experimental data, but the current large uncertainties on the measurement preclude quantitative conclusions about the contributions of the various effects.

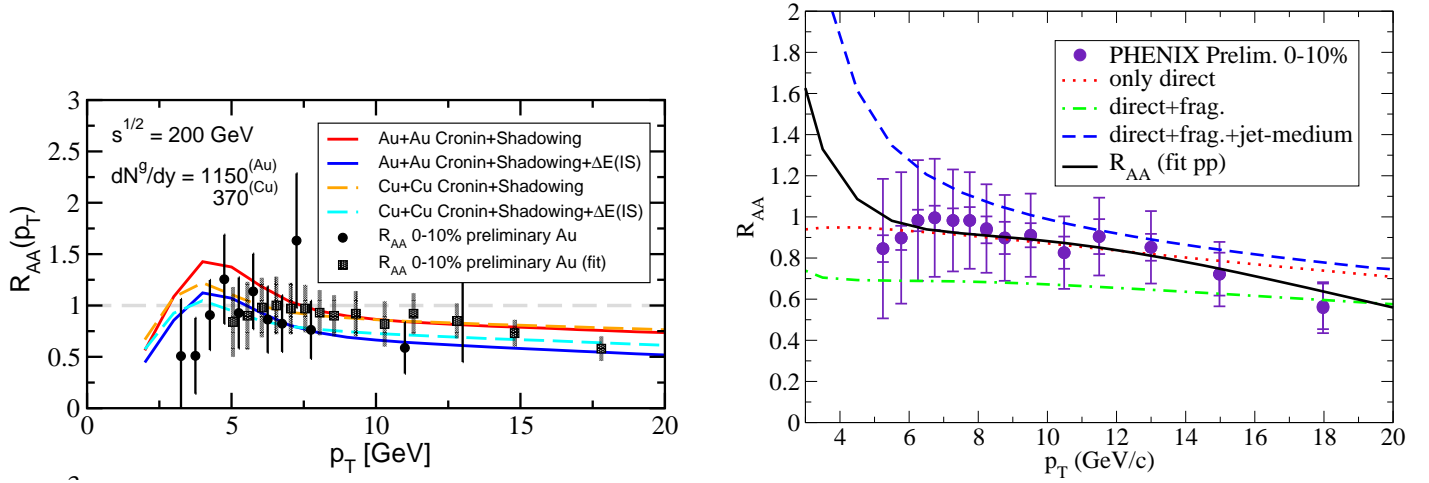


Figure 15: Nuclear modification factor  $R_{AA}$  for prompt photons in central Au+Au collisions at  $\sqrt{s_{NN}} = 200$  GeV as a function of  $p_T$ , [122] compared to various model calculations. Left panel: Model curves by Vitev, including initial state energy loss [114]. Right panel: Model curves by Qin et al showing separate contributions of direct, fragmentation and medium induced photons [40]. The black solid line shows the effect of adjusting the  $p + p$  reference in the calculation to the measured spectrum. Both panels ©American Physical Society.

$\hat{q} \propto$	ASW $\hat{q}_0$ [GeV <sup>2</sup> /fm]	HT $\hat{q}_0$ [GeV <sup>2</sup> /fm]	AMY $\hat{q}_0$ [GeV <sup>2</sup> /fm]
$T^3$	10	2.3	4.2
$\epsilon^{3/4}$	18.5	4.5	
$s$		4.3	

Table 1: Values of the initial transport coefficient  $\hat{q}_0$  ( $\tau = \tau_0 = 0.6$  fm/c) at the center of the most central collision (0-5%) as determined by comparing calculations of  $R_{AA}$  with a medium density space-time profile taken from a 3D hydrodynamical evolution and three different parton energy loss models [84].

### 6.4.2 Light hadron suppression

Parton energy loss leads to a suppression of the pion yield at high  $p_T$ . A recent measurement of  $R_{AA}$  of  $\pi^0$  by the PHENIX experiment is shown in Fig. 16. A clear suppression is visible at high  $p_T$ . The suppression increases with centrality and is approximately  $p_T$ -independent for  $p_T > 4$  GeV/c. The value of  $R_{AA}$  at high  $p_T$  for central collisions is around 0.2.

Figure 17 compares calculations of the nuclear modification factor using a 3D hydrodynamical evolution for the medium density and three different parton energy loss formalisms to experimental data on  $\pi^0$  suppression from PHENIX in Au+Au collisions at  $\sqrt{s_{NN}} = 200$  GeV and two different centralities. The hydrodynamical simulation is tuned to fit RHIC data with a  $p_T < 2$  GeV and provides space-time profiles for the medium properties. The only free parameter in the calculation is an overall proportionality constant between the local transport coefficient and the medium density. This parameter was set using the value of  $R_{AA}$  at  $p_T = 9.5$  GeV in central collisions. The behaviour with  $p_T$  and centrality are parameter free predictions. It is interesting to note that all three model calculations show only a very weak dependence of  $R_{AA}$  on  $p_T$ , in agreement with the data. In the model calculations, the independence of  $R_{AA}$  on  $p_T$  does not have a simple interpretation; it comes about as a result of the interplay between the shape of the parton spectrum and the energy-dependence of energy loss, which is partially due to the kinematic cut-off  $\Delta E < E$ .

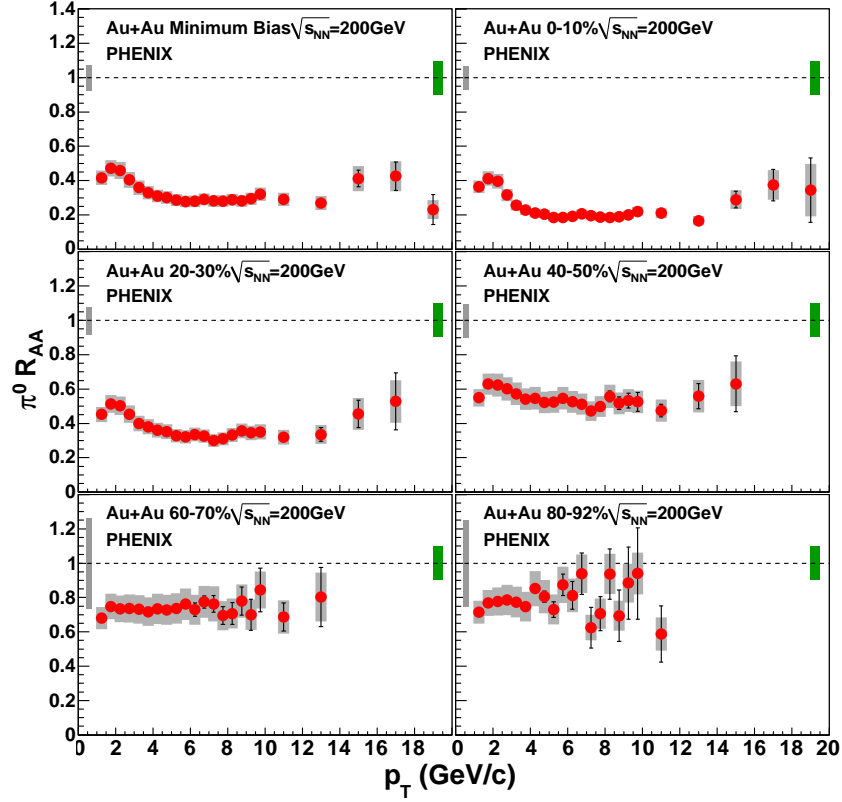


Figure 16: Nuclear modification factor  $R_{AA}$  as a function of  $p_T$  for  $\pi^0$  as measured by PHENIX in Au+Au collisions at  $\sqrt{s_{NN}} = 200$  GeV. The different panels show different centrality selections. The error bands around the dashed line at  $R_{AA} = 1$  indicate the uncertainty from the number of binary collisions (left band) and the normalization uncertainty in the  $p + p$  reference data (right band). Figure reproduced with permission from [123] (©American Physical Society).

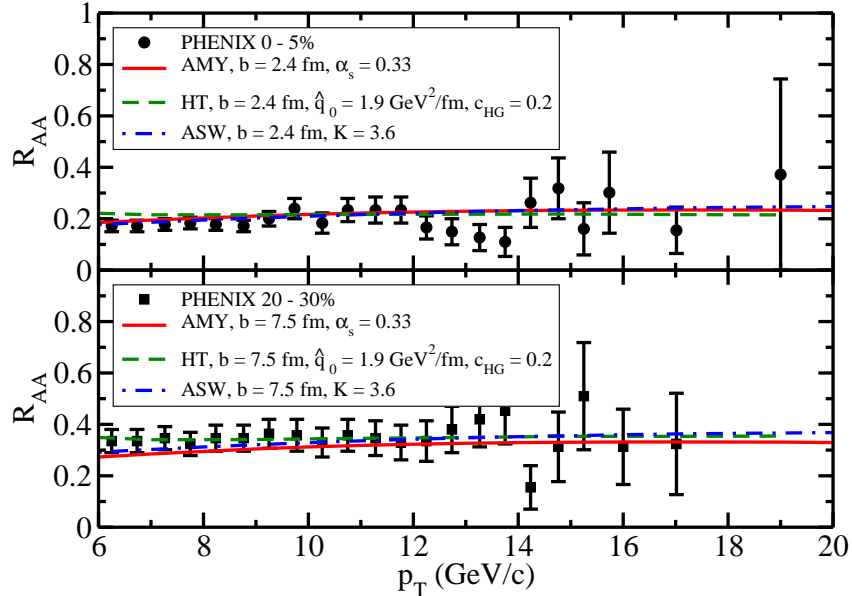


Figure 17: Nuclear modification factor  $R_{AA}$  as a function of  $p_T$  as measured by PHENIX for  $\pi^0$  compared to calculations using a 3D hydrodynamical medium evolution and 3 different energy loss formalisms: Higher Twist (HT), Hard Thermal Loop (AMY) and multiple soft gluon scattering (ASW). The upper panel shows results for 0-5% central Au+Au collisions at  $\sqrt{s_{NN}} = 200$  GeV and the lower panel shows 20-30% central collisions. Figure reprinted with permission from [84] (©American Physical Society).

The resulting values of  $\hat{q}_0$ , the transport coefficient at thermalization ( $\tau = 0.6$  fm/c) at the center of the most central collisions (0-5% centrality) are given in Table 1. The extracted values for  $\hat{q}$  depend on whether the local transport coefficient is assumed to be proportional to the energy density  $\epsilon$  (to the appropriate power  $3/4$ ), the third power of the temperature  $T$  or the entropy density  $s$ . In addition, there are significant differences between the energy loss formalisms: the Hard Thermal Loop formalism (AMY) gives  $\hat{q}_0 = 4.1$  GeV<sup>2</sup>/fm, while the higher twist formalism gives a lower value of 2.3 GeV<sup>2</sup>/fm and the multiple soft scattering approach (ASW) gives a much larger value of 10 GeV<sup>2</sup>/fm.

It is interesting to note that in this comparison, the HT and AMY formalisms give similar medium density parameters, while it can be seen in Fig. 10 that AMY generally has a larger suppression at given  $T$  and  $L$  than HT. Also, in Fig. 10, the suppression for ASW is closer to HT for  $L = 2$  than to AMY, while in this comparison ASW needs a much larger value of  $\hat{q}_0$ . The qualitative difference between the comparison to  $R_{AA}$  in Fig. 17 and the fragmentation functions in the Fig. 10 is probably due to differences in the treatment of the medium in the hydrodynamical calculations of Fig. 17 and Ref. [84]: for the AMY calculation, no energy loss was taken into account for  $\tau < \tau_0$  and the hadronic phase at late times, while for the HT calculation in the same paper, the density was taken to be constant for  $\tau < \tau_0$  and energy loss was also calculated in the hadronic phase. The ASW calculation in that paper calculated no energy loss for  $\tau < \tau_0$  but did continue the energy loss calculation in the hadronic phase. The treatment of the density for early times  $\tau < \tau_0$ , when the medium is very dense, has a large impact on the extracted medium density. A factor 2 difference was found between the case where  $\hat{q} = 0$  is taken for  $\tau < \tau_0$  compared to constant  $\hat{q} = \hat{q}_0$  for the initial stage in Ref. [90].

Thus far, the importance of the early-time dynamics in the modeling of parton energy loss has not been generally realised in the literature. Future studies will need to explore this aspect further, for example by using the exact same treatment for side-by-side comparisons of other model aspects. Uncertainties in the initial density of the system should be taken into account when determining the medium density from energy loss measurements and will likely give a sizable contribution to the overall uncertainty. The present authors feel that taking  $\hat{q} = 0$  for  $\tau < \tau_0$  is unrealistic, since it also implies a very sharp rise of the density at thermalization  $\tau \approx \tau_0$ . A more realistic lower limit of the medium density at early times is needed, but there currently exists no commonly accepted estimate.

At the moment of writing, a comparable calculation of  $R_{AA}$  with a hydrodynamic medium evolution using the GLV energy loss formalism was not available. Early work by Hirano and Nara [124] uses full hydrodynamic evolution, but only a schematic form of the GLV energy loss formalism, and can therefore not be compared directly.

### 6.4.3 Di-hadron correlations and $I_{AA}$

The measurement of inclusive spectra and the nuclear modification factor integrates over a large range of parton energies and over the entire collision geometry. Di-hadron correlation measurements provide more differential information on the partonic kinematics and a different geometrical bias. Comparing results may therefore provide more insight in for example the path length dependence of energy loss.

The left panel of Fig. 18 shows example distributions of the azimuthal angle difference  $\Delta\phi$  between charged *associated* particles and high  $p_T$  ( $8 < p_T < 15$  GeV/c) *trigger* particles. In all panels, two peaks are visible, which is a clear di-jet signature. For the lower  $p_T$  associated hadrons (upper panel), a clear increase is visible in the combinatorial background when comparing d+Au (left column) and central Au+Au collisions (right column). The near-side peak around  $\Delta\phi = 0$  above background has similar magnitude in d+Au and central Au+Au, while a clear suppression of the yield is visible in the recoil at  $\Delta\phi = \pi$ . It is also interesting to note that the width of the correlation peaks is similar in d+Au and Au+Au; no sign is seen of the transverse momentum kicks from the medium, neither at the near side (jet broadening) nor in the recoil (acoplanarity). Since both jet broadening and acoplanarity are at some level unavoidable consequences of the energy loss process, this leads to the conclusion that either

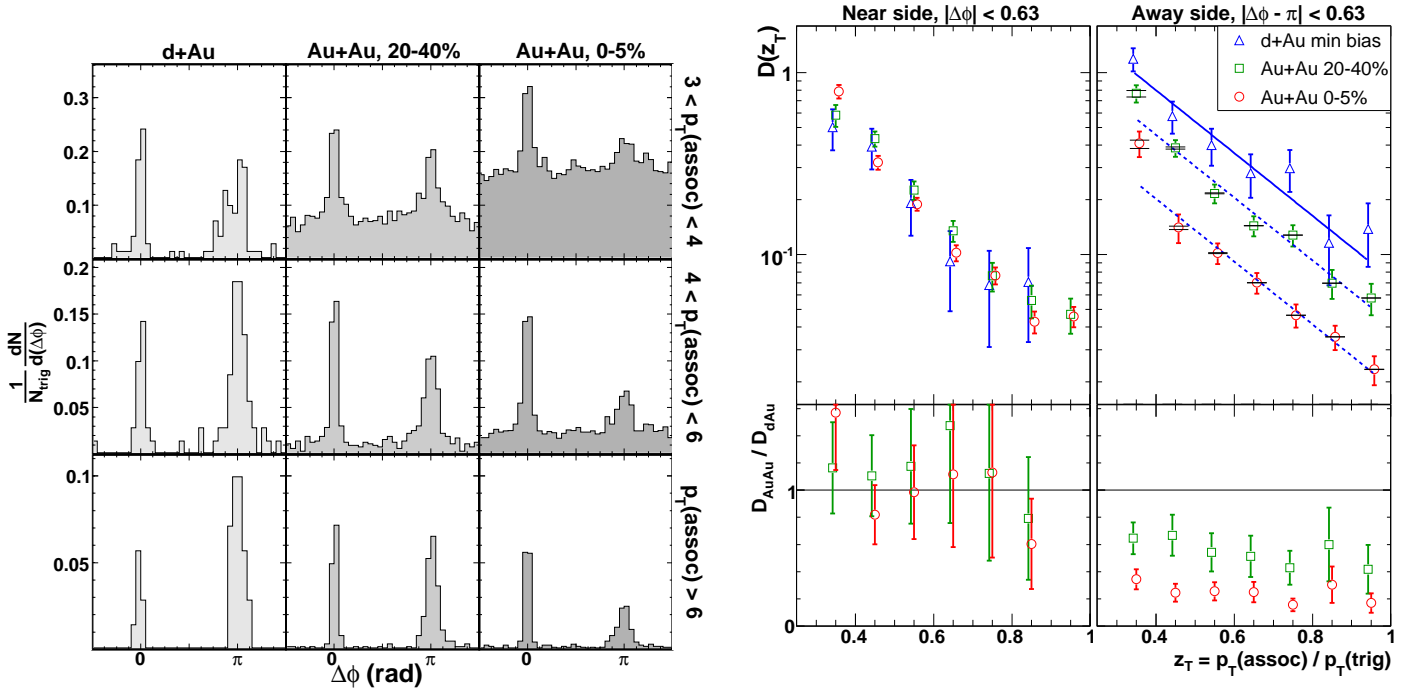


Figure 18: (Left) Distributions of azimuthal angle difference  $\Delta\phi$  between charged associated particles and a high- $p_T$  charged trigger particle ( $8 < p_T < 15$  GeV/c) for different system sizes (d+Au, mid-peripheral and central Au+Au) at  $\sqrt{s_{NN}} = 200$  GeV/c and different  $p_T$ -ranges for the associated particles, including uncorrelated background. The distributions are normalized per trigger particle. (Right) Associated yield on the near side yield  $|\Delta\phi| < 0.63$  (left panels) and recoil  $|\Delta\phi - \pi| < 0.63$  (right panels), as a function of  $z_T = p_T^{\text{assoc}} / p_T^{\text{trig}}$  for trigger particles with ( $8 < p_T < 15$  GeV/c) and three different system sizes at  $\sqrt{s_{NN}} = 200$  GeV/c. The lower panels show the ratio of the Au+Au result to the d+Au reference measurement. Both panels are reprinted with permission from [125] (©American Physical Society).

the transverse kicks are small compared to the trigger and associated hadron momenta, so that the angular broadening is small, or that the selection of high-momentum particles biases towards partons that had little or no interaction with the medium. Note that only 20–30% of the recoil yield is visible in Au+Au, so a significant fraction of back-to-back di-hadrons that is present in the d+Au reference measurement does not pass the  $p_T$ -selection in Au+Au collisions due to energy loss.

A more quantitative representation of the di-hadron results is shown in the right panel of Fig. 18 which shows the per-trigger associated yield, after subtraction of the combinatorial background, on the near side ( $\Delta\phi \sim 0$ , left) and recoil ( $\Delta\phi \sim \pi$ , right) with a trigger particle of  $8 < p_T < 15$  GeV/c for d+Au collisions and Au+Au collisions at two different centralities. The lower panels show the ratio of the Au+Au results to the d+Au reference. On the near side, no modification of the associated yield is seen, while the recoil yield is suppressed by a factor  $\sim 4$ .

It is important to realize that the near-side and recoil yield in this measurement carry different information due to the presence of a trigger particle. The near side measures the yield associated with a trigger particle in the same jet. The absence of suppression on the near side does not necessarily imply that the jets emerge without energy loss; it is also possible that partons lose energy and subsequently fragment in the vacuum, while the lost energy is carried largely by hadrons at lower  $p_T$  or outside the angular region of the measurement. The trigger particle selection would then select partons that have a momentum distribution *after energy loss* that is similar to the d+Au measurement.

Theoretical calculations for the near-side associated yield are quite involved and require the in-



roduction of a new non-perturbative object, the dihadron fragmentation function [126, 127] which contains the correlation between the trigger and the associated hadron. The scale evolution of the di-hadron fragmentation function mixes with the single hadron fragmentation functions. The calculation of medium-modified di-hadron fragmentation has only been carried out in the HT formalism, we refer the reader to Ref. [128] for details. Figure 19, compares theoretical calculations for the case of one scattering and one emission in the medium with experimental data on the centrality and associated  $p_T$  dependence of the associated yield. Note that since the transport coefficients have been fit to the  $R_{AA}$ , there are no free parameters in this calculation. The agreement is excellent for the case of the highest associated  $p_T$  and gradually moves away from the data as the range of  $p_T$  for the associated hadron is lowered.

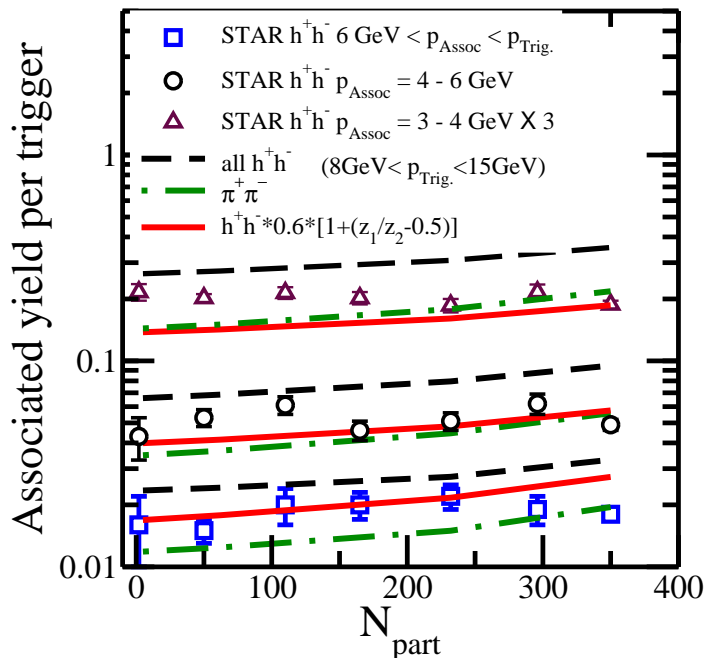


Figure 19: The associated yield per trigger for a trigger with  $8 \text{ GeV} < p_T < 15 \text{ GeV}$  for three different ranges of associated  $p_T$  and for all centralities. The dashed line represents the results for the associated yield of charged hadrons where the initial condition for the dihadron fragmentation function is taken from JETSET. The dot-dashed line is the result for charged pions where the initial condition is taken from JETSET. The red lines are the results for the associated yield of charged hadrons where the initial condition has been fitted to the associated yield of charged hadrons in  $p$ - $p$  collisions in STAR. Reproduced from [128] (©American Physical Society).

The recoil yield, on the other hand, consists of fragments from the recoil parton (back-to-back with the triggered parton) which propagate independently. Energy loss of the recoil parton must lead to reduced high- $p_T$  recoil particle yield per trigger. At lower associated  $p_T$ , enhanced yield has been observed, suggesting that the radiated energy remains correlated with the trigger particle [129, 130].

It is also interesting to note that the away-side suppression in the di-hadron measurement is independent of  $z_T$  in the range shown in Fig 18. This suggests that the longitudinal momentum distribution of high- $p_T$  fragments is unmodified in Au+Au collisions, which could mean that the measured yield is mostly from partons that have little or no interaction with the medium, while, on the other hand, partons that did interact with the medium only produce associated yield at lower  $p_T$ . However, it should be kept in mind that the steeply falling parton  $p_T$  spectrum, combined with approximately exponential fragmentation functions imply that the trigger  $p_T$  selection provides only limited control over the initial state parton kinematics. More complete modeling is needed to provide quantitative limits on the

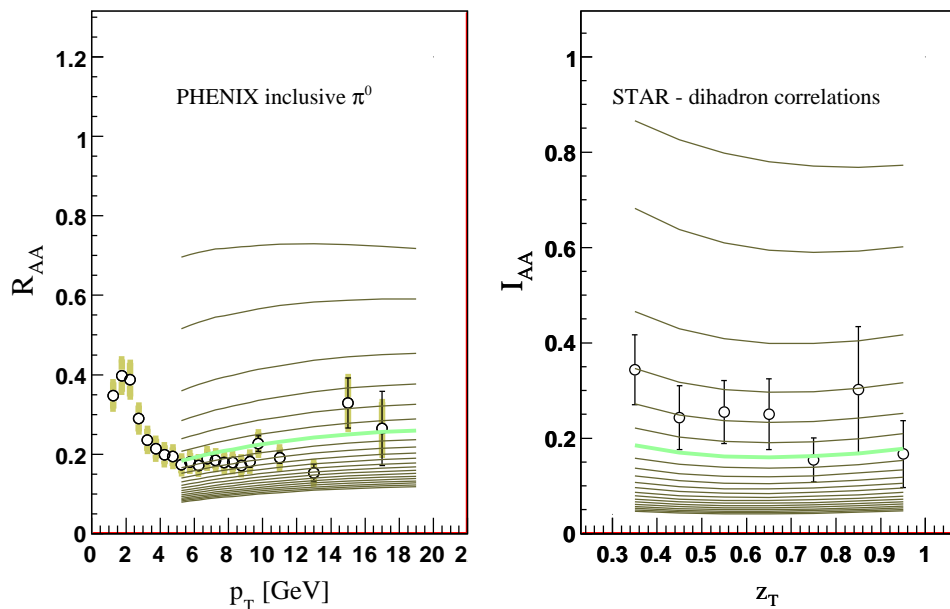


Figure 20: Model curves from a model with a hydrodynamical evolution of the medium and energy loss using the multiple soft scattering approximation (ASW quenching weights) compared to measurements of  $\pi^0$   $R_{AA}$  (left panel) and charged particle  $I_{AA}$ . The broad green line indicates the best simultaneous fit to both experimental results Figure reproduced with permission from [90] (©IOP Publishing).

qualitative trends discussed above. First measurements with experimentally controlled parton energies via  $\gamma$ -hadron correlations and direct jet reconstruction are now becoming available, which can be more straightforwardly interpreted in terms of parton energies. These will be discussed in more detail in Sections 6.4.8.

#### 6.4.4 Model comparisons of $R_{AA}$ and $I_{AA}$

Early comparisons of theory to data [91, 92, 93] have focused on the nuclear modification factor  $R_{AA}$ . As shown in Fig. 17, most energy loss formalisms can be tuned to describe  $R_{AA}$ , including the observed independence of  $R_{AA}$  on  $p_T$ . To further validate energy loss calculations, a simultaneous comparison to observables with different geometrical and fragmentation biases is needed.

Figure 20 shows a comparison of a model using a hydrodynamical evolution for the medium density profile and the ASW multiple soft scattering formalism for gluon radiation [90]. The model can describe the measurements of the nuclear modification factor  $R_{AA}$  and the recoil suppression  $I_{AA}$  with a common scale factor  $K$  between the energy density in the hydrodynamical model and the transport coefficient  $\hat{q}$ . The obtained values for  $K$  are in the range 3–5, indicating that the transport coefficient is larger than the perturbative estimate of Baier ( $\hat{q} \approx 2\epsilon^{3/4}$ ) [131]. These values are in approximate agreement with the values of  $\hat{q}_0$  in Table 1 and also with an earlier fit by Renk and Eskola [89].

#### 6.4.5 Path length dependence of energy loss

Conceptually, a measurement of the path-length dependence of energy loss is very interesting, since it would directly show to what extent the LPM interference is present. As discussed in Section 2.2, LPM interference effects lead to energy loss proportional to  $L^2$  in the infinite energy limit. Elastic energy loss, on the other hand, would be proportional to  $L$ .

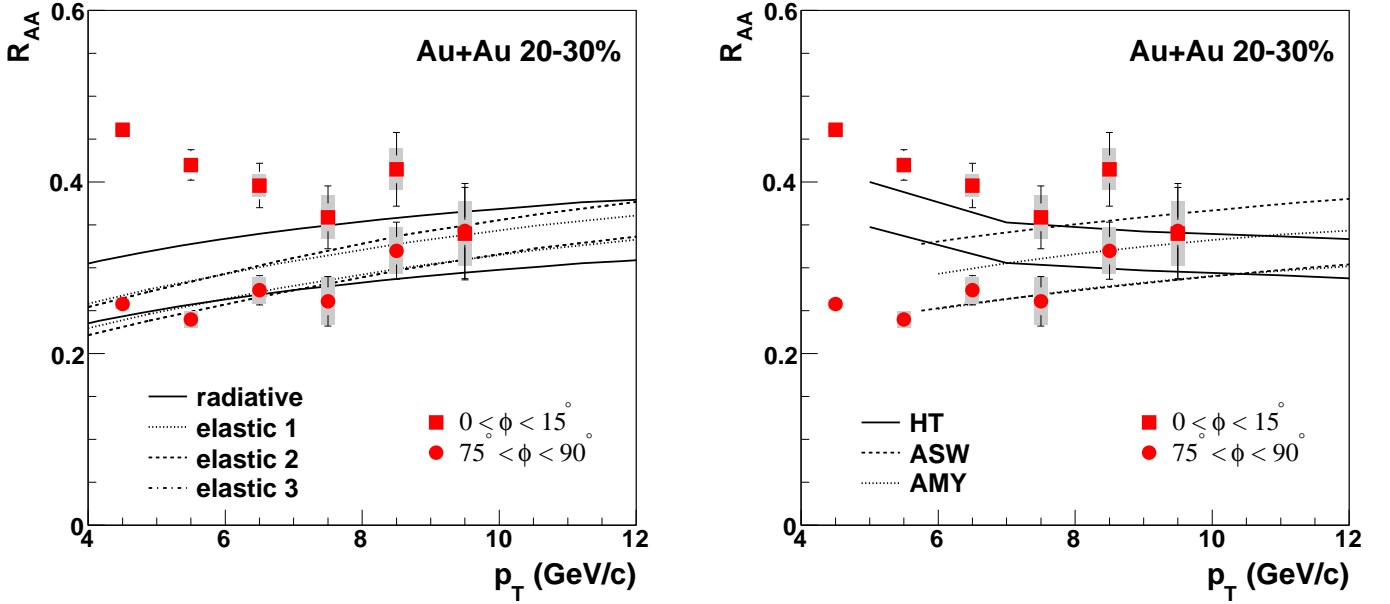


Figure 21: Nuclear modification factor  $R_{AA}$  for  $\pi^0$  emitted at angles close to the reaction plane and perpendicular to the reaction plane ( $75^\circ < \phi < 90^\circ$ ) as measured by PHENIX in 20-30% central Au+Au collisions at  $\sqrt{s_{NN}} = 200$  GeV [132]. The curves in the left panel represent calculations with a hydrodynamic medium, comparing radiative energy loss with three scenarios for elastic energy loss (see also Fig. 22) [96]. The curves in the right panel represent calculations with a hydrodynamic medium at fixed impact parameter ( $b = 7.5$  fm) in the same centrality range and using three different energy loss formalisms [84].

Experimentally, the path length of the partons through the medium can be varied by selecting different centralities and/or using different size nuclei. For this purpose, Cu+Cu collisions have been used at RHIC [133, 134], but so far no detailed comparisons with model calculations with a realistic hydrodynamic medium have been performed.

More differential control of the geometry is obtained by measuring  $R_{AA}$  as a function of the emission angle with respect to the reaction plane, or by measuring elliptic flow  $v_2$  at high  $p_T$ . The most accurate measurement of this type has been performed by PHENIX. Fig. 21 shows the measured  $R_{AA}$  for  $\pi^0$  produced in 15 degree angular intervals around the reaction plane (short path length, square markers) and perpendicular to the reaction plane (long path length, circle markers) in mid-central (20-30% centrality) collisions are compared to two sets of model calculations using a hydrodynamical medium. In the left panel, model calculations for radiative energy loss (solid curves) and elastic energy loss are shown [96]. The three different calculations using elastic energy all have energy loss proportional to  $L$  with a gaussian spread of different widths. The elastic models are seen to have in general a smaller difference between  $R_{AA}$  for hadrons emitted in the reaction plane and perpendicular to the reaction plane than the radiative calculation, as expected from the different  $L$  dependence. The data are more in agreement with the radiative energy loss curves at the highest  $p_T$ , although the differences between the models are small. The out-of-plane measurement shows significant deviations from the model curves at  $p_T < 6$  GeV/ $c$ , possibly due to contributions from hydrodynamical flow of the soft matter.

The right panel of Figure 21 shows a comparison to three different calculations with radiative energy loss (the same calculations as Fig. 17). It can be seen in the figure that the ASW energy loss formalism leads to the largest difference between in-plane and out-of-plane suppression, which is closest to the experimental result. The statistical uncertainties in the measurement are still sizable and will be reduced in the future when larger data samples are analyzed.

According to model calculations, the recoil suppression  $I_{AA}$  also has a significant sensitivity to the path length dependence of energy loss. The reason for this sensitivity is that the trigger particle selects partons on the near side that have little or no energy loss and therefore a short path length. As a result, the recoil parton has a longer-than-average path length. This so-called ‘surface bias’ effect was first pointed out by Dainese, Loizides and Paic in [87]. Later, it was pointed out by Renk [135] that there is an important interplay between the expansion of the medium and this path-length bias effect. The longest path-lengths arise for partons that originate close to the surface, but then travel inwards. These partons only pass through the center of the collision after a few fm/ $c$ . In the presence of rapid longitudinal expansion, the medium will have cooled down significantly by that time and thus despite the long path length, the average medium density along the path is significantly reduced.

Fig. 22 (right panel) shows a comparison of the measured recoil yield with high  $p_T$  trigger particles  $8 < p_T < 15$  GeV/ $c$  with calculations using ASW quenching weights for radiative energy loss and the same three implementations of elastic energy loss that were used in the left panel of Fig. 21, based on Gaussian energy loss fluctuations with different mean and width for the Gaussian. In each calculation, the medium density has been tuned to reproduce the inclusive hadron suppression  $R_{AA}$  (left panel). The figure (right panel) clearly shows that all three elastic energy loss models underpredict the recoil suppression, due to the combination of the path length bias and the linear dependence of elastic energy loss on  $L$ , thus indicating that radiative energy loss, with a quadratic dependence on  $L$ , is dominant for light hadrons. Comparing the left panel of Fig. 21 and the right panel of Fig. 22, we also note that the recoil suppression  $I_{AA}$  is more sensitive to the path length dependence of energy loss than the angle dependence of  $R_{AA}$ .

#### 6.4.6 Colour factor dependence: quark versus gluon energy loss

Radiative energy loss is expected to be  $C_A/C_F = 9/4$  times larger for high energy gluons than high-energy light quarks. It has been suggested that this difference is experimentally accessible by comparing

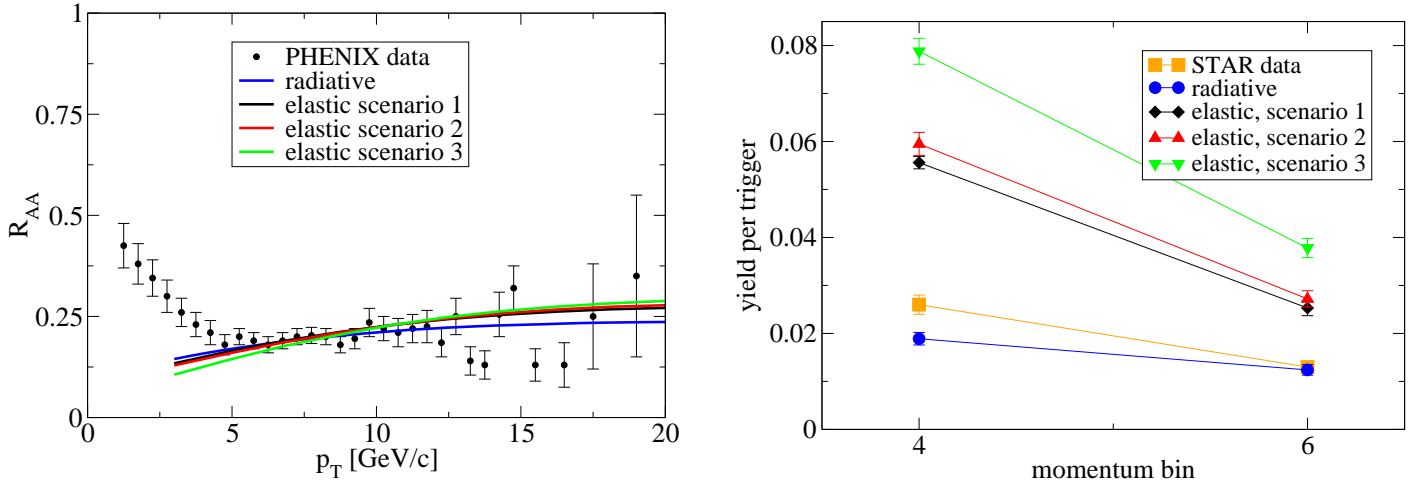


Figure 22: Comparison of energy loss calculations with the nuclear modification factor  $R_{AA}$  from Fig. 17 (left panel) and the recoil yield measurement from Fig. 18 (right panel, yellow points). One of the calculations uses radiative energy loss and the other three use different schematic implementations of elastic energy loss. The calculations use the same geometry from a hydrodynamic evolution and have been tuned to reproduce the inclusive hadron suppression measurement  $R_{AA}$ . Figures reprinted from [96] with permission (©American Physical Society).

nuclear modification factors for (anti-)protons and pions. In  $e^+e^-$  collisions at LEP, it has been observed that gluon jets are more likely to produce (anti-)protons than quark jets [136]. One could therefore use anti-protons to ‘tag’ gluon jets and expects to see a larger suppression for (anti-)protons than for pions.

There are several caveats to this simple expectation. First of all, the argument crucially depends on the difference between (anti-)proton production from gluon and quark fragmentation. The gluon to proton fragmentation function is not accurately known; in fact, recent extractions of fragmentation functions from experimental data use the RHIC  $p-p$  data to constrain this [137, 138]. It has also been shown in more detailed calculations using the AKK fragmentation functions, that while the expected difference between quarks and gluon  $R_{AA}$  is almost a factor 2, the effect is diluted when comparing protons and pions, because pions are produced by gluon as well as quark fragmentation [139]. Finally, it should be realised that quark showers contain gluons and vice versa, so that the distinction between quark and gluon energy loss in a full shower evolution not be clear. One specific implementation of this effect are ‘jet conversion’ processes in the medium. A calculation of this effect shows a reduced  $p/\pi$  ratio in heavy ion collisions compared to  $p-p$  collisions [140]. Measurements performed by STAR [120], do not show a larger suppression of (anti-)protons compared to pions.

#### 6.4.7 Heavy quark energy loss

Due to their large mass ( $m \gg \Lambda_{\text{QCD}}$ ), heavy quarks move at speeds smaller than the speed of light through the medium. As a result, they cannot emit gluons at small angles, the so-called ‘dead cone effect’, and therefore lose less energy than light quarks (see Section 4.1) [73]. To verify whether radiative energy loss is dominant for heavy quarks, measurements have been performed of heavy flavor production using semi-leptonic decays into electrons.

The upper panel of Figure 23 shows a comparison of predictions using only radiative energy loss by Armesto et al, using the parameters obtained from the light quarks measurements in Fig. 20, to measurements of the nuclear modification factor of non-photonic electrons (electrons which are not from photon conversion or light hadron decay) from heavy flavor decays by STAR and PHENIX at

<sup>2</sup>See footnote with Fig. 12 for the systematic uncertainties.

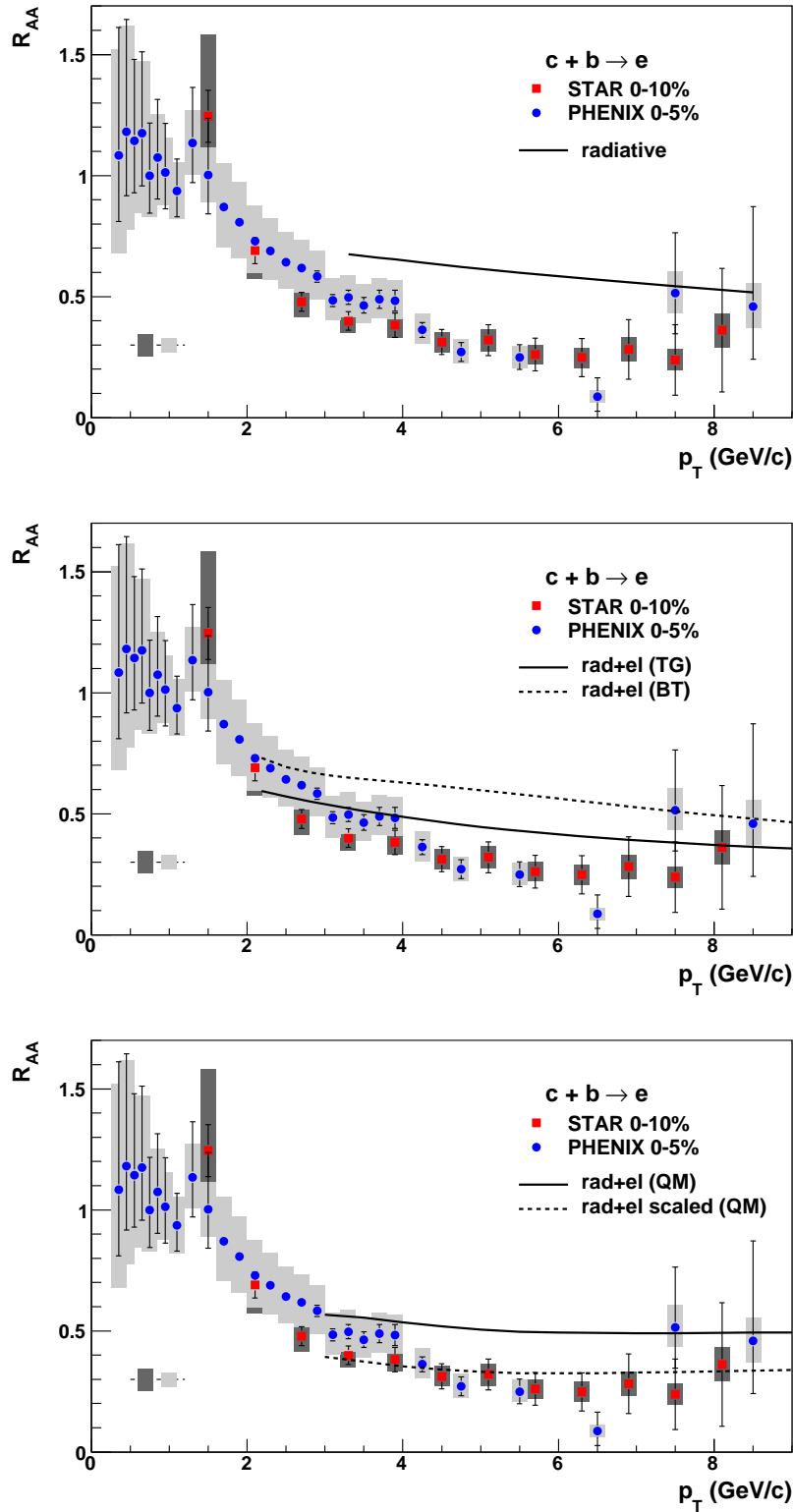


Figure 23: Nuclear modification factor  $R_{AA}$  for non-photon electrons from heavy flavor decays as measured by STAR [99] and PHENIX [141] in central Au+Au collisions at  $\sqrt{s_{NN}} = 200$  GeV compared to three different model calculations. The uncertainty bands on the lower left indicate the overall normalisation uncertainty. <sup>2</sup> Top panel: radiative energy loss only [90] (see also Fig. 20). Middle panel: radiative and elastic energy loss [66]. Bottom panel: radiative and elastic energy loss [75].

RHIC [90]. The measured suppression of non-photonic electrons is larger than the model predicts. The extracted  $K$ -factor would be larger than 25, while the value for light quarks was between 2 and 5. These results indicate that the suppression of heavy quarks is larger than expected, possibly similar to light quark suppression. It is worth noting that the systematic uncertainties on the measurements are sizable. These uncertainties are expected to be quite strongly correlated point-to-point. As a result, the data are not strictly inconsistent with the expectation from radiative energy loss. For a more detailed discussion of the systematic uncertainties and the implications for energy loss we refer to [90].

Various mechanisms have been proposed to explain the observed large suppression. For example, it has been argued that elastic energy loss may play a significant role for heavy quarks, because the radiative energy loss is reduced [66]. A detailed evaluation of the combined effect of radiative and elastic energy loss has been performed using the opacity expansion for radiative energy loss and elastic energy loss based on the HTL calculation by Thoma, Gyulassy (TG) [70] and Braaten, Thoma (BT) [71]. The same mechanism should be present for light quarks, so the model was fitted first to the light quarks and the predicted suppression of non-photonic electrons is compared to the measurements in the middle panel of Fig. 23. The discrepancy between the model and the experiment is smaller than when only radiative energy loss is taken into account (compare to upper panel), but the calculation still gives less suppression than measurement.

Recently, it was pointed out that heavy and light quarks probe the medium at different scales and may therefore effectively see a different medium [75]. This is illustrated in the bottom panel of Fig. 23 which compares non-photonic electron  $R_{AA}$  with model curves using a Woods-Saxon overlap geometry with an initial temperature of  $T = 400$  MeV at the hottest point. The solid line shows the result using HTL values for the transport coefficients  $\hat{q} \approx 2\text{GeV}^2/\text{fm}$ ,  $\hat{e}$  and  $\hat{e}_2$  (see also Section 4.2), while the dashed line shows the result with relative increase of the energy loss for heavy quarks by about 30%, which brings the model into agreement with the data. The same calculation also describes the measured elliptic flow for light hadrons and non-photonic electrons.

Other models, which include hadron formation inside the medium followed by dissociation and recombination [142] or resonant scatterings [143] can also be tuned to describe the measurement. The implications of such models for light quark energy loss have not been studied in detail.

High- $p_T$  measurements of heavy flavor production at RHIC have so far relied on electrons from semi-leptonic decay and therefore do not distinguish between charm and bottom. The difference in mass between charm quarks ( $m \approx 1.3 \text{ GeV}/c^2$ ) and bottom quarks ( $m \approx 4.2 \text{ GeV}/c^2$ ) leads to a different momentum dependence of the dead-cone effect, which will be explored by future measurements. At high  $p_T$ , the charm quark behaves as a light quark, so that comparisons to light hadrons are a measure of the difference between quark and gluon energy loss. Calculations have shown that this effect leads to large effects in the heavy-to-light ratios at RHIC and LHC [144]. Future measurements will certainly be sensitive to these effects.

#### 6.4.8 $\gamma$ -hadron and jet based measurements at RHIC

In recent years, two new types of measurements of parton energy loss are being explored at RHIC:  $\gamma$ -hadron correlations and jet reconstruction. Both measurements provide experimental control over the initial state parton kinematics: in the case of  $\gamma$ -hadron measurements, the photon and the recoil jet have equal  $p_T$ , while in the case of jet reconstruction, the parton energy is measured by summing up the energies of the fragments.

The  $\gamma$ -hadron measurement is conceptually appealing, and has been advocated for a long time [149, 150], but it is experimentally difficult because of the low rates and the large background from  $\pi^0$  decays. First results from PHENIX [145] and STAR (preliminary) [146] are shown in Fig. 24 and compared to model calculations. Both experiments show a recoil suppression of 0.3, which is similar to the value found for di-hadron suppression in Fig. 18 (charged hadrons) and the right panel of Fig. 24

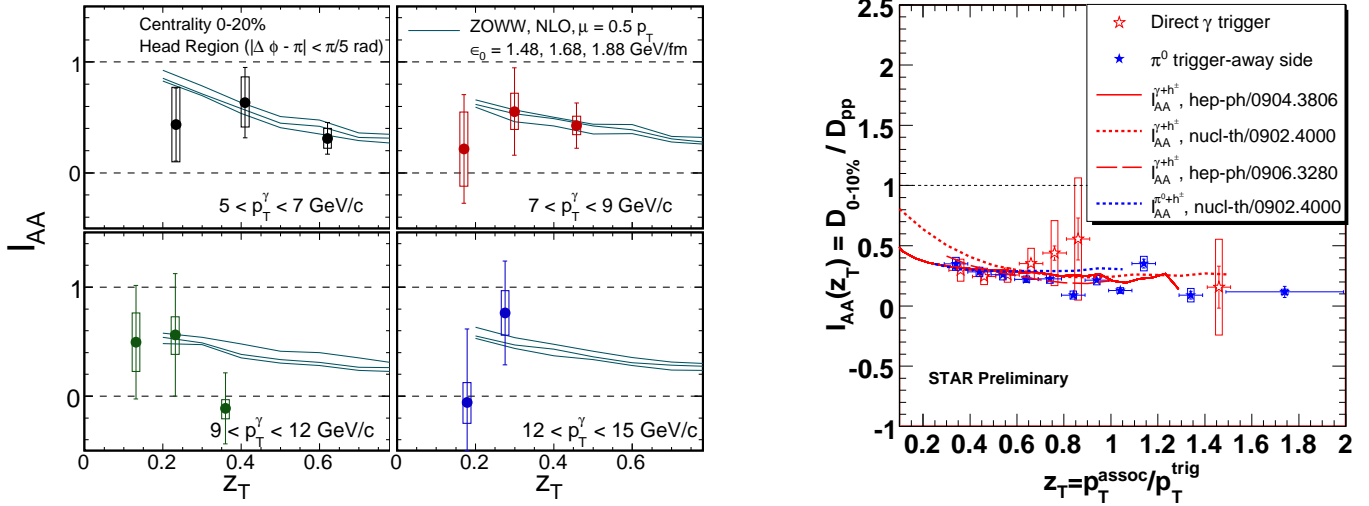


Figure 24: Recoil hadron suppression for direct photons measured by PHENIX (left panel) [145] and STAR (right panel) [146] in central Au+Au collisions compared to  $p + p$ . The PHENIX measurement (left panel) is presented for four ranges in  $p_T^\gamma$  between 5 and 15 GeV/c and compared to energy loss calculations by Zhang, Owens and Wang (ZOWW) [147]. The preliminary STAR measurement (right panel) has  $8 < p_T^\gamma < 16$  GeV/c and is compared to the ZOWW calculation (dotted curves), a calculation by Renk [148] and an AMY-based calculation that takes into account parton-photon conversions in the medium (dashed line) [40] and a similar measurement for  $\pi^0$  recoil. Figures reproced with permission from [145] ((©American Physical Society) and [146].

( $\pi^0$ -charged hadron pairs) despite the different geometrical and fragmentation bias.

The  $\gamma$ -hadron measurements are compared to model calculations by three groups. The calculation by Zhang, Owens and Wang [147], which is shown in both panels of Fig. 24 uses NLO pQCD to calculate the initial photon rate, including fragmentation photons but uses a simplified geometry (hard spheres) and an energy loss calculation without energy loss fluctuations. The calculation by Renk [148] (solid line in the right panel of Fig. 24) uses a more realistic geometry and ASW quenching weights for energy loss. The third calculation in the right panel of Fig. 24 (dashed line) uses a 3D hydro model for the medium and an AMY-based energy loss formalism, which includes production of photons by interactions with the medium [40]. All three model calculations are in good agreement with the measurement, indicating that the measured recoil suppression is consistent with the hadron suppression measurements.

For sufficiently high photon energy, one would expect to see the  $z$ -dependent suppression of the fragmentation functions, similar to what is shown in Fig. 10, although the effect may be weaker for a realistic nuclear geometry than for the fixed-length calculations presented in Fig. 10. Some of the model curves in Fig. 24 indeed show a rise at small  $z_T = p_T / p_T^\gamma \sim 0.2$ , where no measurements are available due to the large combinatorial background at low  $p_T$ . Future runs at RHIC will bring larger data samples and correspondingly reduced uncertainties.

Experimentally, jet measurements have the advantage of a large cross section, but a good jet analysis is complicated, especially in the presence of uncorrelated backgrounds from the underlying heavy ion event. Jet measurements are being actively pursued at RHIC, by both STAR [151, 152, 153] and PHENIX [154]. Initially, it was thought that it would be necessary to reject all particles below a certain transverse momentum threshold from the analysis to reduce the background, but experience with data has shown that this is not necessary. This enables infrared safe algorithms to be used, such as the recently developed SIScone algorithm [155] and fast  $k_T$  [156] and anti- $k_T$  algorithms [157].

In collisions of elementary particles,  $e^+ + e^-$ ,  $p + p$ , and  $p + \bar{p}$ , reconstructed jet energies provide



an accurate measure of the underlying parton momentum as evidenced by kinematic reconstruction of  $W \rightarrow q\bar{q}$  [158, 159, 160] and  $t \rightarrow bW \rightarrow q\bar{q}$  decays [161, 162]. The accurate mapping between parton energy and jet energy is a phenomenological implication of QCD factorization: an infrared and collinear safe jet definition is insensitive to details of the soft QCD processes in jet fragmentation and therefore measures properties of the ‘hard partons’. In heavy-ion collisions, jet-fragmentation is modified by interactions with the medium, thereby modifying the longitudinal and transverse structure of the jet. In addition, part of the jet energy may be transported outside the jet cone by large angle radiation, thus reducing the reconstructed jet energy. A number of different experimental analyses are being performed, which are sensitive to different aspects of the medium modification of jet energies. The available preliminary results show an increasing suppression when using a smaller jet radius in the reconstruction algorithm, suggesting that jet broadening is an important effect [152]. For large radius,  $R = 0.4$ , the jet suppression is much smaller than the inclusive hadron suppression, indicating that a large fraction of the radiated energy is recovered by jet reconstruction.

Attempts have also been made to measure fragmentation functions, *i.e.* the longitudinal distribution of particles in jets, with the aim to characterize the softening of the fragmentation due to medium interactions. Such measurements, however, are complicated by potential interplays between the softening of the fragmentation and the jet energy reconstruction. Preliminary results that attempt to circumvent this problem by using di-jet events, where the jet energy is measured in one jet and the fragment distribution is studied in the recoil jet, show a large suppression of the overall recoil jet rate, but no apparent modification of the fragment distribution in the reconstructed recoil jets [163].

## 6.5 Outlook: how to reduce uncertainties

In the above various measurements have been compared to theoretical calculations to extract medium parameters. In some cases, such as the heavy flavor measurements, the experimental uncertainties are sizable, of the order of 20% and seem to limit the extraction of medium properties. As mentioned in Section 6.1, the first approach to improving this situation should be by defining more selective observables using theoretical insight and modeling. For example, one might expect a measurement of recoil suppression  $I_{AA}$  of heavy quarks to be sensitive to the path length dependence of energy loss, like in the case of light hadrons. This is clearly a challenging measurement, so it would be worth to first explore the potential in model calculations.

However, it is also worth to consider the origins of the various experimental uncertainties to see whether improvements are possible. In this section, we will briefly discuss the various sources of uncertainties in the measurements and which improvements are planned with future RHIC upgrades.

### Statistical errors, luminosity

The most straightforward source of uncertainties are statistical uncertainties. These uncertainties are always due to counting statistics in the experiment and can therefore be reduced by increasing the number of analyzed events, either by improving luminosity or by longer running times, and sometimes by selecting a process with a larger cross section. The beam luminosity and effective running time at RHIC have steadily increased over the years. The largest event samples were taken in run 4 and run 7, with run 7 having about twice the integrated luminosity of run 4. It is important to realize that not all observables can make full use of the luminosity, because the event rates may be too high to record all events. Both STAR and PHENIX can select events with large energy depositions in the electromagnetic calorimeters with an on-line trigger, so that measurements with high- $p_T$  photons,  $\pi^0$  and electrons can make use of the full luminosity. Both experiments are also continually improving the detector read-out rates to be able to record a larger fraction of the total luminosity for other (un-triggered) measurements.

If a signal has a large background, the statistical uncertainty is driven by the amount of background. This explains the relatively large statistical uncertainties on direct photon measurements (decay pho-

ton background) and to a lesser extent the non-photon electron measurements (conversion electron background).

### Background uncertainties

Apart from the statistical uncertainties on a background, there are also systematic uncertainties. For example, in the case of the decay photon background for direct photons, the background level is set by the  $\pi^0$  spectrum, which is known to finite precision. The contributions of higher-mass mesons are less precisely known. The main source of the conversion electron background for the (non-photon) electron spectrum are also photons from  $\pi^0$  decay, so here again the subtraction relies on the knowledge of the  $\pi^0$  spectrum, in addition to a precise knowledge of the amount and composition of the detector materials.

If the signal is smaller than the background, a relatively small uncertainty in the background level may translate into a large uncertainty on the signal. Larger data samples can improve the knowledge of the background level, but only up to the level of the intrinsic systematic uncertainties.

### Intrinsic systematic uncertainties

Every experimental set-up has intrinsic lower limits to the experimental uncertainties. The two dominant effects are uncertainties in the detection efficiency and in the energy or momentum scale. Experimental efficiency is generally calculated using detector response simulations, which have a finite precision. Details of what limits the uncertainty differ from detector to detector, but it is safe to say that a precision of better than a few per cent in the detection efficiency is difficult to attain. In addition, energy scale calibration uncertainties may introduce significant uncertainties in the yields at a given  $p_T$ . For example, with a power law spectrum  $1/p_T^6$ , an energy scale uncertainty of 0.5% leads to a 3% uncertainty on the yield. These types of uncertainties limit, for example, the  $\pi^0$  spectrum at intermediate  $p_T$  in Figs 16 and 17.

### Normalization uncertainties

For spectra and  $R_{AA}$ , normalization uncertainties are a significant contribution, see Figs 12, 16, and 23, where this type of uncertainty is indicated by a separate error band without data point. There are two main contributions: the absolute normalisation of the  $p+p$  reference measurement and the determination of the number of binary collisions  $N_{coll}$ .

The normalisation uncertainty of  $p+p$  reference measurements is due to a significant contribution of low-multiplicity events, including double-diffractive collisions, to the total cross section. Some of these low-multiplicity events are not detected by the experiment. The measurement in  $p+p$  can be given in terms of multiplicity per event ( $d^2N/dydp_T$ ) or differential cross section  $d^2\sigma/dydp_T$ . The normalisation uncertainty is slightly different for these two types of measurement; in one case it enters as an uncertainty in the total number of events, while in the other case it enters as an uncertainty in the total cross section, which can be measured independently, using a Vermeer scan. Both methods lead to a total uncertainty on the absolute cross section of 5-10%.

To calculate  $R_{AA}$  or  $R_{CP}$  in heavy ion events, the number of binary collisions (or overlap function  $T_{AA}$ ) is used. This quantity is derived from Glauber models of the total cross section (cf Section 5.1). The uncertainty on this calculation is indicated separately in Fig. 16 as a grey band on the left side of each panel. The result is accurate for central events, but for peripheral collisions the uncertainties can be sizable. This uncertainty can possibly be reduced with dedicated studies of peripheral events, but some of the uncertainty is inherent in the Glauber modeling.

The normalisation uncertainty is strongly reduced when concentrating on central events, where the determination of  $N_{coll}$  is quite reliable. The types of normalisation uncertainty discussed here only affect measurements that involve an absolute cross-section and therefore do not affect di-hadron measurements and elliptic flow.

When comparing theory calculations to experimental data, all of the above sources of uncertainties need to be taken into account. For example, in Fig. 12, there are three types of uncertainties indicated, statistical, systematic and an overall normalisation uncertainty. The systematic uncertainties are some-

what correlated between points and are due to the sources listed above under background uncertainties and intrinsic uncertainties. For the  $\pi^0$  spectrum in the left panel of Fig. 12, statistical uncertainties are dominant only for  $p_T > 16$  GeV/ $c$ . At lower  $p_T$ , the systematic uncertainty of about 5-10% on each data point and the overall uncertainty of about 10% are dominant. Reducing the systematic uncertainties is very difficult, and often requires building new detectors.

For the non-photonic electron measurements in the right panel of Fig. 12 and in Fig. 23, the statistical uncertainties are dominant for  $p_T > 5$  GeV/ $c$ , so that longer running times or larger luminosity will still improve the precision of the result. Note also that the statistical uncertainties for the STAR measurement are larger, due to a smaller analyzed (triggered) data sample. Also for this measurement, reducing the systematic uncertainties below the current value of 15 – 20% is difficult to impossible. The precision of the di-hadron suppression and the  $\gamma$ -hadron measurements are still limited by statistical uncertainties, so that future runs with larger luminosity will improve the precision.

## 7 Outlook: parton energy loss at LHC

In the near future, the LHC will start colliding protons and nuclei at energies far greater than RHIC energies (maximum energies are  $\sqrt{s_{NN}} = 5.5$  TeV for Pb+Pb and  $\sqrt{s} = 14$  TeV for p+p, but the initial runs will be at lower energy).

First results from the LHC experiments should already provide an important test of the understanding of parton energy loss developed at RHIC: if the same models and theory can be applied to describe the LHC results, that would be an important sign that our basic understanding of parton energy loss is correct. However, the LHC will provide access to a far greater number of jet observables.

Our current understanding of RHIC results indicate that jet energy loss is typically a few GeV with important tails to much larger energy losses. Since typical jet energies at RHIC are 10–20 GeV, the energy loss is not much smaller than the jet energy, which complicates the theoretical treatment of energy loss. At LHC, large numbers of jets with energies above 100 GeV will be produced, while the medium density is only expected to increase by a modest factor of 3–5 [164]. This makes it possible to cleanly separate jets from the underlying event. In addition, the regime where  $\Delta E < E$ , where theory calculations are better controlled, may become experimentally accessible. Luminosity upgrades at RHIC will also extend the accessible  $p_T$ -range there, reaching parton energies of 40–50 GeV. The large jet rates at 100 GeV at LHC will further enable more differential studies of *e.g.* jet structure using sub-jet distributions [165].

### 7.1 Experimental capabilities at the LHC

ALICE [166, 167] is the dedicated heavy-ion detector, which has been optimized for large track densities in heavy-ion collisions and features powerful particle identification. ATLAS [168, 169] and CMS [170] will also perform heavy-ion measurements with their detector systems that are more conventional for high- $p_T$  and jet measurements, including large calorimeter coverage. For a complete review of the potential of hard probes at the LHC, see [112, 171].

The LHC detectors are all equipped with high-precision vertex detectors for secondary vertex reconstruction of heavy flavor decays. This will allow to separate charm and beauty from the outset, providing critical tests of the mass and flavour dependence of energy loss, which will show whether radiative energy loss is dominant or not. Since the dead-cone effect should be less pronounced for the lighter charm quark than for the heavy bottom quark, comparing the suppression of charm and bottom provides direct sensitivity to the dead-cone effect. On the other hand, comparing charm fragmentation at high  $p_T$  with light parton fragmentation, which is a mix of quark and gluon fragmentation, provides sensitivity to the difference between quarks and gluons [144]. In addition, heavy quark fragmentation studies should be possible at LHC, but these have not yet been explored in detail.

Finally,  $\gamma$ -jet and  $Z^0$ -jet events will be studied to provide a well-defined calibration of the jet energy measurement. The total rates of these events are significantly lower than inclusive jets, so that differential measurements of jet fragmentation will most likely be performed with single jets or di-jet events.

### 7.2 Theoretical issues: From analytical approaches to Monte-Carlo

While the single hadron formalism has been the central theme in this review we now report on the emerging new directions in jet modification theory which are being tailored to calculate multi-hadron final states.

The computation of multihadron final states for jets in vacuum is now a rather well established procedure. The standard method uses Monte-Carlo routine to compute the underlying jet shower by sampling the DGLAP splitting functions repeatedly in order to sequentially decompose a single virtual

parton into a shower of lower virtuality partons, using the Sudakov prescription. We refer the reader to Refs. [172, 173] for details on these algorithms. At any given step in this routine one typically has a hard virtual parton which will survive for a time which is inversely proportional to its virtuality and then split into two partons with lower virtuality and so on. At low enough virtuality, this ‘‘DGLAP’’ shower routine is terminated and a phenomenological hadronization routine is invoked to convert the parton shower into a shower of hadrons.

In a medium, the showering and hadronisation process becomes far more complicated, due to additional radiations and the possible exchange of color with the medium [174]. In addition, hadronisation through recombination of shower partons with partons from the medium might play a role. At the LHC, given the energies of the jets, one expects a large part of the jet to exit the medium in partonic form and continue to shower. Finally one expects a considerable part of this escaped and modified jet to hadronize independently of the medium. While the very soft part of this hadronic spectrum from the jet will still become indistinguishable from the harder hadrons from the medium, the high  $p_T$  part of the jet should be separable from the medium. The major challenge is to model the partonic splittings which now contain a vacuum like part where a higher virtuality parton splits into lower virtuality partons interfering with an in-medium part where scatterings in the medium may raise the virtuality of the hard parton and cause it to split into two.

There are currently three different routines: JEWEL [165], Q-PYTHIA [175] and YaJEM [176], in the published literature, which have been benchmarked with single hadron data. A series of other Monte Carlo generators (e.g. the AMY based Monte Carlo MARTINI) is in the development stage. Each of these uses a somewhat different set of approximations and calculational techniques. Of these Q-PYTHIA [175] is closest in spirit to the traditional vacuum Monte-Carlo routines. Here the authors add a medium-induced contribution to the vacuum splitting function and use this to calculate an in-medium Sudakov form factor. They now have a probability that the jet will emit a gluon while propagating over a certain distance and also the probability that it will not radiate. This is then iteratively applied to compute a shower distribution. In the case of JEWEL [165], the authors attempt an original algorithm. The very process of single gluon radiation is calculated via a numerical algorithm. Here, the random process of scattering is used to modify the formation time of the radiated gluon in a stochastic process. More scatterings tend to increase the transverse momentum of a gluon which has not completely formed. As the transverse momentum is increased the formation time of the gluon shrinks till it is formed within the next time step. After this the process begins anew. JEWEL also includes the elastic loss that the hard jet encounters every time it scatters. In YaJEM [176], the author modifies the vacuum DGLAP shower that is contained within PYTHIA. This is done by randomly modifying the virtuality of an intermediate state due to scattering in the medium. This leads to a change in the radiation pattern and thus to a different shower pattern. In MARTINI [177], analytical energy loss routines computed within the AMY formalism are used to modify the shower distribution in PYTHIA prior to hadronization.

These Monte-Carlo routines along with others being developed represent the next wave of jet modification calculations. These will no longer be limited to the single hadron or dihadron level but will be able to compute a whole host of full jet observables. They will also provide the experimental community with multiple event generator codes which will provide necessary input and benchmarks for the experimental analysis of multihadron final states.

## 8 Conclusion

In this review, we have discussed in some detail the theoretical formalisms describing parton energy loss in cold and hot QCD matter. Conceptually, there are two main mechanisms for energy loss: elastic and radiative. For radiative energy loss off high-momentum partons in a dense medium, the formation times are large, so that the Landau-Pomeranchuk-Migdal (LPM) effect plays an important role, leading to energy loss scaling with the square of the path length ( $L^2$ ). At the same time, a high-momentum parton is also expected to reduce its virtuality even in the absence of a medium, leading to a jet of hadrons. The interplay (and interference) between vacuum radiation and medium-induced radiation is therefore also expected to play an important role.

Due to the complex nature of the energy loss process and in-medium modification of the fragmentation function, different theoretical formalisms have chosen different approximations in the calculation. A side-by-side comparison of the medium modifications to the fragmentation functions for a fixed-length homogeneous medium was presented in Fig. 10 and shows important quantitative differences between different formalisms.

Unfortunately, fixed length, homogeneous hot QCD matter is not experimentally available, but instead a rapidly expanding medium is produced in heavy ion collisions. Comparing Fig. 17 and 10, we concluded that the way in which the partons sample the evolving medium is an important aspect of the modeling for heavy ion collisions, which currently precludes the precise determination of the medium density or transport coefficient from experiment.

There are, however, qualitative features of radiative energy loss that can be addressed with experimental data despite the uncertainties in some of the quantitative details of the calculations. The comparison of measured nuclear modification factor  $R_{AA}$  and the recoil suppression  $I_{AA}$  indicate that there is a leading  $L^2$  dependence to the energy loss (cf. Fig. 22), which is a first indication that the LPM interference effect indeed plays an important role in parton energy loss.

Another prediction of radiative energy loss is that heavy quarks lose less energy than light quarks due to the dead-cone effect. The measured suppression of heavy quarks at RHIC is larger than expected from pure radiative energy loss, indicating that other effects play a role. Possibilities include the presence of elastic energy loss and the possible influence of the larger scale at which transport coefficients should be evaluated due to the larger mass of the heavy quark.

Future measurements at RHIC and LHC will include  $\gamma$ -jet measurements and measurements with kinematically reconstructed jets, which will provide more differential control of the partonic kinematics. Such measurements will be more directly comparable to the theoretically calculated fragmentation functions in Fig. 10.

An important ongoing theoretical development is the use of Monte Carlo techniques, which has two important aspects. On the one hand, Monte Carlo techniques can be used to explore the effect of certain limitations of the analytical calculations of energy loss, most notably the effect of kinematic limits. On the other hand, Monte Carlo event generators can be used to calculate more exclusive (multi-hadron) observables, and thus provide a reliable tool to explore observables based on reconstructed jets, such as fragmentation function and jet broadening measurements.

All in all, a quantitative understanding of the theory and phenomenology of parton energy loss based on the RHIC measurements is starting to emerge, including some areas of apparent disagreement between the data and theory. As a result, all the tools and understanding are available to start devising critical tests of the theoretical understanding using future measurements at RHIC and LHC. The much larger momentum range available at LHC will likely make the regime where the energy loss is significantly smaller than the jet energy experimentally available. This regime is the most suited for pQCD based theoretical treatment and therefore promises to provide the most unambiguous tests of our understanding of fragmentation and energy loss in a hot QCD medium.

## Acknowledgements

The authors would like to thank William Horowitz, Guangyou Qin, Thorsten Renk, Carlos Salgado and Werner Vogelsang for providing numerical data from their calculations. The authors also thank Nestor Armesto, Ulrich Heinz, , Peter Jacobs, Berndt Müller, Jamie Nagle and Carlos Salgado for reading an earlier version of the manuscript and providing feedback. The research of A.M. is supported in part by the U. S. Department of Energy under grant number DE-FG02-01ER41190.

## References

- [1] X.N. Wang and M. Gyulassy, Phys. Rev. Lett. 68 (1992) 1480.
- [2] STAR, C. Adler et al., Phys. Rev. Lett. 89 (2002) 202301.
- [3] PHENIX, K. Adcox et al., Phys. Rev. Lett. 88 (2002) 022301.
- [4] D. Antreasyan et al., Phys. Rev. D19 (1979) 764.
- [5] H. Fritzsche, M. Gell-Mann and H. Leutwyler, Phys. Lett. B47 (1973) 365.
- [6] D.J. Gross and F. Wilczek, Phys. Rev. Lett. 30 (1973) 1343.
- [7] H.D. Politzer, Phys. Rev. Lett. 30 (1973) 1346.
- [8] A.D. Martin et al., Eur. Phys. J. C14 (2000) 133.
- [9] J. Pumplin et al., JHEP 07 (2002) 012.
- [10] S. Albino, B.A. Kniehl and G. Kramer, Nucl. Phys. B725 (2005) 181.
- [11] B. Jager et al., Phys. Rev. D67 (2003) 054005.
- [12] J.C. Collins, D.E. Soper and G. Sterman, Phys. Lett. B134 (1984) 263.
- [13] J.C. Collins, D.E. Soper and G. Sterman, Nucl. Phys. B261 (1985) 104.
- [14] J.C. Collins, D.E. Soper and G. Sterman, Nucl. Phys. B308 (1988) 833.
- [15] J.C. Collins, D.E. Soper and G. Sterman, Adv. Ser. Direct. High Energy Phys. 5 (1988) 1.
- [16] Y.L. Dokshitzer, Sov. Phys. JETP 46 (1977) 641.
- [17] V.N. Gribov and L.N. Lipatov, Sov. J. Nucl. Phys. 15 (1972) 438.
- [18] G. Altarelli and G. Parisi, Nucl. Phys. B126 (1977) 298.
- [19] J. wei Qiu and G. Sterman, Nucl. Phys. B353 (1991) 137.
- [20] R. Doria, J. Frenkel and J.C. Taylor, Nucl. Phys. B168 (1980) 93.
- [21] C. Di’Lieto et al., Nucl. Phys. B183 (1981) 223.
- [22] A. Idilbi and A. Majumder, (2008), arXiv:0808.1087.
- [23] HERMES, A. Airapetian et al., (2009), arXiv:0906.2478.
- [24] X.N. Wang and M. Gyulassy, Phys. Rev. Lett. 68 (1992) 1480.

- [25] M. Gyulassy and X. nian Wang, Nucl. Phys. B420 (1994) 583.
- [26] X.N. Wang, M. Gyulassy and M. Plumer, Phys. Rev. D51 (1995) 3436.
- [27] R. Baier et al., Phys. Lett. B345 (1995) 277.
- [28] R. Baier et al., Nucl. Phys. B483 (1997) 291.
- [29] R. Baier et al., Nucl. Phys. B484 (1997) 265.
- [30] R. Baier et al., Phys. Rev. C58 (1998) 1706.
- [31] HERMES, A. Airapetian et al., Nucl. Phys. B780 (2007) 1.
- [32] X. feng Guo and X.N. Wang, Phys. Rev. Lett. 85 (2000) 3591.
- [33] A. Majumder and B. Muller, Phys. Rev. C77 (2008) 054903.
- [34] A. Majumder, (2009), arXiv:0912.2987.
- [35] P. Arnold, G.D. Moore and L.G. Yaffe, JHEP 11 (2001) 057.
- [36] P. Arnold, G.D. Moore and L.G. Yaffe, JHEP 12 (2001) 009.
- [37] P. Arnold, G.D. Moore and L.G. Yaffe, JHEP 06 (2002) 030.
- [38] S. Turbide et al., Phys. Rev. C72 (2005) 014906.
- [39] G.Y. Qin et al., Phys. Rev. Lett. 100 (2008) 072301.
- [40] G.Y. Qin et al., (2009), arXiv:0906.3280.
- [41] U.A. Wiedemann, Nucl. Phys. B582 (2000) 409.
- [42] U.A. Wiedemann, Nucl. Phys. B588 (2000) 303.
- [43] U.A. Wiedemann, Nucl. Phys. A690 (2001) 731.
- [44] C.A. Salgado and U.A. Wiedemann, Phys. Rev. D68 (2003) 014008.
- [45] N. Armesto, C.A. Salgado and U.A. Wiedemann, Phys. Rev. D69 (2004) 114003.
- [46] M. Gyulassy, P. Levai and I. Vitev, Nucl. Phys. B571 (2000) 197.
- [47] M. Gyulassy, P. Levai and I. Vitev, Phys. Rev. Lett. 85 (2000) 5535.
- [48] M. Gyulassy, P. Levai and I. Vitev, Nucl. Phys. B594 (2001) 371.
- [49] M. Gyulassy, P. Levai and I. Vitev, Phys. Lett. B538 (2002) 282.
- [50] M. Djordjevic and M. Gyulassy, Nucl. Phys. A733 (2004) 265.
- [51] M. Djordjevic, M. Gyulassy and S. Wicks, Phys. Rev. Lett. 94 (2005) 112301.
- [52] C.W. Bauer et al., Phys. Rev. D63 (2001) 114020.
- [53] C.W. Bauer and I.W. Stewart, Phys. Lett. B516 (2001) 134.



- [54] R.B. Neufeld and B. Muller, Phys. Rev. Lett. 103 (2009) 042301.
- [55] G.Y. Qin et al., Phys. Rev. Lett. 103 (2009) 152303.
- [56] J. Casalderrey-Solana, E.V. Shuryak and D. Teaney, J. Phys. Conf. Ser. 27 (2005) 22.
- [57] PHENIX, S.S. Adler et al., Phys. Rev. Lett. 97 (2006) 052301.
- [58] STAR, B.I. Abelev et al., Phys. Rev. Lett. 102 (2009) 052302.
- [59] J.M. Maldacena, Adv. Theor. Math. Phys. 2 (1998) 231.
- [60] S.S. Gubser, Phys. Rev. D74 (2006) 126005.
- [61] C.P. Herzog et al., JHEP 07 (2006) 013.
- [62] S.S. Gubser, S.S. Pufu and A. Yarom, JHEP 09 (2007) 108.
- [63] P.M. Chesler and L.G. Yaffe, Phys. Rev. Lett. 99 (2007) 152001.
- [64] A. Majumder, R.J. Fries and B. Muller, Phys. Rev. C77 (2008) 065209.
- [65] P. Arnold and W. Xiao, Phys. Rev. D78 (2008) 125008.
- [66] S. Wicks et al., Nucl. Phys. A784 (2007) 426.
- [67] W.A. Horowitz and B.A. Cole, (2009), arXiv:0910.1823.
- [68] S. Jeon and G.D. Moore, Phys. Rev. C71 (2005) 034901.
- [69] Theory and experimental collaboration on hot qcd matter (techqm).
- [70] M.H. Thoma and M. Gyulassy, Nucl. Phys. B351 (1991) 491.
- [71] E. Braaten and M.H. Thoma, Phys. Rev. D44 (1991) 2625.
- [72] M.G. Mustafa and M.H. Thoma, Acta Phys. Hung. A22 (2005) 93.
- [73] Y.L. Dokshitzer and D.E. Kharzeev, Phys. Lett. B519 (2001) 199.
- [74] B.W. Zhang, E. Wang and X.N. Wang, Phys. Rev. Lett. 93 (2004) 072301.
- [75] G.Y. Qin and A. Majumder, (2009), arXiv:0910.3016.
- [76] A. Majumder, Phys. Rev. C80 (2009) 031902.
- [77] R.D. Woods and D.S. Saxon, Phys. Rev. 95 (1954) 577.
- [78] A. Bialas, M. Bleszynski and W. Czyz, Nucl. Phys. B111 (1976) 461.
- [79] M.L. Miller et al., Ann. Rev. Nucl. Part. Sci. 57 (2007) 205.
- [80] G. Policastro, D.T. Son and A.O. Starinets, Phys. Rev. Lett. 87 (2001) 081601.
- [81] C. Nonaka and S.A. Bass, Phys. Rev. C75 (2007) 014902.
- [82] C. Hartnack et al., Eur. Phys. J. A1 (1998) 151.

- [83] F. Cooper and G. Frye, Phys. Rev. D10 (1974) 186.
- [84] S.A. Bass et al., Phys. Rev. C79 (2009) 024901.
- [85] B.G. Zakharov, JETP Lett. 65 (1997) 615.
- [86] P. Arnold, Phys. Rev. D79 (2009) 065025.
- [87] A. Dainese, C. Loizides and G. Paic, Eur. Phys. J. C38 (2005) 461.
- [88] K.J. Eskola et al., Nucl. Phys. A696 (2001) 715.
- [89] T. Renk and K.J. Eskola, Phys. Rev. C75 (2007) 054910.
- [90] N. Armesto et al., (2009), arXiv:0907.0667.
- [91] E. Wang and X.N. Wang, Phys. Rev. Lett. 89 (2002) 162301.
- [92] I. Vitev and M. Gyulassy, Phys. Rev. Lett. 89 (2002) 252301.
- [93] K.J. Eskola et al., Nucl. Phys. A747 (2005) 511.
- [94] STAR, C. Adler et al., Phys. Rev. Lett. 90 (2003) 082302.
- [95] T. Renk, Phys. Rev. C77 (2008) 017901.
- [96] T. Renk, Phys. Rev. C76 (2007) 064905.
- [97] PHENIX, A. Adare et al., Phys. Rev. D76 (2007) 051106.
- [98] STAR, J. Adams et al., Phys. Lett. B637 (2006) 161.
- [99] STAR, B.I. Abelev et al., Phys. Rev. Lett. 98 (2007) 192301.
- [100] PHENIX, A. Adare et al., Phys. Rev. Lett. 97 (2006) 252002.
- [101] M. Cacciari et al., JHEP 07 (2004) 033.
- [102] P. Aurenche et al., Eur. Phys. J. C13 (2000) 347.
- [103] D0, V.M. Abazov et al., Phys. Rev. Lett. 101 (2008) 062001.
- [104] CDF, T. Aaltonen et al., Phys. Rev. D80 (2009) 111106.
- [105] J. Pumplin et al., Phys. Rev. D80 (2009) 014019.
- [106] B.A. Kniehl, G. Kramer and B. Potter, Nucl. Phys. B582 (2000) 514.
- [107] European Muon, J. Ashman et al., Z. Phys. C57 (1993) 211.
- [108] J.W. Cronin et al., Phys. Rev. D11 (1975) 3105.
- [109] A. Accardi, (2002), arXiv:hep-ph/0212148.
- [110] A. Accardi et al., (2009), arXiv:0907.3534.
- [111] A. Majumder, (2009), arXiv:0901.4516.

- [112] A. Accardi et al., (2004), arXiv:hep-ph/0310274.
- [113] K.J. Eskola, H. Paukkunen and C.A. Salgado, JHEP 04 (2009) 065.
- [114] I. Vitev and B.W. Zhang, Phys. Lett. B669 (2008) 337.
- [115] PHENIX, S.S. Adler et al., Phys. Rev. Lett. 98 (2007) 172302.
- [116] STAR, J. Adams et al., Phys. Rev. Lett. 91 (2003) 072304.
- [117] M. Hirai, S. Kumano and T.H. Nagai, Phys. Rev. C76 (2007) 065207.
- [118] I. Vitev, Phys. Rev. C75 (2007) 064906.
- [119] PHENIX, S.S. Adler et al., Phys. Rev. C69 (2004) 034909.
- [120] STAR, B.I. Abelev et al., Phys. Rev. Lett. 97 (2006) 152301.
- [121] STAR, B.I. Abelev et al., Phys. Lett. B655 (2007) 104.
- [122] PHENIX, S.S. Adler et al., Phys. Rev. Lett. 94 (2005) 232301.
- [123] PHENIX, A. Adare et al., (2008), arXiv:0801.4020.
- [124] T. Hirano and Y. Nara, Phys. Rev. C69 (2004) 034908.
- [125] STAR, J. Adams et al., Phys. Rev. Lett. 97 (2006) 162301.
- [126] A. Majumder and X.N. Wang, Phys. Rev. D70 (2004) 014007.
- [127] A. Majumder and X.N. Wang, Phys. Rev. D72 (2005) 034007.
- [128] A. Majumder, E. Wang and X.N. Wang, Phys. Rev. Lett. 99 (2007) 152301.
- [129] STAR, J. Adams et al., Phys. Rev. Lett. 95 (2005) 152301.
- [130] PHENIX, A. Adare et al., Phys. Rev. C78 (2008) 014901.
- [131] R. Baier and D. Schiff, JHEP 09 (2006) 059.
- [132] PHENIX, S. Afanasiev et al., (2009), arXiv:0903.4886.
- [133] PHENIX, A. Adare et al., Phys. Rev. Lett. 101 (2008) 162301.
- [134] S. Collaboration, (2009), arXiv:0911.3130.
- [135] T. Renk, Phys. Rev. C74 (2006) 024903.
- [136] DELPHI, P. Abreu et al., Eur. Phys. J. C17 (2000) 207.
- [137] S. Albino, B.A. Kniehl and G. Kramer, Nucl. Phys. B803 (2008) 42.
- [138] D. de Florian, R. Sassot and M. Stratmann, Phys. Rev. D76 (2007) 074033.
- [139] T. Renk and K.J. Eskola, Phys. Rev. C76 (2007) 027901.
- [140] W. Liu, C.M. Ko and B.W. Zhang, Int. J. Mod. Phys. E16 (2007) 1930.

- [141] PHENIX, A. Adare et al., Phys. Rev. Lett. 98 (2007) 172301.
- [142] A. Adil and I. Vitev, Phys. Lett. B649 (2007) 139.
- [143] H. van Hees et al., Eur. Phys. J. C61 (2009) 799.
- [144] N. Armesto et al., Phys. Rev. D71 (2005) 054027.
- [145] PHENIX, A. Adare et al., Phys. Rev. C80 (2009) 024908.
- [146] STAR, A.M. Hamed, Nucl. Phys. A830 (2009) 451c.
- [147] H. Zhang et al., Phys. Rev. Lett. 103 (2009) 032302.
- [148] T. Renk, Phys. Rev. C80 (2009) 014901.
- [149] X.N. Wang and Z. Huang, Phys. Rev. C55 (1997) 3047.
- [150] F. Arleo et al., JHEP 11 (2004) 009.
- [151] STAR, S. Salur, Eur. Phys. J. C61 (2009) 761.
- [152] for the STAR, M. Ploskon, (2009), arXiv:0908.1799.
- [153] STAR, J. Putschke, Eur. Phys. J. C61 (2009) 629.
- [154] PHENIX, Y.S. Lai, (2009), arXiv:0907.4725.
- [155] G.P. Salam and G. Soyez, JHEP 05 (2007) 086.
- [156] M. Cacciari and G.P. Salam, Phys. Lett. B641 (2006) 57.
- [157] M. Cacciari, G.P. Salam and G. Soyez, JHEP 04 (2008) 063.
- [158] ALEPH, S. Schael et al., Eur. Phys. J. C47 (2006) 309.
- [159] DELPHI, J. Abdallah et al., Eur. Phys. J. C55 (2008) 1.
- [160] L3, P. Achard et al., Eur. Phys. J. C45 (2006) 569.
- [161] CDF, A. Abulencia et al., Phys. Rev. Lett. 99 (2007) 182002.
- [162] D0, V.M. Abazov et al., Phys. Rev. Lett. 101 (2008) 182001.
- [163] STAR, E. Bruna, (2009), arXiv:0907.4788.
- [164] P.F. Kolb, J. Sollfrank and U.W. Heinz, Phys. Rev. C62 (2000) 054909.
- [165] K. Zapp et al., Eur. Phys. J. C60 (2009) 617.
- [166] ALICE, F. Carminati, (ed. ) et al., J. Phys. G30 (2004) 1517.
- [167] ALICE, B. Alessandro, (ed. ) et al., J. Phys. G32 (2006) 1295.
- [168] ATLAS, P. Steinberg, J. Phys. G34 (2007) S527.
- [169] ATLAS, H. Takai, J. Phys. G30 (2004) S1105.

- [170] CMS, D.G. d'Enterria, (Ed. ) et al., J. Phys. G34 (2007) 2307.
- [171] N. Armesto, (ed. ) et al., J. Phys. G35 (2008) 054001.
- [172] R.D. Field, Redwood City, USA: Addison-Wesley (1989) 366 p. (Frontiers in physics, 77).
- [173] R.K. Ellis, W.J. Stirling and B.R. Webber, Camb. Monogr. Part. Phys. Nucl. Phys. Cosmol. 8 (1996) 1.
- [174] S. Sapeta and U.A. Wiedemann, Eur. Phys. J. C55 (2008) 293.
- [175] N. Armesto, L. Cunqueiro and C.A. Salgado, Eur. Phys. J. C63 (2009) 679.
- [176] T. Renk, Phys. Rev. C80 (2009) 044904.
- [177] B. Schenke, C. Gale and S. Jeon, (2009), arXiv:0909.2037.